

**PEPTIDE AND NONPEPTIDE APPROACHES TO TARGET PROTEIN-
PROTEIN INTERACTIONS FOR THE TREATMENT OF CANCER**

by

Xu Ran

**A dissertation submitted in partial fulfillment
of the requirements for the degree of
Doctor of Philosophy
(Medicinal Chemistry)
in The University of Michigan
2015**

Doctoral Committee:

**Professor Shaomeng Wang, Chair
Research Professor Scott D. Larsen
Professor Henry I. Mosberg
Assistant Professor Zaneta Nikolovska-Coleska**

© Xu Ran 2015

DEDICATION

This work is dedicated to my beloved family members.

ACKNOWLEDGMENTS

I would like to express my gratitude to my advisor Dr. Shaomeng Wang for his guidance and support for my PhD studies during the past five years. It has been a great honor for me to work in Professor Wang's Lab, where I was exposed to diverse scientific disciplines, cutting-edge techniques, and challenging but rewarding projects, and learned how technology transfer of research benefits academia, industry and patients.

I would like to acknowledge my committee members, Dr. Scott Larsen, Dr. Henry Mosberg and Dr. Zaneta Nikolovska-Coleska, for their valuable advice for this thesis.

I am grateful for my amazing colleagues: Dr. Yujun Zhao for his consistent advice concerning my chemistry experiments, and also his invaluable suggestions in data interpretation and career planning; Dr. Steven Kawamoto for his pioneer work in triazole-stapled peptides and his help in initiating the RAP1 project. I would like to thank Dr. Liu Liu for his obtaining biochemical data for both of the projects; Dr. Chao-Yie Yang for his computational analyses of proposed molecules; Drs. Longchuan Bai and Jianfeng Lu for testing compounds in cell based assays for the Bromodomain and the RAP1 projects; and Donna McEachern and Sally Przybranowski for testing bromodomain inhibitors in animal models. I would also like to thank the rest of our laboratory members for constructive discussions and invaluable feedbacks.

I would like to thank my collaborators: Drs. Ming Lei and Yong Chen; Drs. Jeanne A. Stuckey, Jennifer Meagher and Krishnapriya Chinnaswamy for their help in

expressing proteins and solving X-ray crystal structures for the RAP1 and the Bromodomain projects. I would also like to thank Drs. Duxin Sun, Xiaoqin Li, Bo Wen and Ruijuan Luo for the microsomal stability and pharmacokinetic analyses of bromodomain inhibitors.

I would also like to thank Dr. Ari Gafni for letting me use their circular dichroism spectrometer, and Dr. Katarzyna Sobczyk-Kojiro for the advice and training she provided for using their peptide synthesizer.

Lastly and most importantly, my family members: my wife Jing, my parents and in-laws, whose support made this happen.

TABLE OF CONTENTS

DEDICATION	ii
ACKNOWLEDGMENTS	iii
LIST OF TABLES	viii
LIST OF FIGURES	ix
LIST OF SCHEMES	x
ABSTRACT	xi
CHAPTER 1 Introduction: protein-protein interactions as anticancer drug targets.....	1
1.1 General survey of clinical anticancer drugs	1
1.2 Progress of targeting protein-protein interactions	3
1.3 Oncogenic PPIs and ligand design strategy.....	4
CHAPTER 2 Design of stapled peptides targeting RAP1/TRF2 and RAP1/IKK interaction.....	10
2.1 Introduction	10
2.1.1 Function of RAP1 and its interaction with TRF2 and IKK.....	10
2.1.2 Analysis of the TRF2-RAP1 protein-protein interaction.....	12
2.1.3 Stapled α -helical peptides.....	14
2.2 Design and synthesis of high-affinity stapled peptides binding to RAP1.	16
2.2.1 Design and optimization of tracers for fluorescence polarization assay.	16
2.2.2 Truncation study.....	17
2.2.3 Triazole stapling.....	18
2.2.4 Mutation of interacting residues.....	21
2.2.5 Improvement of water solubility	24
2.3 Stapled peptide down-regulates NF- κ B activation and inhibits cell growth in breast cancer cell lines.....	25
2.3.1 Stapled peptide down-regulates NF- κ B activation in HeLa and MDA-MB-157 cell-lines.	25
2.3.2 Cell growth inhibition by the stapled peptides.	25
2.4 Summary and discussion	26
2.5 Future directions.....	28

2.5.1 Further modification of peptide-based α -helix mimetics.	28
2.5.2 Non-peptide α -helix mimetics.	30
2.6 Experiments.....	31
2.6.1 Peptide synthesis	31
2.6.2 Fluorescence polarization assay	31
2.6.3 Circular Dichroism	33
2.6.4 Proteolytic stability assays	33
2.6.5 Molecular modeling.....	34
2.6.6 Cellular assays.....	34
CHAPTER 3 Structure-based design and synthesis of novel small-molecular inhibitors targeting BET bromodomains.	38
3.1 Introduction	38
3.1.1 Epigenetic histone modifications	38
3.1.2 Bromodomains as acetylated lysine binding partners	39
3.1.3 Pharmacological significance of BET bromodomains	40
3.1.4 Development of BET bromodomain inhibitors for cancer treatment.....	42
3.2 Structure-based design of novel BET bromodomain inhibitors.	44
3.3 Structure activity relationship studies of the new class of BET bromodomain inhibitors. .	47
3.3.1 SAR of “head” groups.....	48
3.3.2 SAR of five-membered aromatic system as “tail” groups.....	49
3.4 Selectivity of new BRD4 inhibitors in biochemical and cellular assays	53
3.4.1 Selectivity among BET family bromodomains	53
3.4.2 Selectivity among bromodomains from other families	54
3.5 RX-series BET bromodomain inhibitors selectively induce cell-cycle arrest and apoptosis in leukemia cell-lines.....	55
3.6 SAR of mono- or bicyclic aromatics as “tail” group.....	58
3.7 Pharmacokinetic and antitumor efficacy studies	60
3.8 Synthesis of γ -carboline-containing compounds as BET bromodomain inhibitors.	61
3.9 Future Directions	65
3.10 Experiments.....	66

3.10.1 Synthetic methods and characterizations of BET bromodomain inhibitors	66
3.10.2 Biochemical assays.....	86
3.10.3 Cellular assays	89
3.10.4 Molecular modeling.....	90
3.10.5 Crystallization and structure determination.....	91
3.10.6 Pharmacokinetic analysis	92
3.10.7 <i>In vivo</i> antitumor efficacy.....	92
CHAPTER 4 Perspective of targeting protein-protein interactions using peptide or non-peptide small-molecules for cancer targeted therapy	93
REFERENCES.....	97

LIST OF TABLES

Table 1 Sequence and K_d value of tracers binding to RAP1 protein.....	17
Table 2 Binding affinities of truncated TRF2 peptides to RAP1.	18
Table 3 Binding affinities of peptides mutated at solvent-exposed residues.....	19
Table 4 Binding affinities of stapled peptides and unstapled precursors.	19
Table 5 Binding affinities of stapled peptides with modification at Ile283.	22
Table 6 Contribution of stapling and Ile283 modification to the K_i	23
Table 7 SAR of new BET inhibitors with modification “head” groups.	48
Table 8 SAR of new BET inhibitors with modification “tail” groups.	51
Table 9 Binding affinities of new BET inhibitors among BET family members.....	54
Table 10 Binding affinities of selected BET inhibitors to other family bromodomains measured by Bio-Layer Interferometry.	54
Table 11 Cell growth inhibitory activity of new BET inhibitors in acute leukemia cell lines.	56
Table 12 Structure and binding affinities of compounds with mono- and bi-cyclic aromatic “tails”.	59
Table 13 RX-201 concentrations in mouse plasma and tumor.	60

LIST OF FIGURES

Figure 1 Smac mimetics bind to XIAP.....	6
Figure 2 Bcl-2 family inhibitors.....	8
Figure 3 MDM2/p53 inhibitors.....	8
Figure 4 Crystal structure of the RAP1/TRF2 complex.....	12
Figure 5 Analysis of TRF2 α_1 and RAP1 interactions.....	14
Figure 6 All-hydrocarbon and triazole stapling strategies.....	15
Figure 7 Circular dichroism spectra of selected peptides.....	20
Figure 8 Modeled binding pose of mutated residues: I283F and I283W.....	21
Figure 9 Binding model of 19T to RAP1.....	23
Figure 10 Structures and RAP1 binding affinities of optimized stapled peptides for cellular studies.....	24
Figure 11 Stapled peptide down-regulates NF- κ B activation in cell.....	25
Figure 12 Cell growth inhibition of 14TnPip and 14TnPip (-) in MDA-MB-157 and HeLa cell lines.....	26
Figure 13 Trypsin digestion assay using Ac-ARA-NH ₂ as negative control.....	28
Figure 14 Proposed modification strategies to improve cellular activity (Type I mimetics).....	29
Figure 15 Selected non-peptide proteomimetic scaffolds (Type III mimetics).....	31
Figure 16 Transcriptional regulations by HATs, bromodomains and HDAC.....	39
Figure 17 Co-crystal structure of BRD4 BD1 with a K-Ac containing peptide.....	40
Figure 18 BRD4 transcriptionally activates oncogenes <i>c-MYC</i> and <i>BCL2</i> family in MLL-fusion leukemia.....	42
Figure 19 Potent and selective BET bromodomain inhibitors.....	42
Figure 20 Co-crystal and modeled structures of I-BET 151 (4).....	45
Figure 21 Design of γ -carboline core structure.....	46
Figure 22 Modeled structures of compound 5 bound to BRD4 BD1 and BRD4 BD2.....	47
Figure 23 Co-crystal structures of 6 and 12 with BRD4 BD2.....	50
Figure 24 Co-crystal structure and schematic representation of 18 interactions.....	53
Figure 25 New BET bromodomain inhibitors down-regulate target oncoprotein expression and induce apoptosis in MV4-11 cells.....	57
Figure 26 New BET bromodomain inhibitors induce apoptosis in Molm-13 cells.....	58
Figure 27 RX-201 concentrations in mice plasma and tumor.....	60
Figure 28 Antitumor activity of RX-201 in a mouse xenograft model.....	61
Figure 29 Charge difference is important in cellular activity of stapled peptides.....	95

LIST OF SCHEMES

Scheme 1 Synthetic route to γ -carboline core structure.	62
Scheme 2 General synthetic method for 6-11.	62
Scheme 3 Synthetic method for 5.....	63
Scheme 4 General synthetic route for 12-19.	64
Scheme 5 General synthetic route for five-membered heterocyclic boronates.	64

ABSTRACT

Protein-protein interactions (PPIs) are macromolecular contacts critical in physiological processes and they play a role in both normal cellular processes and disease pathogenesis. Targeting PPIs represents a new but poorly explored therapeutic strategy. In this thesis, I have investigated peptide and nonpeptide approaches to two separate PPIs.

Repressor activator protein 1 (RAP1) is a binding partner of telomeric repeat-binding factor 2 (TRF2) for the regulation of telomere function. A previous study has suggested that RAP1 recruits I κ B kinases (IKK) to NF- κ B complex phosphorylate p65 S536 and activates NF- κ B pathway. Knocking down RAP1 sensitizes breast cancer cells apoptosis *via* NF- κ B suppression. We employed a structure-based design strategy to develop a series of triazole-stapled α -helical peptides based upon the TRF2 sequence to block both RAP1/TRF2 and RAP1/IKK interactions. The most potent peptide synthesized binds to RAP1 with a K_i value of 7 nM, and is 400-fold more potent than the initial TRF2 peptide. Cellular studies show that an optimized peptide dose-dependently down-regulates p65 phosphorylation and inhibits cell growth in the HeLa and MDA-MB-157 cancer cell lines. This study generates the first-in-class inhibitor targeting RAP1, which can be used as a pharmacological tool to study NF- κ B signaling in certain type of cancer.

Bromodomain and extra terminal (BET) proteins, including BRD2, BRD3 and BRD4, are epigenetic readers and play a key role in regulation of gene transcription by

binding to acetylated lysine residues on histone tails. Small-molecule inhibitors of BET have therapeutic potential for the treatment of human cancers and other diseases. We have carried out structure-based design, synthesis and evaluation of γ -carboline-containing compounds as a new class of small molecule BET inhibitors. Our most potent inhibitor (compound 18, RX-37) binds to BET bromodomain proteins (BRD2, BRD3 and BRD4) with K_i values of 3.2-24.7 nM and demonstrates high selectivity over other bromodomain proteins. RX-37 potently and selectively inhibits cell growth in human acute leukemia cell lines harboring rearranged mixed lineage leukemia 1 gene. Further modification of RX-37 yielded RX-201 which shows high oral bioavailability and *in vivo* efficacy in mice. This study has introduced a new chemical scaffold with potential therapeutic value in clinic.

CHAPTER 1

Introduction: protein-protein interactions as anticancer drug targets.

1.1 General survey of clinical anticancer drugs

Cancer is one of the most life-threatening illnesses in the world, causing the death of 8.2 million people worldwide in 2012¹. The efforts in development of clinical anticancer drugs have been a major task in academia and in the pharmaceutical industry through the decades, and have recorded a number of successes and challenges in patient response and toxicities as well as drug resistance².

Classical chemotherapy which directly blocks DNA replication and cell division was firstly introduced in 1946 when nitrogen mustard, a DNA-alkylating substance successfully induced remission in lymphoma³. Subsequent discoveries of new agents in this class including methotrexate⁴ (antifolate), vinca alkaloids⁵ (targeting mitotic spindle), platinum derivatives⁶ (DNA cross-linker), nucleoside analogues⁷ (DNA polymerase inhibitor) and taxanes^{8,9} (tubulin) are still the major clinical chemotherapeutics currently and can successfully treat leukemia, ovarian, testicular and other types of cancer. However, the lack of selectivity between cancer and normal cells leads to toxicities for human organs and normal physiological functions as these drugs target rapidly dividing cells².

Limitations of chemotherapy gave rise to “targeted therapies” which can more successfully differentiate tumor cells from normal cells, thus achieving higher specificity

and lower toxicity. Protein targets that play a more important role in cancerous than in normal cells were identified and targeted with drugs that could offer clinical benefit to cancer patients².

Several clinical successes were mainly oncogenic signaling intermediates such as the BCR-ABL kinase inhibitor imatinib¹⁰⁻¹² (Gleevec; Novartis), the EGFR inhibitor Gefitinib^{13, 14} (Iressa; AstraZeneca) and monoclonal antibodies targeting cell surface receptors such as trastuzumab^{15, 16} (Herceptin; Genetech/Roche). Even though these new approaches have generally milder side-effects than the older cytotoxic drugs, new challenges regarding the persistence of these agents have emerged and have resulted occasionally in relapse of the therapeutic response¹⁷. For example, the resistance mechanisms for imatinib in BCR-ABL are mutations and amplification of target fusion protein, over-expression of multidrug-resistance protein 1, or activation of an alternative survival signaling pathway^{18, 19}. Combination therapies of drugs targeting different signaling pathways or design of single drugs targeting multiple targets have been tested in clinical trials in the past decade, but few have shown long-term success^{20, 21}.

Thus, new targeted therapies have emerged, aimed at “tumor-supportive cellular machineries”, such as chromatin modifiers, protein chaperones or the proteasome². Upon approval of bortezomib^{22, 23} (Velcade; Millennium Pharmaceuticals) and SAHA^{24, 25} (Vorinostat, Zolinza/Merck) for the treatment of different types of lymphoma, an increasing number of targets have been validated and agents binding to those proteins were identified and optimized for pre-clinical or clinical development²⁶⁻²⁸. Whether and

to what extent these new targets could overcome previous limitations and provide clinical benefit still await examination with more clinical evidence.

In both classes of targeted therapies: signaling intermediates and cellular machineries, protein-protein interactions (PPIs) have been viewed as offering attractive new anticancer drug targets, because of their essential role in organizing molecular processes and maintaining intra- and extracellular physiological function^{26, 29}. Altered cellular signals that were transduced *via* PPIs may finally give rise to various malignances^{26, 29}. There are estimated 650,000 distinct PPIs, most of whose functions are still to be clarified³⁰. Targeting protein-protein interactions has become therefore a “gold mine” for scientists who seek a better understanding of biological systems, and more importantly, design of new anticancer therapies.

1.2 Progress of targeting protein-protein interactions

PPIs normally refer to physical contacts between two or more proteins forming complexes that contribute to certain biological events such as molecular dynamics, enzymatic reactions and signaling transductions²⁹. Inhibitors of PPIs are either orthosteric inhibitors that competitively bind to protein interfaces or allosteric inhibitors that induce conformational changes thus disrupting the protein complex³¹. Current research is mostly focussed on orthosteric inhibitors³².

Twenty years ago, PPIs were considered as “undruggable” targets because crystal structures disclosed at that time showed a much larger (1,000-2,000 Å²) and flatter interface area than traditional deep cavities (~300-500 Å²) familiar in small molecule

binding³². Even though some peptide hormones had been approved as drugs for clinical use³³, poor cell-permeability and bioavailability issues hampered their application for intracellular targets²⁹. Employment of computational techniques in drug discovery in the 1990's led to the first clinical PPI modulators, including aggrastat³⁴ (tirofiban) which was derived from virtual screening leads and was approved as an anticoagulant³⁵. Natural products like taxanes were among the first anticancer drugs that modulate tubulin PPI interactions⁸.

The last decade has witnessed amazing progress in the study of PPIs. Computer-assisted structural analysis and rational design revealed the existence of small “hot spots” on the interfaces that contributed most of the binding free-energy³⁶. This discovery further strengthened the possibility of designing “drug-like” small-molecules as potent PPI inhibitors by utilizing these “hot spots”³⁷. In addition to this, a number of cell-permeable peptide-based molecules were reported to target intracellular PPI targets^{30, 38}.

1.3 Oncogenic PPIs and ligand design strategy

Traditionally, PPI inhibitors have high molecular weights (>500 Da) and high LogP values (>5) compared to typically drug-like small-molecules. This violates two principals of “Lipinski's rule of five”^{39, 40}, and reduces their chances of entering clinical trials. Recent discoveries of new pathologically important PPIs however revealed protein interfaces with the different sizes and shapes which led to novel PPI inhibitors with diverse physicochemical properties, from peptide based compounds (>2000 Da) to drug-like small molecules (<500 Da)³⁰.

The shapes of PPI interfaces can be classified according to the conformation of interacting peptide sequences as: (1) continuous short loops, (2) α -helices, β -sheets or turns and (3) tertiary structures. The difficulties associated with the design of small molecule PPIs increase as the conformation becomes more complex³².

In the first class of the PPI interface, which normally comprise 3-4 continuous residues and adopt unstructured loop conformation, short peptide segments can be converted to either small molecule peptide mimetics or to nonpeptide small molecules.

XIAP, an inhibitor of apoptosis proteins (IAP), is an example of the first class of the PPI interface. It binds to the BIR domain of caspase-3, caspase-7 and caspase-9 and inhibits the caspases' proapoptotic activity⁴¹. An endogenous ligand of XIAP, the second mitochondrial activator of caspases (Smac) which competes with caspases for binding to the BIR domain of XIAP can reactivate caspases and induce cancer cells to undergo apoptosis⁴². The Smac motif at the interface is a four-residue peptide, AVPI, all of whose hydrophobic side chains interact with hot-spot residues Glu314, Leu307, Trp310 and Trp323 on the XIAP BIR3 domain⁴³. Peptide mimetics utilizing these interactions have resulted in discovery of seven clinical drugs and currently, five Smac mimetic compounds are active in clinical trials for various types of cancer (**Figure 1**)³².

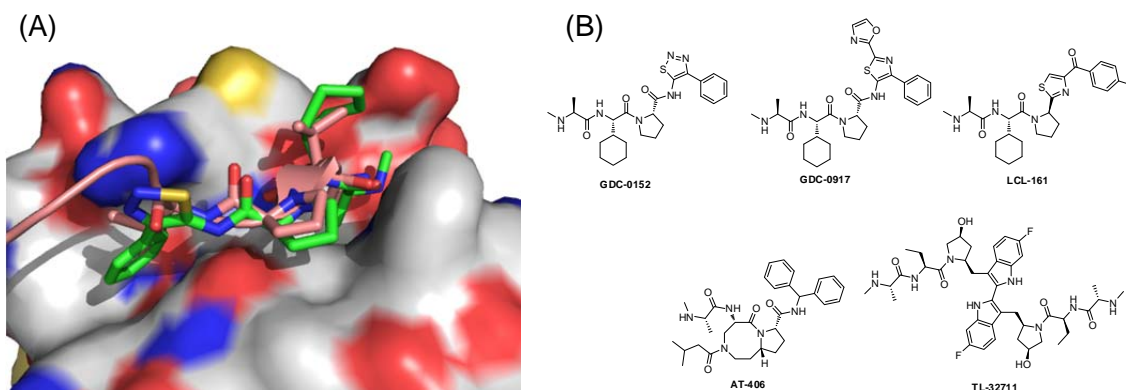


Figure 1 Smac mimetics bind to XIAP. (A) GDC-0152 (green) binds to XIAP (surface) overlaid with Smac peptide (pink). (B) Structures of Smac mimetics in clinical trials.

Besides peptide-based small molecules, there are also some nonpeptide small molecules that mimic the interaction of short peptides. A typical example is the bromodomain-containing proteins, which mainly interact with only one residue from the interacting partner⁴⁴. Bromodomain and extra terminal (BET) proteins are epigenetic “readers” that recognize histone acetyl-lysine markers and recruit transcriptional complexes to the corresponding site for gene transcription⁴⁵. BET proteins contain a deep hydrophobic pocket for acetyl-lysine recognition, which makes it plausible to design nonpeptide-based small molecules. The details of BET inhibitor design will be discussed below in CHAPTER 3.

The second class of PPI interfaces consists of well-defined secondary structures such as the α -helix. For example, two cell apoptosis related PPIs, that between Bcl-2 family proteins, and that between oncogenic protein MDM2 and tumor suppressor p53, have a well-defined helical structure^{46,47}.

As the interface of the Bcl-2/BAX interaction is quite large, two strategies have been employed for the design of PPIs. One strategy called for the design of stapled peptides. Hydrocarbon stapled BH3 peptides, prepared by olefin-metathesis reactions have been shown to have *in vivo* activities in animal models because they have an improved helical propensity as well as stability to proteolysis that benefits their cell-permeability and pharmacokinetic profiles³⁸. In the second approach, non-peptide small-molecule inhibitors, such as ABT-737⁴⁸, were designed. ABT-737 was designed using a fragment-based approach, which covers all the interacting hot spots residues and achieves sub-nanomolar affinity for the protein (**Figure 2**). ABT-263, an optimized version of ABT-737 is now in Phase I/II clinical trials^{29, 49}. ABT-263, with a molecular weight of 975 Da and a cLogP value of 12.4, is clearly an outlier of the “Lipinski’s rule of five”, but surprisingly, is orally bioavailable. The interface of MDM2/p53 is smaller than the interface in the Bcl-2 family protein PPIs, and this allows traditional drug screening approaches to succeed. Nutlin-3a, a small molecule inhibitor of the MDM2/p53 interaction, was discovered by high-throughput screening, followed by extensive medicinal chemistry optimization⁵⁰. MI-888⁵¹, a designed spiro-oxindole compound, was shown to mimic three key interacting residues in p53: Phe19, Trp23 and Leu26 for interaction with MDM2 but has an affinity 1000-times superior to that of p53 (**Figure 3**). MI-77301⁵², an analog of MI-888, has advanced into clinical development.

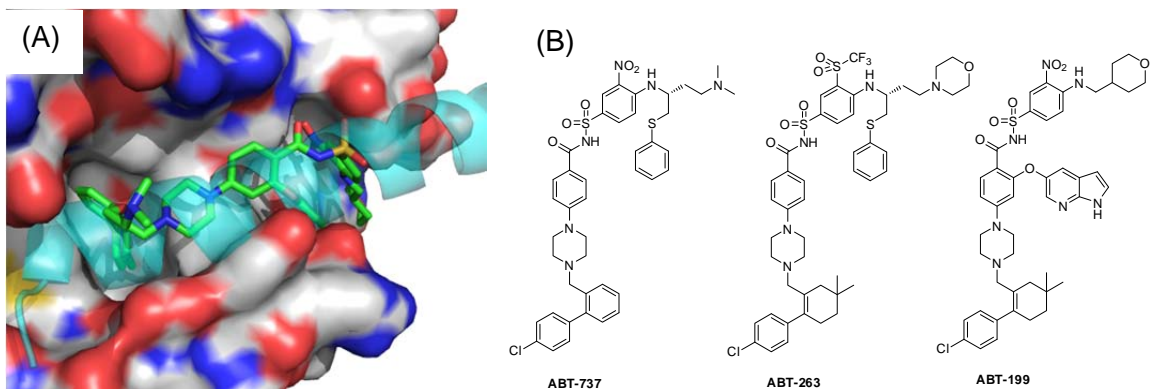


Figure 2 Bcl-2 family inhibitors. (A) ABT-199 (green) binds to Bcl-2 (surface) overlaid with BAX BH3 helix (cyan). (B) Structures of nonpeptide Bcl-2/Bcl-xL inhibitors.

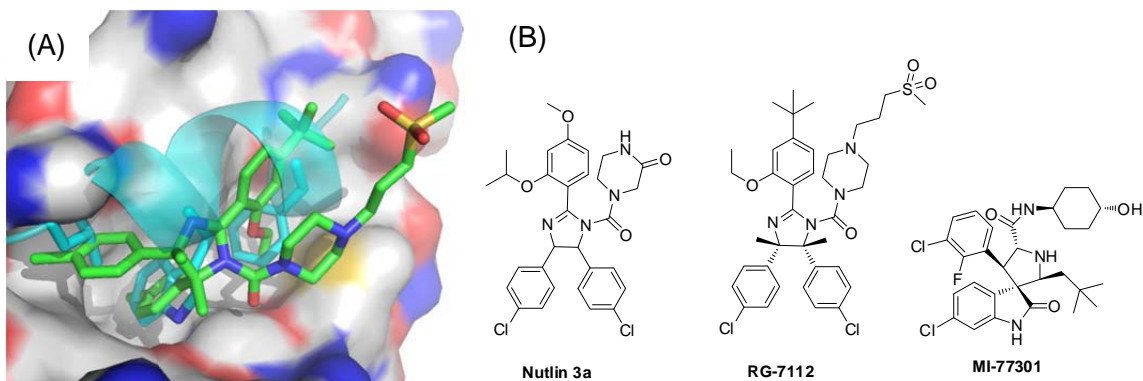


Figure 3 MDM2/p53 inhibitors. (A) RG-7112 (green) binds to MDM2 (surface) overlaid with p53 helix (cyan). (B) Structures of MDM2 inhibitors.

Tertiary structures, while fewer than the α -helical structures discovered in PPI interfaces, contribute to some key pathological events in inflammation and HPV infection^{53, 54}. However, due to their structural complexity, there have been very few successes in academic studies and no clinical trials have been reported.

In the following chapters, two projects will be presented. These projects use either peptide or nonpeptide molecules targeting two protein-protein interfaces for the discovery of novel anticancer therapeutics.

CHAPTER 2

Design of stapled peptides targeting RAP1/TRF2 and RAP1/IKK interaction.

2.1 Introduction

2.1.1 Function of RAP1 and its interaction with TRF2 and IKK

Repressor Activator Protein 1 (RAP1) is an evolutionarily conserved telomere-associated protein that was initially discovered as a protean regulator in budding yeast⁵⁵, where it either represses or activates transcription of genes at its DNA binding site and also preserves the topological structure of the chromosome tail.

Later studies in fission yeast and mammals revealed a different mechanism for the impact of RAP1 on telomere integrity. It forms a six-subunit protein complex named shelterin⁵⁶, which facilitates telomere folding and prevents the single strand overhang from being processed by DNA repair machinery⁵⁷⁻⁵⁹. Unlike budding yeast RAP1, mammalian and fission yeast RAP1 binds to telomere DNA *via* its interacting partner in the shelterin complex, the Telomeric Repeat binding Factor 2 (TRF2) in mammalian cells or Tar-EnvZ hybrid molecule (Taz1) in fission yeast⁶⁰. The biophysical explanation for “losing” its direct DNA binding property is loss of the second Myb-like domain during evolution. Removal of RAP1 from mouse telomere does not affect telomere capping, or the viability and fertility of the animal, but induces chromosome recombination which leads to homology-directed repair (HDR) in absence of nonhomologous end joining (NHEJ)⁵⁷. HDR threatens telomere integrity and alters telomere length and is related to senescence and cancer^{61, 62}.

In recent years, several telomere-independent functions of RAP1, including gene transcription⁶³⁻⁶⁶ and NF- κ B activation⁶⁷ have been discovered.

Martinez *et al.*⁶³ and Yeung *et al.*⁶⁵ reported that RAP1 binds to both telomere and extratelomeric region through a (TTAGGG)(2) consensus motif, regulating transcription of metabolic related genes such as *Ppara* and *Pgc1- α* . *In vivo* experiments showed that RAP1 deficiency leads to metabolic disorders and accumulation of excess fat, and thus forges a link between RAP1 transcriptional regulation and obesity^{65, 66}. Surprisingly, studies also revealed that RAP1 binds to DNA in a TRF2-independent manner, indicating either that RAP1 may directly interact with DNA or that there is an unidentified partner that recruits the protein to DNA⁶⁵.

RAP1 was also implicated as an NF- κ B regulator through a genome-wide gain-of-function screen⁶⁷. Free RAP1 was detected in cytoplasm where it recruits I κ B kinases (IKK) to NF- κ B, phosphorylates p65 at Ser536 and activates NF- κ B pathway. In turn, the activated NF- κ B induces RAP1 expression thus forming a feedback loop which further amplifies the activation. Knock down of RAP1 with *sh*RNA sensitizes TNF α induced apoptosis in breast cancer cell lines⁶⁷. Accordingly, blocking RAP1/IKK interaction with a PPI inhibitor might have a similar effect as RAP1 knockdown and hence, targeting the RAP1/IKK interaction with synthetic chemical entities could also be the basis of a strategy for the development of clinical therapeutics for cancer.

2.1.2 Analysis of the TRF2-RAP1 protein-protein interaction.

Although the precise details of the interaction between RAP1 to IKK are still limited, the crystal structure of human RAP1 and its shelterin partner TRF2 was determined several years ago (**Figure 4**, PDB ID: 3K6G)⁶⁸.

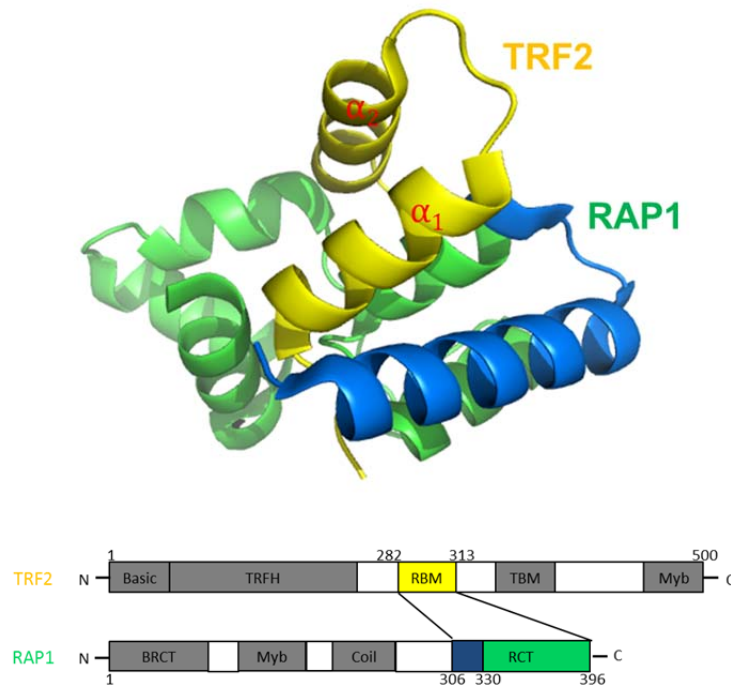


Figure 4 Crystal structure of the RAP1/TRF2 complex. Helix α_1 of TRF2 RBM (yellow) interacts with RAP1 RCT (green) and a shared binding motif (blue) of RAP1 RCT to both TRF2 and IKK.

The RAP1 Binding Motif (RBM) of TRF2 adopts two α -helices with which to interact with a six-helical bundled RAP1 C-Terminus (RCT), an evolutionarily conserved motif for RAP1 protein-protein interactions. The two helices of RBM, α_1 and α_2 are both three-turn short helices linked by four unstructured residues that enable them to fold and clamp onto the surface of RCT⁶⁸. The crystal structure also provides conformation for

part of the IKK interacting motif in RAP1 (Val306-Ser330)⁶⁷, which locates mainly at a 19-residued α -helix, interacting closely with α_1 of TRF2 (**Figure 4**). This observation reveals on RAP1, an interacting motif shared by TRF2 and IKK, and indicates that the short helix α_1 which binds to the RAP1/TRF2 interface might be able to block both PPIs of RAP1/TRF2 and RAP1/IKK either by competitively binding the same location or inducing conformational change from an allosteric site. In our study, we applied a structure-based design strategy and developed a potent inhibitor, which blocks RAP1/TRF2 interaction in biochemical assays, and functions intracellularly as an NF- κ B inhibitor. This mechanism is associated with disruption of the RAP1/IKK interaction.

Our analysis of the TRF2 / RAP1 interface at the helical α_1 fragment showed the helix to be located at a large and flat hydrophobic area where the six residues Ile283, Thr287, Leu288, Ala291, Phe292 and Leu295 in TRF2 interact with corresponding hydrophobic pockets in RAP1⁶⁸ (**Figure 5A**). Meanwhile, two hydrogen bond interactions from the backbone of Thr281 and Ile283 on N-terminal loop anchor the following helix to the surface (**Figure 5B**). Two charged residues, Lys289 and Lys293, are exposed to solvent and contribute to the solubility of the peptide (**Figure 5C**).

Typically, a hydrophobic surface like this is considered undruggable as it is very difficult to design potent, specific and drug-like small-molecular inhibitors⁶⁹. We therefore took advantage of the α_1 helix sequence and performed extensive modifications of the peptide to enhance its binding affinity and cell-permeability. Although such peptide-based compounds may not be suitable for clinical development, they may be used

as pharmacological tools for target validation as well as further investigation of physiological functions of RAP1^{57, 63, 65-67, 70}.

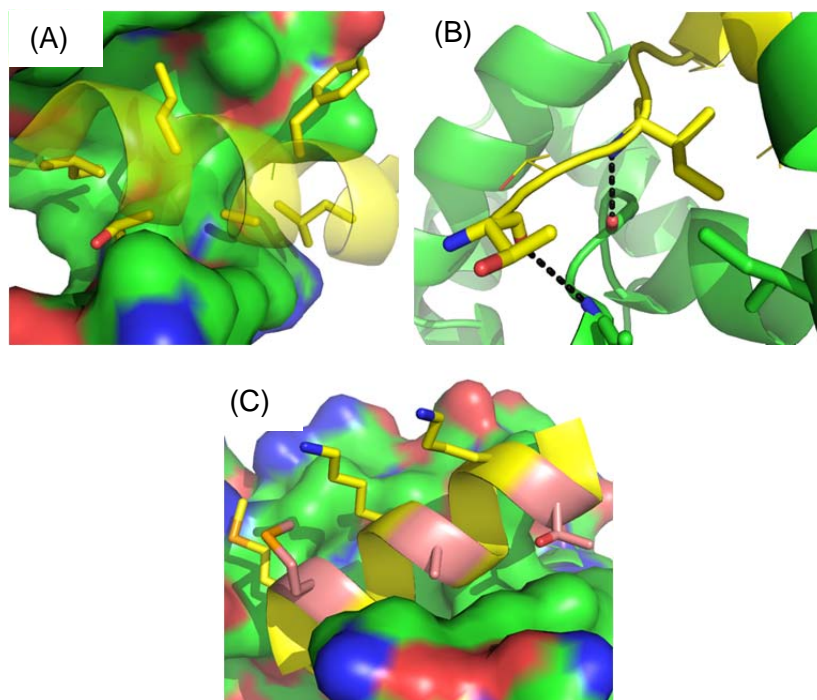


Figure 5 Analysis of TRF2 α_1 (yellow) and RAP1 (green) interactions. (A) Hydrophobic interacting residues (sticks). (B) N-terminal hydrogen bond interactions (dashed lines). (C) Solvent-exposed residues (sticks), residues to be stapled (pink sticks).

2.1.3 Stapled α -helical peptides.

The major obstacle for peptides to approach intracellular targets and become therapeutic agents is the lack of drug-like properties, including potency, cell permeability and resistance to proteolysis⁶⁹. One of the reasons is that short helical peptide tends to adopt an extended structure when dissolved in aqueous solution³⁸. Such loss of secondary structure results in a high energy barrier for restoration of the active conformation and exposure of amide bonds make peptides more susceptible to digestion by proteases. To

overcome these weaknesses, chemical modifications *via* introduction of conformational restrictions that have been intensively studied in the past 20 years³⁰ include hydrogen-bonding surrogates⁷¹⁻⁷⁴, photocontrolled α -helices⁷⁵ and various types of stapled peptides^{38, 69, 76-86}. Among the strategies that were pursued, the all hydrocarbon “stapled” BH3 helical peptides furnished by ring-closing metathesis (RCM) reaction successfully activated leukemia cell-line apoptosis in animal models³⁸ (**Figure 6A**). This breakthrough discovery expanded the role of α -helical peptides from tool molecules for target validation to potential drug candidates for clinical therapeutics. An all-hydrocarbon stapled peptide ALRN-5281 which is a growth-hormone-releasing hormone agonist entered clinical trials in 2013 for the treatment of rare endocrine disorders⁸⁷.

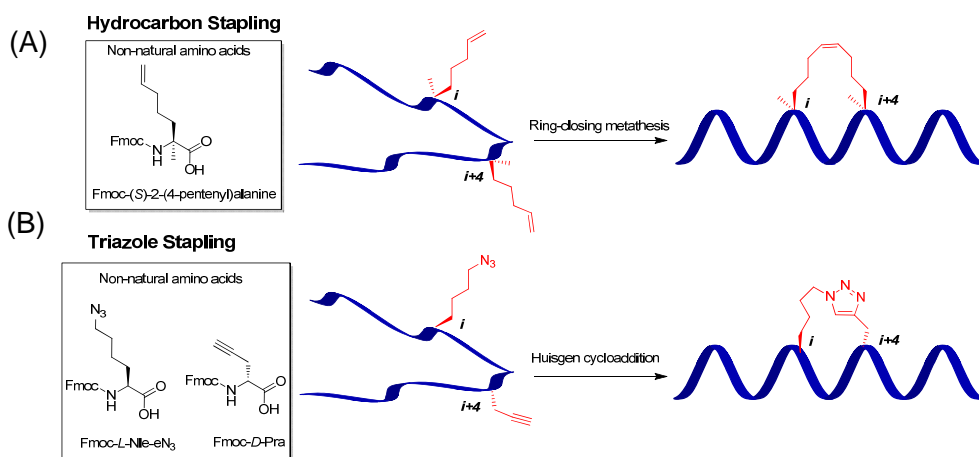


Figure 6 All-hydrocarbon and triazole stapling strategies. (A) Hydrocarbon stapling applies RCM reaction. (B) Triazole stapling uses Huisgen cycloaddition (click chemistry).

Another stapling strategy using Huisgen cycloaddition (click chemistry) yielded a triazole-stapled BCL9 peptide in our laboratory in 2012 (**Figure 6B**)⁸⁶. The investigation suggested that the triazole-stapled peptide had improved binding affinity, enzymatic stability and helical propensity in biochemical assays. To further explore the application

of triazole-stapled peptides in cell-based assays, we employed the triazole-stapling strategy described in this study to develop a potent and cell-permeable TRF2 peptide as an inhibitor of RAP1/TRF2.

2.2 Design and synthesis of high-affinity stapled peptides binding to RAP1.

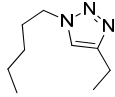
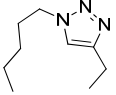
2.2.1 Design and optimization of tracers for fluorescence polarization assay.

The fluorescence polarization (FP) assay is widely used in testing the binding affinities of ligands that block protein-protein interactions⁸⁸. A tracer molecule attached to a fluorescein can be excited by polarized light. When the tracer binds to a protein, the molecule absorbs energy and emits polarized fluorescence as if it is in a stationary state. As long as there are unlabeled ligands binding competitively with the tracer, the energy level emitted would be decreased as more tracer molecules are free in solution⁸⁹. To establish an FP assay targeting RAP1/TRF2 interaction, a tracer molecule that binds to target protein RAP1 must be designed and synthesized.

Wild-type 16-residue TRF2 peptides were labeled with 5-carboxyfluorescein (5-FAM) at either the N-terminus or the C-terminus using two β -alanine molecules as a spacer (**Table 1**). Our saturation experiments showed that the tracer labeled at the C-terminus has a K_d value of 0.3 μ M, 7-times better than the tracer labeled at the N-terminus. Thus, we developed a competitive FP assay using the tracer labeled at the C-terminus (**cF**) for initial binding experiments, but further optimized the assay by using a more potent stapled peptide subsequently labeled with FAM (**14TnF**, $K_d=11$ nM).

As shown in **Table 1**, the K_d values of **14TnF** and **14TcF** are comparable while **nF** and **cF** have a 7-fold difference. One of the possible explanations is that labeling fluorescein at C-terminus might have a stronger α -helix induction effect than fluorescein at the N-terminus for unstapled peptides, as it was linked directly to the α -helical portion, and this effect gets weaker as the conformation of **14TnF** and **14TcF** are stabilized by staples.

Table 1 Sequence and K_d value of tracers binding to RAP1 protein.

ID	Sequence	K_d (μ M)
nF	FAM- β A- β A-TTIGMMTLKAAFKTLS-NH ₂	2.2
cF	Ac-TTIGMMTLKAAFKTLS- β A- β A-K(FAM)-NH ₂	0.3
14TnF	 FAM- β A- β A-TTFGMMTLK*AFK [^] LS-NH ₂	0.011
14TcF	 Ac-TTFGMMTLK*AFK [^] LS- β A- β A-K(FAM)-NH ₂	0.011

*L-configuration, ^D-configuration

2.2.2 Truncation study

Before introducing the staple, we firstly determined the minimum sequence that is required for RAP1 interaction. As truncated versions of TRF2 peptides have poor water solubility, a solvent-exposed residue Met286 was mutated to Lys to generate **2**, which binds to RAP1 with a K_i value of 2 μ M, very similar to that of the wild-type (**WT**) peptide (**Table 2**). Truncation of **2** by 1-2 residues from either N or C-terminus gave **9-12** with weaker or abolished binding affinity to RAP1. These data thus suggest that 16 residues are necessary for achieving good binding affinity.

Table 2 Binding affinities of truncated TRF2 peptides to RAP1.

ID	Sequence	K _i (μM)
WT	Ac-TTIGM M TLKAAF T LS-NH ₂	2.0±0.1
2	Ac-TTIGM M K TLKAAF T LS-NH ₂	1.8±0.1
9	Ac-TTIGM M K TLKAAF T L-NH ₂	5.8±0.1
11	Ac-TTIGM M K TLKAAF T -NH ₂	No Binding
12	Ac-TIGM M K TLKAAF T L-NH ₂	19.5±0.9
10	Ac-IGM M K TLKAAF T L-NH ₂	39.1±0.4

2.2.3 Triazole stapling

Triazole-stapled peptides were furnished by Huisgen 1,3-dipolar cycloaddition reaction, also called “click chemistry”. In our study on BCL9 peptides⁸⁶, two non-natural amino acids norleucine-εN₃ (Nle-εN₃) and propargylglycine (Pra) were inserted at the *i* and *i*+4 residues respectively (**Figure 6B**), with Nle-εN₃ adopting an *L*-configuration and Pra adopting either the *L* or *D*-configuration. *L*-Nle-εN₃ was prepared from Fmoc-protected lysine using the reported method⁹⁰.

To determine the location of these stapling residues, a lysine screening was performed on “solvent-exposed” residues Met285, Met286, Ala290 and Thr294 to examine the tolerance for a long side chain in these positions (**Figure 5C, Table 3**). Our binding data show that **1** (M285K) decreases binding affinity to 10-fold, while **2-4** all bind to RAP1 at a level comparable to that of **WT**. Based on these data, Met286, Ala290 and Thr294 were selected as residues to be replaced by *L*-Nle-εN₃ and Pra. The other two non-interacting residues, Lys289 and Lys293 were kept in the sequence for reasons related to solubility.

Table 3 Binding affinities of peptides mutated at solvent-exposed residues.

ID	Sequence	IC ₅₀ (μM)	K _i (μM)
WT	Ac-TTIGM ²⁸⁶ MTLKA ²⁹⁰ AFK ²⁹⁴ TLS-NH ₂	7.4	2.0±0.1
1	Ac-TTIG ^K MTLKA ²⁹⁰ AFK ²⁹⁴ TLS-NH ₂	53.8	19.6
2	Ac-TTIGM ^K TLKA ²⁹⁰ AFK ²⁹⁴ TLS-NH ₂	6.5	2.2
3	Ac-TTIGM ²⁸⁶ MTL ^K KA ²⁹⁰ AFK ²⁹⁴ TLS-NH ₂	11.3	4.0
4	Ac-TTIGM ²⁸⁶ MTLKA ²⁹⁰ AF ^K LS-NH ₂	5.9	2.0

Table 4 Binding affinities of stapled peptides and unstapled precursors.

Ac-TTIGM ²⁸⁶ MTLKA ²⁹⁰ AFK ²⁹⁴ LS-NH ₂					
ID	Met286	Ala290	Thr294	IC ₅₀ (μM)	K _i (μM)
WT	Met	Ala	Thr	7.4	2.6
5 5T^a	<i>L</i> -Nle-εN ₃	<i>D</i> -Pra	Thr	137.1	50.2
				43.3	15.7
6 6T	<i>L</i> -Nle-εN ₃	<i>L</i> -Pra	Thr	37.8	13.7
				36.5	13.2
7 7T	Met	<i>L</i> -Nle-εN ₃	<i>D</i> -Pra	>15μM ^b	-
				0.7±0.1	0.14±0.03
8 8T	Met	<i>L</i> -Nle-εN ₃	<i>L</i> -Pra	6.03	2.1
				67.4	24.6

^aT means the triazole-stapled version of the corresponding peptide sequence.

^bNo binding up to 15 μM and precipitated.

L-Nle-εN₃ and Pra (*L* or *D*) were inserted to either Met286-Ala290 or Ala290-Thr294 locations to give four stapled peptides and their unstapled precursors were also prepared (**Table 4**). As predicted, applying *D*-Pra in the sequence gives the much more weakly binding unstapled peptides **5** and **7**. However, their stapled counterparts: **5T** and **7T**, exhibit improved binding affinities. The binding affinity of **7T** for example, was improved from >15 μM to 0.14 μM. Interestingly, *L*-Pra-containing peptides **6** and **8** bind

more potently than the unstapled **5** and **7**, but **6T** and **8T**, failed to show any improvement after being stapled.

To investigate how triazole stapling affects the secondary structure of these peptides and their binding affinities, we selected **5T**, **7T**, **14** and **14T** to test their helical propensity using circular dichroism spectrometry. Since the solubility of unstapled peptide **7** was poor, we used a modified version: **14** with an I283F mutation in the sequence of **7**. As shown in **Figure 7**, the unstapled peptide **14** ($K_i = 18 \mu\text{M}$) adopts a random coil conformation in aqueous solution but after conversion to its stapled form **14T** ($K_i = 0.019 \mu\text{M}$), the α -helical conformation is restored and this results in a 1000-fold improvement in its binding affinity (**Table 5**). In contrast, the stapled **5T**, which fails to improve α -helical population, binds weakly to RAP1 (**Table 4**). In addition to improved helical propensity, the stapled peptides show better solubility than their unstapled counterparts. For example, **7T** dissolves completely in buffer at $100 \mu\text{M}$, while **7** is precipitated at $15 \mu\text{M}$.

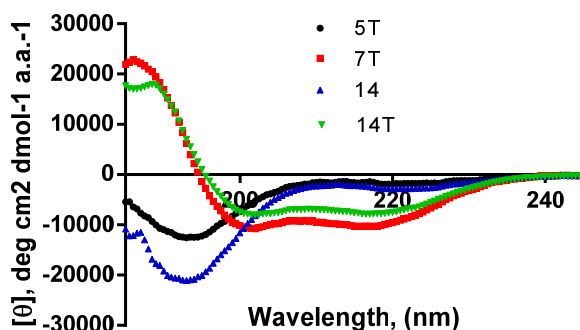


Figure 7 Circular dichroism spectra of selected peptides.

2.2.4 Mutation of interacting residues

In an effort to further enhance the binding affinities, we examined the effect of mutations of hydrophobic residues in the α_1 helix on their interactions with RAP1. Structural analysis showed that Ile283 sits in a large hydrophobic pocket in RAP1 in which a larger hydrophobic group could be tolerated. We modeled a number of compounds containing larger hydrophobic groups to replace Ile283 and showed that replacement of Ile283 with compounds containing Phe or Trp may enhance the interactions of the peptide with RAP1 (**Figure 8**).

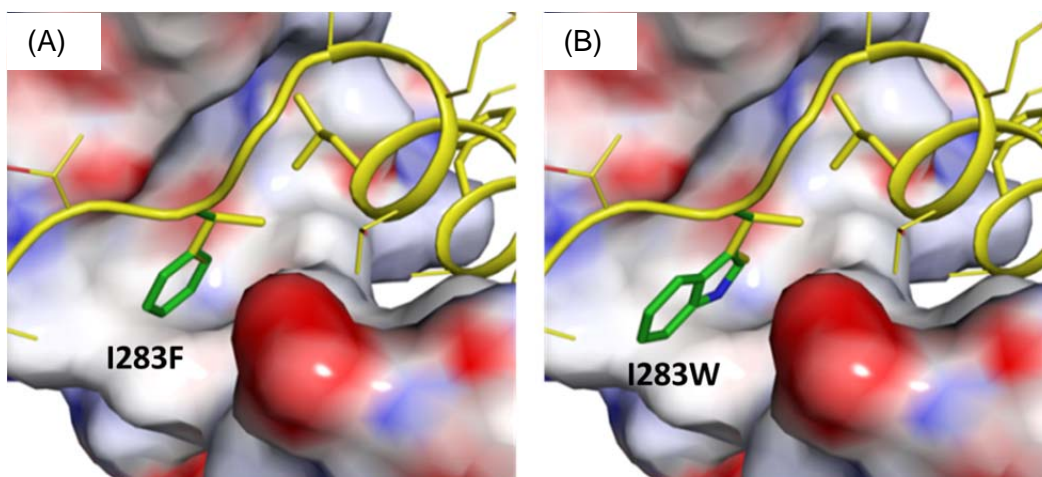
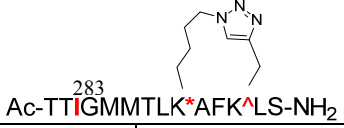


Figure 8 Modeled binding pose of mutated residues: (A) I283F and (B) I283W. TRF2 α_1 (yellow), modeled mutations (green) and RAP1 (surface) are as depicted.

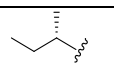
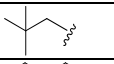
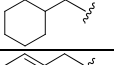
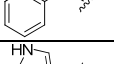
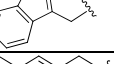
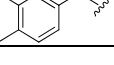
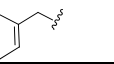
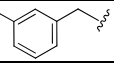
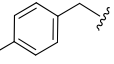
Based on our modeling studies, further modifications were performed using **7T** as a template in which Ile283 was replaced with a larger natural or non-natural amino acid. As shown in **Table 5**, the binding affinities of the resulting peptides improve as the size of the hydrophobic moieties becomes larger (**7T**, **14T**, **16T-18T**). However, **15T** with a Trp residue has an affinity similar to that of **7T** but less than that of **18T** with a naphthyl

group, due perhaps to the polar nitrogen atom which is unfavorable in this hydrophobic environment. As the binding affinities of **14T** and **18T** are in a comparable range, further modifications were made to **14T** by introducing a chlorine substitution in different positions of the Phe283 phenyl group. This yielded **19T**, **20T** and **21T**, and while **20T** and **21T** have a binding affinity similar to that of **14T**, **19T** is three-fold more potent. To understand the structural basis for the improved binding affinity of **19T** over **14T**, we modeled the binding mode of **19T** (**Figure 9**), which shows that the Cl atom in the 2-position of the phenyl ring has additional interactions with the F336 residue of RAP1, which are absent in **14T**, **20T** and **21T**.

Table 5 Binding affinities of stapled peptides with modification at Ile283.



Ac-TTIGMMTLK*AFK^ALS-NH₂

ID	Ile283	IC ₅₀ (μM)	K _i (μM)
7T		0.696	0.14±0.03
17T		0.276	0.053±0.0110
16T		0.182	0.032±0.004
14T		0.121	0.019±0.030
15T		0.614	0.13±0.05
18T		0.104	0.016
19T		0.065	0.007±0.001
20T		0.118	0.019±0.001
21T		0.134	0.022±0.001

*L-configuration, ^D-configuration

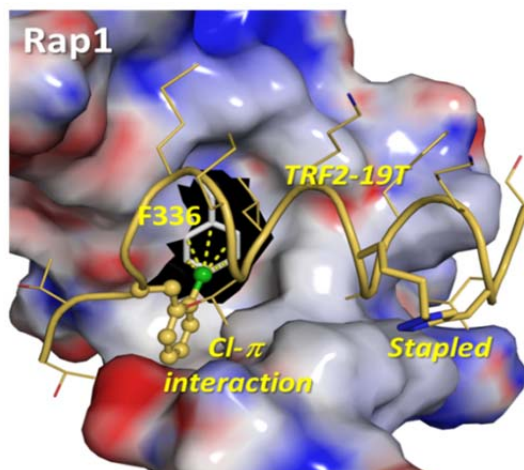


Figure 9 Binding model of **19T** to RAP1. TRF2 α_1 (yellow), the chloride atom (green), Cl- π interaction (dashed lines), F336 from RAP1 (grey stick) and RAP1 (surface) are as depicted.

Table 6 Contribution of stapling and Ile283 modification to the K_i .

Ac-TT²⁸³IGMMTLK²⁹⁰AAFK²⁹⁴LS-NH₂

ID	Ile283	Ala 290	Thr294	K_i (μ M)	Fold improved v.s WT
WT	Ile	Ala	Thr	2.6	1
22	2Cl-Phe			0.26	10.0
7T	Ile	Triazole stapled		0.14 \pm 0.03	18.6
19T	2Cl-Phe			0.007 \pm 0.001	371.4
14T	Phe			0.019 \pm 0.030	136.8

The unstapled peptide **22** with mutation at Ile283 was also synthesized in order to evaluate the individual contributions of stapling and mutation to potency. As shown in **Table 6**, the “mutation only” peptide **22** binds to RAP1 with a K_i value of 0.26 μ M, while the “staple only” peptide **7T** binds to RAP1 with a K_i value of 0.14 μ M, indicating that using mutation or stapling alone gave 10-20 fold improvement of binding affinity over that of the wild-type peptide (**WT**). Combination of stapling and mutation leads to

400-fold improvement in binding compared to the **WT**, suggesting a cooperative effect of stapling and mutation. Another potent peptide, **14T** is about 150-times more potent than **WT**, and since preliminary cellular tests using the WST assay showed that **14T** dose-dependently inhibits growth of the MDA-MB-231 breast cancer cell line while **19T** was much weaker (data not shown), we finally chose **14T** for additional investigations.

2.2.5 Improvement of water solubility

Since this peptide is largely hydrophobic and precipitates were observed in 100 μM cell cultures, we next sought to improve its solubility. To this end, we introduced a hydrophilic group: 3-(4-methylpiperazin-1-yl)propanoic acid, to the N-terminus of **14T** using two β -Ala residues as a spacer. This gave **14TnPip** (**Figure 10**) which dissolves in cell culture at 300 μM without visible precipitation, and binds to RAP1 with a K_i value of 10 nM. To further address the specificity issue, an inactive control molecule **14TnPip (-)** was made by using the D-isoform of Phe283 on **14TnPip**. Competitive binding experiments showed that this control molecule was about 100-fold less potent than **14TnPip** in binding to RAP1.

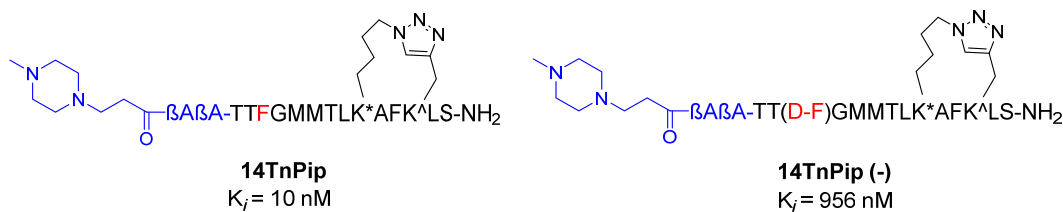


Figure 10 Structures and RAP1 binding affinities of optimized stapled peptides for cellular studies. **L*-configuration, ^*D*-configuration.

2.3 Stapled peptide down-regulates NF- κ B activation and inhibits cell growth in breast cancer cell lines.

2.3.1 Stapled peptide down-regulates NF- κ B activation in HeLa and MDA-MB-157 cell-lines.

Teo *et. al.*⁶⁷ have shown that knock-down of RAP1 by RNA_i down-regulates the level of phosphorylated p65 (P-p65) within 60 minutes in the HeLa cell line and several breast cancer cell lines. We analyzed the effect of **14TnPip** and **14TnPip(-)** to see if they have similar effects in the same cell lines. As shown in **Figure 11**, **14TnPip** dose-dependently down-regulates P-p65 level while the control molecule has no significant effect at 300 μ M, the highest concentration tested. Similar data were obtained using the MDA-MB-157 breast cancer cell line. Taken together, these data indicate that the stapled peptide penetrates the cell-membrane and inhibits p65 phosphorylation.

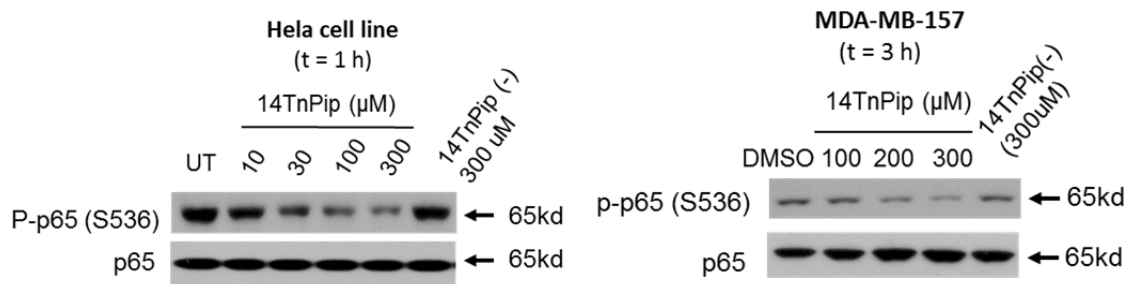


Figure 11 Stapled peptide down-regulates NF- κ B activation in cell.

2.3.2 Cell growth inhibition by the stapled peptides.

As knocking-down RAP1 also sensitizes cancer cell lines to apoptosis⁶⁷, we tested our stapled peptides in a cell-growth inhibition assay using the same cell lines that were discussed above.

In our evaluation, **14TnPip** was found to be able to dose-dependently inhibit proliferation of the MDA-MB-157 and the HeLa cell lines, while the control peptide **14TnPip (-)** is only effective at its highest concentration (**Figure 12A**). When comparing the cell survival rate in both cell lines treated at 100 μM , significant differences were observed between the active and control molecules (**Figure 12B**), suggesting at least some specificity for these molecules.

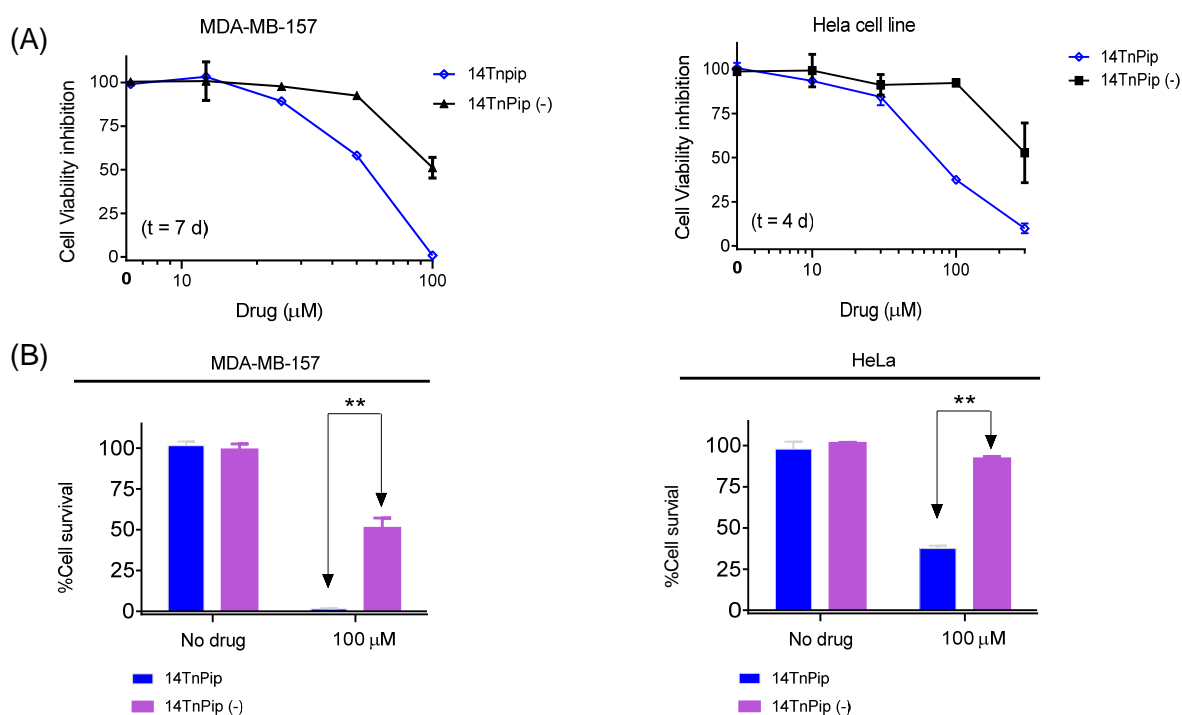


Figure 12 Cell growth inhibition of **14TnPip** and **14TnPip(-)** in MDA-MB-157 and HeLa cell lines. (A) Dose-dependent curves. (B) Histograms showing cell survival rate at 0 or 100 μM concentrations.

2.4 Summary and discussion

Our design of stapled-peptide inhibitors of RAP1 starts with the co-crystal structure of RAP1 RCT domain complexed with the RBM domain of TRF2. Review of

the structure suggests that a 16mer peptide from TRF2 may serve as a template for the design of peptide-based inhibitors of the RAP1/TRF2 protein-protein interaction. We first designed and developed a fluorescence polarization assay by synthesis of a fluorescent tagged TRF2 peptide. A truncation study established that the 16-residues from TRF2 are the minimum sequence associated with good affinity to RAP1. Lysine screening identified the potential stapling sites. Triazole stapling based upon the wild-type TRF2 sequence yielded **7T** as the most potent peptide, 18-fold more potent than the wild-type peptide. Further modifications of Ile283, replacing it with larger natural or non-natural hydrophobic residues resulted in a number of potent stapled peptides, such as **14T** and **19T**, which bind to RAP1 at 19 nM and 7 nM, respectively. To address the solubility issue concerning these peptides, we synthesized a new analogue of **14T** by attaching a soluble group to its N-terminus through a spacer, yielding **14TnPip**. We also synthesized a control molecule for **14TnPip** by replacing the natural *L*-isoform of Phe283 with a *D*-isoform, resulting in **14TnPip(-)**. Testing of **14TnPip** and **14TnPip(-)** revealed that **14TnPip** dose-dependently down regulates p65 phosphorylation in two cancer cell lines, **14TnPip(-)** being less potent.

In the RAP1 binding assay, **14TnPip** is 100 times more potent than **14TnPip(-)**. However, in the cell growth assay, **14TnPip(-)** is just few fold weaker than **14TnPip**, which suggests there might be some nonspecific effect for the control molecule. As the N-methyl-piperazine moiety is considered to be cytotoxic in some cases, conversion of this group to morpholinyl could be a solution.

Even though the **14TnPip** peptide binds to RAP1 at 10 nM of K_i , its activity in down-regulation of P-p65 (S536) is in the 100 μ M range. The 10000-fold difference may be due to its poor cell-permeability and/or the protease stability of the peptides. Our subsequent evaluations showed that the stapled peptides had $t_{1/2} < 2$ hours in a trypsin digestion assay (**Figure 13**). In order to find a more potent molecule for cellular mechanism study or ultimately for drug development, these two issues have to be addressed.

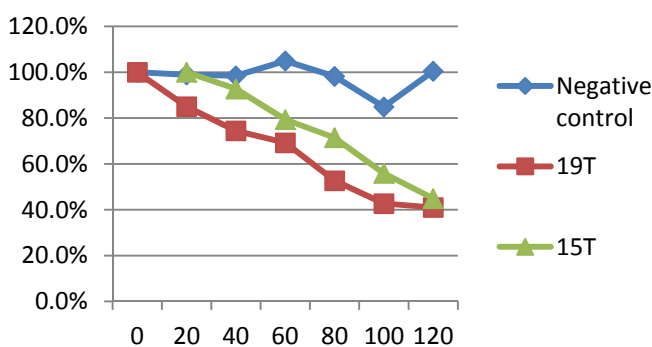


Figure 13 Trypsin digestion assay using Ac-ARA-NH₂ as negative control.

2.5 Future directions

2.5.1 Further modification of peptide-based α -helix mimetics.

Peptide-based α -helix mimetics are also referred to as Type I mimetics³⁰ which include side chain cyclized “stapled” peptides, intramolecular hydrogen bond surrogates, and β or α/β mixed peptide foldamers⁹¹ (**Figure 14**).

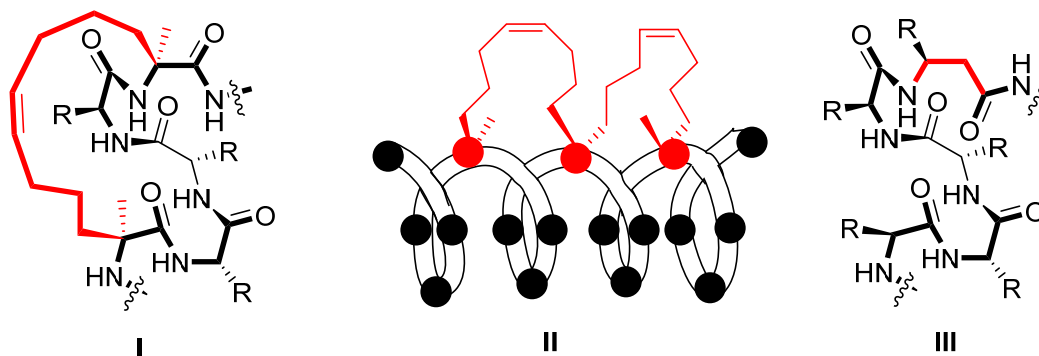


Figure 14 Proposed modification strategies to improve cellular activity (Type I mimetics). All-hydrocarbon stapling (**I**), double stapled stitched peptide (**II**), α/β mixed foldamer (**III**).

These modifications have already seen success in improving enzymatic stability as well as intramolecular activities in a number of cases^{38, 72, 74, 92-94}, especially for the all-hydrocarbon stapled peptide (**I**) which shows *in vivo* activity against cancer³⁸. Comparing the stapling strategies, it is noteworthy that same sequence with different side chain linkers could provide distinct performances in cellular assays^{92, 95}. Thus, replacing the 1,2,3-triazole linker with the all hydrocarbon linker could improve the cellular activity of TRF2 peptides. In addition to the single staple approach, a second cycle could be inserted. This creates a “stitched peptide”⁸⁵ which tends to have a higher α -helical population and reduced exposure of amide bonds for digestion (**II**).

Aside from changing the side chain triazole linker, modification on the backbone by using α/β mixed amino acids (**III**) has been reported to improve the stability to proteolysis of the Puma BH3 peptide⁹⁴. β amino acids alter the enzymatic recognition

motif on the backbone, making the peptide more stable and pharmacodynamically favorable³⁰.

2.5.2 Non-peptide α -helix mimetics.

Non-peptide α -helix mimetics could behave as drug-like small molecules (Type II mimetics) or synthetic molecules that mimic the spatial orientations of the side chain residues (Type III mimetics)³⁰.

For the design of small molecule PPI inhibitors, we can take advantage of the high affinity fluorescent polarization assay and perform high throughput screening with virtual screening effort as a filter for this hydrophobic target. Optimization of the hit by medicinal chemistry efforts could give a small molecule inhibitor with similar binding affinity to that of the peptide but with a more potent activity in cell or animal experiments. If the HTS results are not informative with respect to further modification, another screening approach, a fragment-based screening could be applied using advantages in exploring chemical spaces in PPI interfaces that are large, flat and hydrophobic.

Besides design of small molecules for various PPI interfaces, application of Type III mimetics (**Figure 15**)⁹⁶⁻⁹⁸ is a cheaper and broadly applicable strategy. The interacting side chains i , $i+4$, $i+7$ can be directly installed onto the template at appropriate sites, and this gives these templates an application that is broader than that of the small molecules. In the case of TRF2, there are two combinations: Thr285-Ala289-Leu295 and Leu288-Phe292-Ser296. These two faces can be embedded into a template to make two molecules, both of which should be attached with the N-terminal loop region. If molecules bearing

these features have useful binding affinity to RAP1, further modifications can be made to make the molecule more drug-like.

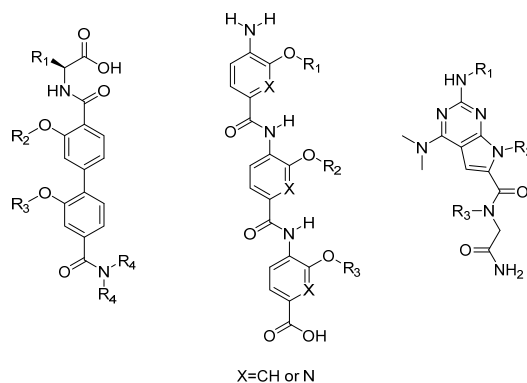


Figure 15 Selected non-peptide proteomimetic scaffolds (Type III mimetics).

2.6 Experiments

2.6.1 Peptide synthesis

All the peptides were synthesized using Fmoc solid phase peptide synthesis (SPPS) strategy using an ABI 433A peptide synthesizer. The conditions regarding synthesis and purification followed previously reported methods⁸⁶.

2.6.2 Fluorescence polarization assay

Competitive FP binding assays were designed and optimized to determine the binding affinities of synthesized peptides to the RAP1 protein. A fluorescent probe (**cF** or **14TnF**) was designed and synthesized by tethering FAM to the C terminal of a stapled TRF2 peptide which binds to RAP1 with high affinity, as determined by preliminary experiments.

The K_d value of the tracer to RAP1 protein was determined by monitoring the total fluorescence polarization of mixtures having the fluorescent probe at a fixed concentration and proteins at increasing concentrations up to full saturation. Fluorescence polarization values were measured using the Infinite M-1000 plate reader (Tecan U.S., Research Triangle Park, NC) in Microfluor 1 96-well, black, round-bottom plates (Thermo Scientific). Serial dilutions of the protein being tested were mixed with the tracer to a final volume of 125 μ l in the assay buffer (100mM potassium phosphate, pH 7.5, 100 μ g/ml bovine γ -globulin, 0.02% sodium azide, Invitrogen, with 0.01% Triton X-100 and 4% DMSO). The final tracer concentration was 2 nM. Plates were incubated at room temperature for 1-2 hours with gentle shaking to assure equilibrium. The polarization values in millipolarization units (mP) were measured at an excitation wavelength of 485 nm and an emission wavelength of 530 nm. Equilibrium dissociation constants (K_d) were then calculated by fitting the sigmoidal dose-dependent FP increases as a function of protein concentrations using Graphpad Prism 5.0 software (Graphpad Software, San Diego, CA). The influence of DMSO, detergent and incubation time was evaluated to determine the optimal conditions under which the K_d value showed minimal variation.

The IC_{50} and K_i values of compounds were determined through a compound dose-dependent competitive binding experiment in which serial dilutions of compounds competed against a fixed concentration of the fluorescent probe for binding to the protein with a fixed concentration (typically 2 to 3 times the K_d values determined above). Mixtures of 5 μ l of the tested compounds in DMSO and 78 μ l of preincubated

protein/probe complex solution in the assay buffer (100mM potassium phosphate, pH 7.5, 100 μ g/ml bovine γ -globulin, 0.02% sodium azide, Invitrogen with 0.01% Triton X-100) were added into assay plates and incubated at room temperature for 1 hour with gentle shaking. Final concentrations of the protein and probe were 40 nM and 2 nM, respectively. Negative controls containing protein/probe complex only (equivalent to 0% inhibition), and positive controls containing only free probes (equivalent to 100% inhibition), were included in each assay plate. FP values were measured as described above. IC₅₀ values were determined by nonlinear regression fitting of the competition curves. The K_i values of competitive inhibitors were calculated using the derived equation described previously, based upon the measured IC₅₀ values, the K_d value of the probe to the protein, and the concentrations of the protein probes in the competitive assays^{99, 100}.

2.6.3 Circular Dichroism

Circular Dichroism experiments were performed using a Jasco J715 spectropolarimeter. Peptides were dissolved in 10 mM phosphate buffer (pH = 7.4) to produce a \sim 100 μ M solution. Spectrum generation and percentage helicity calculation were performed using the same method in the previous study^{86, 101}.

2.6.4 Proteolytic stability assays

In a 12-well plate, peptide (100 μ M) and tryptophan (100 μ M) as an internal label, were co-incubated in presence of trypsin (5 nM) for two hours. Samples were collected at 20, 40, 60, 80, 100, 120 mins time points, quenched with 20% TFA aqueous solution to

make a 50 μ M sample solution which was centrifuged at 13,000 rpm for 5 minutes before being analyzed by HPLC (Method: 20%-50% MeCN in 30 mins). The AUC of peptide peaks were calculated and the percentage remaining was plotted as is shown in **Figure 13**.

2.6.5 Molecular modeling

Based on the crystal structure between RAP1 and TRF2 (PDBID: 3K6G)¹⁰² the chemical linkage between A290 and T294 with different D- and L- conformations were built using MOE program. The designed peptides were minimized to assess the potential clash of the linker with RAP1 and the conformational deviation of the helix from the crystal structure of the unstapled TRF2 peptide. The model structure with least conformational deviation from the wild type peptide was correlated with the highest binding affinity determined from the biochemical assay. The same method was used to model the binding pose of **19T** and gave the modeled structure shown in **Figure 9**.

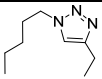
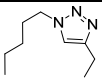
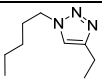
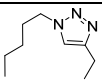
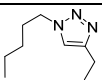
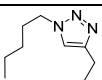
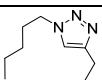
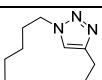
2.6.6 Cellular assays

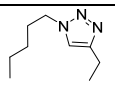
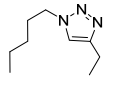
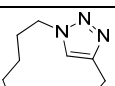
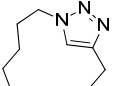
The cell growth inhibition and western-blot analysis followed a similar method reported previously¹⁰³.

Appendix

Structures of TRF2 peptides

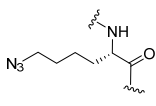
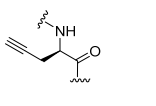
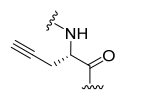
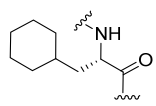
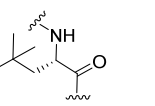
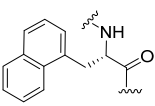
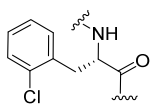
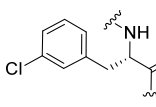
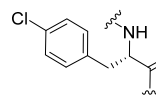
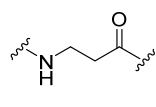
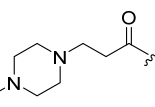
ID	Sequence	m/z $[M+2H]^{2+}/2$ (detected)
WT	Ac-TTIGMRTLKAAFKTLS-NH ₂	878.27
1	Ac-TTIG K MTLKAAFKTLS-NH ₂	876.80
2	Ac-TTIG MK TLKAAFKTLS-NH ₂	876.36
3	Ac-TTIGMRTL K AAFKTLS-NH ₂	906.72
4	Ac-TTIGMRTLKAAF K LS-NH ₂	891.36
5	Ac-TTIGM(L-Nle-εN ₃)TLK(D-Pra)AFKTLS-NH ₂	901.92
5T	 Ac-TTIGM*TLK^AFKTLS-NH ₂	901.92
6	Ac-TTIGM(L-Nle-εN ₃)TLK(L-Pra)AFKTLS-NH ₂	901.90
6T	 Ac-TTIGM*TLK*AFKTLS-NH ₂	901.90
7	Ac-TTIGMRTLK(L-Nle-εN ₃)AFK(D-Pra)LS-NH ₂	916.92
7T	 Ac-TTIGMRTLK*AFK^LS-NH ₂	916.92
8	Ac-TTIGMRTLK(L-Nle-εN ₃)AFK(L-Pra)LS-NH ₂	916.88
8T	 Ac-TTIGMRTLK*AFK*LS-NH ₂	916.84
9	Ac-TTIGMRTLKAAFCTL-NH ₂	834.06
10	Ac-IGMRTLKAAFCTL-NH ₂	731.86
11	Ac-TTIGMRTLKAAFCT-NH ₂	776.46

12	Ac-TIGMRTLKAAF KTL-NH_2	782.34
14	Ac-TT F GMMTLK(L-Nle- ϵN_3)AFK(D-Pra)LS-NH ₂	933.84
14T	 Ac-TT F GMMTLK*AFK^LS-NH ₂	933.84
15	Ac-TT W GMMTLK(L-Nle- ϵN_3)AFK(D-Pra)LS-NH ₂	953.30
15T	 Ac-TT W GMMTLK*AFK^LS-NH ₂	953.42
16	Ac-TT Cha GMMTLK(L-Nle- ϵN_3)AFK(D-Pra)LS-NH ₂	936.78
16T	 Ac-TT Cha GMMTLK*AFK^LS-NH ₂	936.82
17	Ac-TT Tal GMMTLK(L-Nle- ϵN_3)AFK(D-Pra)LS-NH ₂	923.72
17T	 Ac-TT Tal GMMTLK*AFK^LS-NH ₂	923.44
18	Ac-TT(1-Nal)GMMTLK(L-Nle- ϵN_3)AFK(D-Pra)LS-NH ₂	958.82
18T	 Ac-TT(1-Nal)GMMTLK*AFK^LS-NH ₂	958.86
19	Ac-TT(2Cl F)GMMTLK(L-Nle- ϵN_3)AFK(D-Pra)LS-NH ₂	951.22
19T	 Ac-TT(2Cl F)GMMTLK*AFK^LS-NH ₂	950.74
20	Ac-TT(3Cl F)GMMTLK(L-Nle- ϵN_3)AFK(D-Pra)LS-NH ₂	950.86
20T	 Ac-TT(3Cl F)GMMTLK*AFK^LS-NH ₂	951.32
21	Ac-TT(4Cl F)GMMTLK(L-Nle- ϵN_3)AFK(D-Pra)LS-NH ₂	951.24
21T	 Ac-TT(3Cl F)GMMTLK*AFK^LS-NH ₂	950.76

22	Ac-TT(2Cl F)GMMTLKAAFKTLS-NH ₂	913.56
14TnPip (+)	 Pip-βA βA-TTFGMMTLK*AFK^LS-NH ₂	1062.54
14TnPip (-)	 Pip-βA βA-TT(^F)GMMTLK*AFK^LS-NH ₂	1061.67
nF	FAM-βA-βA-TTIGMMTLKAAFKTLS-NH ₂	1107.80
cF	Ac-TTIGMMTLKAAFKTLS-βA-βA-K(FAM)-NH ₂	1193.07
14TnF	 FAM-βA-βA-TTFGMMTLK*AFK^LS-NH ₂	1162.89
14TcF	 Ac-TTFGMMTLK*AFK^LS-βA-βA-K(FAM)-NH ₂	1247.84

*L-configuration ^D-congiguration.

Abbreviations:

<i>L</i> -Nle-εN ₃ 	<i>D</i> -Pra 	<i>L</i> -Pra 	Cha 	Tal 	1-Nal 
2Cl F 	3Cl F 	4Cl F 	βA 	Pip 	

CHAPTER 3

Structure-based design and synthesis of novel small-molecular inhibitors targeting BET bromodomains.

3.1 Introduction

3.1.1 Epigenetic histone modifications

Epigenetics is the study of heritable changes in gene expression in the absence of alterations to the nucleoside sequence¹⁰⁴. The molecular mechanisms of epigenetics include DNA methylation and histone modifications including methylation and acetylation, which are among the most frequently observed. These modifications alter the interaction between histone and DNA or other nuclear proteins, control chromatin folding/unfolding, and consequently modulate gene transcription²⁶. A large number of proteins have been found to be involved in histone modifications and a growing number of these have been implicated in human diseases, including cancer, inflammation and neuropsychiatric disorders^{26, 105}.

Targeting proteins that are involved in these processes led to the design and synthesis of a number of small-molecule regulators, some of which have been approved for the treatment of cancer. A number of other compounds are in clinical trials for cancer, inflammation and neuropsychiatric disorders^{26, 105}.

There are three different types of proteins involved in histone modifications. These are termed “writers”, and include histone acetyltransferases (HATs) and histone methyltransferases (HMTs), “erasers” such as histone deacetylases (HDACs) and histone demethylases (HDMs), and “readers” such as acetyl-lysine readers, which include

bromodomain-containing proteins. These writers, erasers and readers work in concert to modulate the chromatin structure and regulate gene expression^{26,105} (**Figure 16**). In this Chapter, we will focus on structure-based design of a new class of small-molecule inhibitors to target the bromodomain and extra-C terminal domain (BET) protein family.

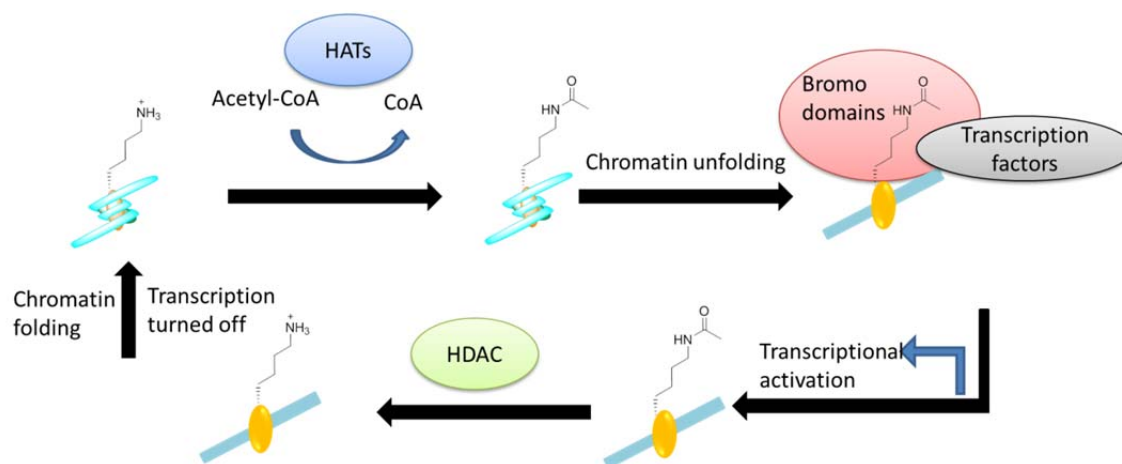


Figure 16 Transcriptional regulations by HATs, bromodomains and HDAC.

3.1.2 Bromodomains as acetylated lysine binding partners

Bromodomains are a group of evolutionarily conserved protein motifs¹⁰⁶ which were initially discovered in the study of *brahma*, a gene required for activation of homeotic genes in *Drosophila*¹⁰⁷. The mechanism by which bromodomains modulate protein-protein interactions was revealed about 12 years ago when 3D structures of bromodomains were determined, and showed direct interaction with acetylated lysines (K-Ac) in histone¹⁰⁸ (**Figure 17**, PDB ID: 3jvk). Structurally, bromodomains adopt a four left-handed helical bundle conformation composed of helices A, B, C and Z. The unstructured loop regions ZA and BC pack against each other and form a hydrophobic

pocket for K-Ac recognition. Despite the length and sequential variation of ZA and BC loops among bromodomain subtypes, the sequence at K-Ac binding site is highly conserved. Normally, an asparagine residue such as Asn140 in BRD4 BD1 will form a hydrogen bond with the oxygen atom of an acetyl carbonyl, while a water-mediated hydrogen bond network was observed to connect the acetyl-lysine with the protein backbone. Beyond the conserved binding motif, variations of residues outside the K-Ac recognition cavity are thought to be important for selectivity¹⁰⁸.

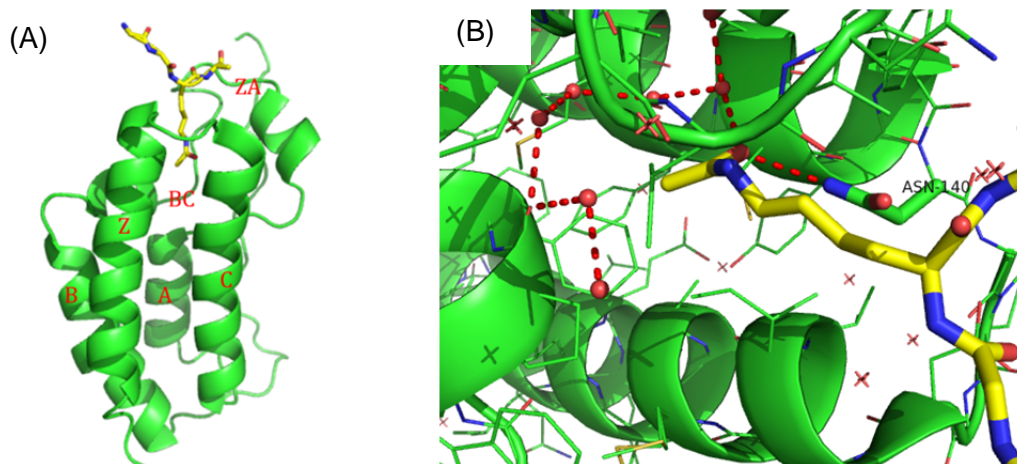


Figure 17 Co-crystal structure of BRD4 BD1 with a K-Ac containing peptide. (A) BRD4 BD1 (green cartoon), K-Ac containing peptide (yellow stick). (B) Detailed interactions at K-Ac recognition site. The K-Ac peptide is shown as yellow sticks with carbon atoms colored in green or yellow, oxygen atoms in red and nitrogen atoms in blue. Water molecules are shown as red spheres and the hydrogen bonds are denoted by cyan dash lines.

3.1.3 Pharmacological significance of BET bromodomains

The Bromodomain and Extra Terminal (BET) proteins (BRD2, BRD3, BRD4, and BRDT) are a group of bromodomain-containing proteins that have been reported to

be involved in a number of pathologically relevant¹⁰⁹ biological events. Small-molecule BET inhibitors contribute to the BET family protein functions as transcriptional activators in cancer¹¹⁰⁻¹¹⁶, inflammation¹¹⁷, HIV infection^{118, 119} and cardiovascular diseases^{116, 118, 119}.

In cancer, the molecular mechanism of BRD4 depends on cellular context of a different subtype. For example, NUT-Midline carcinoma, an aggressive epithelial cancer, is characterized by formation of a fusion protein between the *NUT* coding sequence and BRD3 or BRD4 for oncogenic function¹¹⁰. In hematological malignancies such as MLL-fusion leukemia and acute myeloma, BRD4 transcriptionally activates oncogenes such as *c-MYC* and *BCL2* (**Figure 18**)¹¹⁵. Similarly, inhibition of BET bromodomains in neuroblastomas suppresses *NMYC* transcription¹²⁰. In contrast, the MYC level is independent of BET functions in non-small-cell lung cancer, but it involves modulation of *FOSL1* by BET inhibition¹¹². BRD2-BRD4 proteins also have been shown to interact directly with the androgen receptor (AR) and function as co-activators of AR, and BET inhibition is effective *in vitro* and *in vivo* against castration-resistant prostate cancer¹¹⁴.

BET-dependent transcriptional regulation has also been found in other human diseases and conditions. For example, in inflammation, BRD2-4 is related to lipopolysaccharide (LPS) induced lethal septic shock¹¹⁷. BRD4 is also linked to the regulation of cardiomyocyte hypertrophy that can prevent heart failure^{121, 122}. Further mechanism studies show that BRD4 binds to positive transcription elongation factor (P-TEFb) and regulates Pol II-dependent transcription¹²³. This interaction is also important

in HIV replication because BRD4 competitively binds to P-TEFb with Tat resulting in HIV latency¹¹⁸. Meanwhile, a Tat-independent mechanism was also reported to involve BRD2 as an endogenous regulator of HIV latency¹²⁴. BRD2 has also been reported to be related to metabolism¹²⁵ and lymphomagenesis¹²⁶. Inhibition of a testis specific BET family member BRDT, results in reduction of spermatogenesis and testis volume which offers a new approach to male contraception¹²⁷.

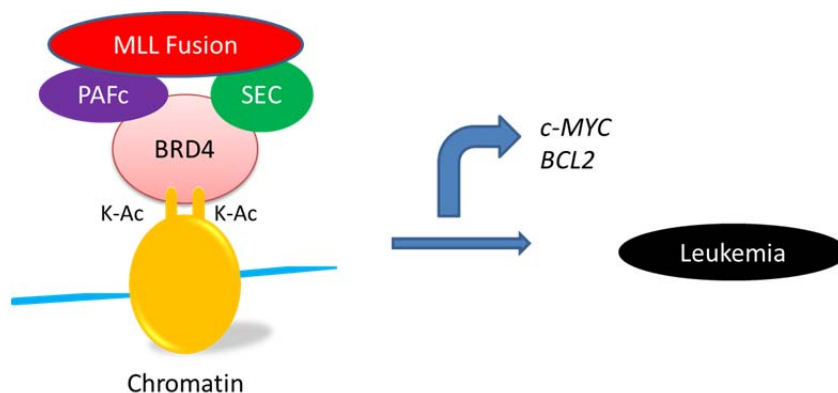


Figure 18 BRD4 transcriptionally activates oncogenes *c-MYC* and *BCL2* family in MLL-fusion leukemia.

3.1.4 Development of BET bromodomain inhibitors for cancer treatment

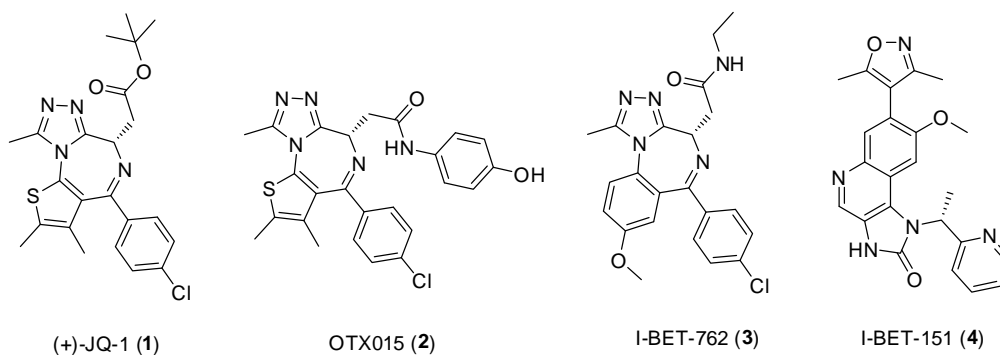


Figure 19 Potent and selective BET bromodomain inhibitors.

Small molecular inhibitors that bind selectively to BET family bromodomain proteins have been reported to be able to down-regulate pathogenic gene transcription, and demonstrate strong *in vivo* activity in animal models, especially in the area of oncology^{110, 112, 114, 115}. In October 2014, there were reported to be six BET bromodomain inhibitors in clinical trials for the treatment of various types of cancer (<https://clinicaltrials.gov>).

Studies of selective BET bromodomain inhibitors in academia started from Bradner's group at the Dana-Farber Cancer Institute¹¹⁰. They synthesized JQ-1 (**Figure 19**), a thienotriazolodiazepine type of compound which had been initially disclosed in a Mitsubishi Tanabe Pharma patent^{128, 129}. JQ-1 has served as a pharmacological tool with which to elucidate the functions of BET family proteins and their pharmacological significance as a class of drug targets^{111-114, 118, 124, 127, 130-135}. In 2012, a Swiss biotech company Oncoethix licensed OTX015¹³⁶, a JQ1 analog discovered by Mitsubishi, and initiated a Phase I clinical trial for the treatment of different forms of human cancer^{137, 138}.

I-BET 762, a benzotriazolodiazepine molecule was discovered by GlaxoSmithKline (*GSK*) via phenotypic and chemoproteomic screenings¹³⁹. This was initially reported as an anti-inflammatory therapeutic agent but it has also shown antitumor effects in other studies¹¹⁷ and it is now in Phase I clinical trials for treatment of NUT-midline carcinoma¹⁴⁰. In addition to I-BET 762, *GSK* also published I-BET 151, a new chemical scaffold featuring dimethylisoxazole as an acetyl-lysine mimetic (**Figure**

19) This molecule showed significant improvement in plasma exposure compared to JQ1 and I-BET 762, and effectively prolonged survival in a MLL-fusion leukemia model¹¹⁵.

Other BET inhibitors in clinical trial for cancer treatment are TEN-010 and CPI-0610 (structures not disclosed). TEN-010 is now in clinical trials for treatment of solid tumors while CPI-0610 has three clinical trials ongoing mainly addressing hematological malignances¹⁴¹⁻¹⁴⁴.

Despite the fact that there is already more than one candidate in this area, it is well known that different chemical moieties with the same therapeutic target may demonstrate different toxicity and pharmacokinetic profiles which result in different clinical applications. Therefore, we have designed and synthesized several γ -carboline-containing compounds as a new class of potent small-molecule BET inhibitors.

3.2 Structure-based design of novel BET bromodomain inhibitors.

We undertook the design of new BET bromodomain inhibitors based on the 3D co-crystal structure of **4** (I-BET 151) with BRD4 BD1 (**Figure 20A**). The interaction of **4** with the BRD4 BD1 protein can be divided into three regions: the dimethylisoxazole “head” mimics the acetyl-amine, which forms a direct or water-bridged hydrogen bonding network with the Asn140 and Tyr97 residues of BRD4 BD1 in the K-Ac recognition pocket; the “body”, a [6,6,5] tricyclic ring system, which serves as the acetyl-lysine side chain that interacts with the channel; and the “tail”, a pyridyl group which interacts with “WPF shelf”, a hydrophobic pocket outside the K-Ac binding cavity, which is conserved in bromodomain proteins of the BET subfamily¹³⁹. Since **4** also binds to

BRD4 BD2 with a high affinity¹⁴⁵, we also modeled the binding mode of **4** complexed with BRD4 BD2 and found that the binding pose is similar to that observed with BRD4 BD1 (**Figure 20B**).

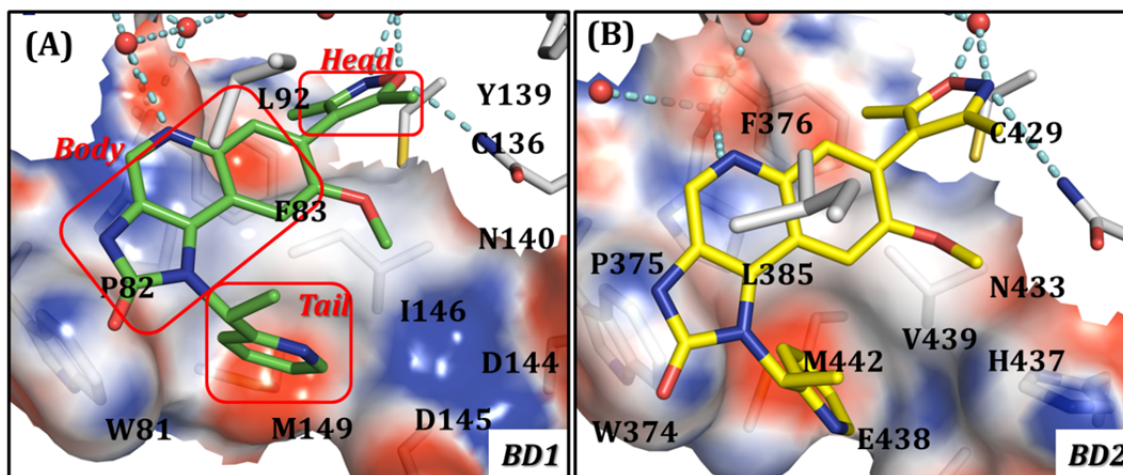


Figure 20 Co-crystal and modeled structures of I-BET 151 (**4**). (A) Co-crystal structure of **4** with BRD4 BD1. (B) Modeled structure of **4** with BRD4 BD2. Compound **4** is shown in stick form with carbon atoms colored in green or yellow, oxygen atoms in red and nitrogen atoms in blue. Electrostatic potential is mapped to the surface of BRD4 BD1 and BD2 proteins where blue, red, grey correspond to positive, negative and neutral charged regions, respectively. Water molecules are shown as red spheres and the hydrogen bonds are denoted by cyan dash lines.

The design of a new class of BET inhibitors started by replacing the [6,6,5]-tricyclic “body” of **4** with a [6,5,6] γ -carboline system. The electron statistics of the two tricyclic systems was mapped in **Figure 21C**, which suggests that both of the structures are conjugated systems with similar shape and electron distribution, and a major difference at the central amine which was converted from an H-bond acceptor to an H-bond donor. Based on this observation, new and potent BET bromodomain inhibitors (RX series) can be discovered by employing the γ -carboline structure and performing

structure-activity relationship (SAR) study using different “head” and “tail” groups
(Figure 21A).

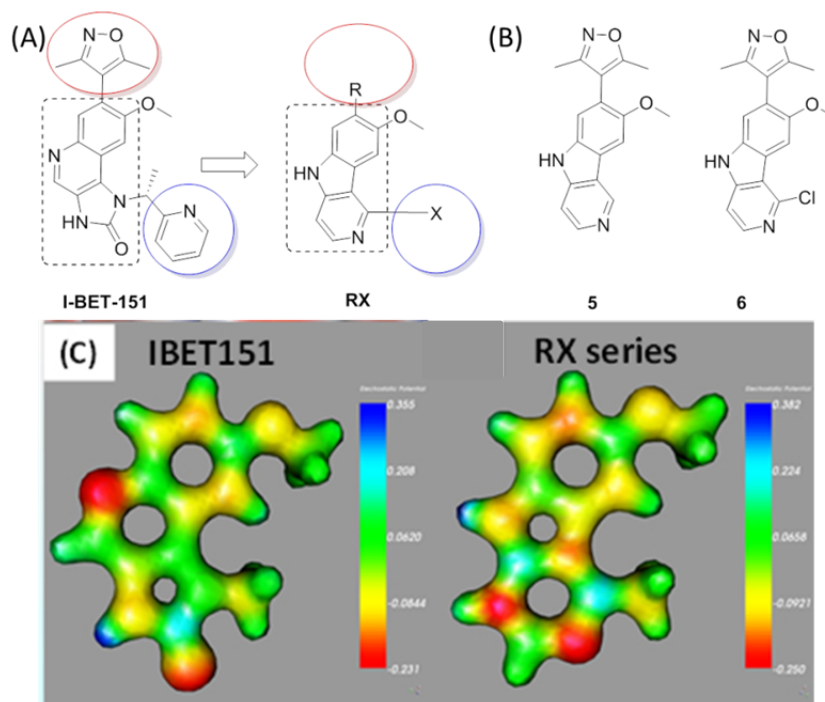


Figure 21 Design of γ -carboline core structure. (A) Conversion from I-BET-151 to RX series with R and X representing the “head” or “tail” group. (B) Structures of new RX series compounds **5** and **6**. (C) Electrostatic potential mapped to the I-BET151 and RX series core fragments.

To test this design idea, two molecules bearing γ -carboline were first synthesized, employing dimethylisoxazole as the “head”, and with either an H (**5**) or a Cl (**6**) atom at the “tail” (Figure 21B). Modeling showed that **5** adopts a binding mode similar to that of the “head” and “body” parts of **4**, but misses a fragment which interacts with the hydrophobic WPF shelf (Figure 22). Binding affinities of **5** and **6** to the two domains of BRD4 were obtained using a Fluorescence Polarization assay. The data showed that **5**

binds to BD1 at 1644 nM, and BD2 at 824 nM; while **6** binds to BD1 at 305 nM, BD2 at 194 nM, respectively (**Table 7**). Although both compounds **5** and **6** are weaker than **4**, we viewed these compounds as promising starting points for further optimization since both compounds miss the important “tail” moiety which interacts with the WPF hydrophobic shelf near Met149 (**Figure 22A**).

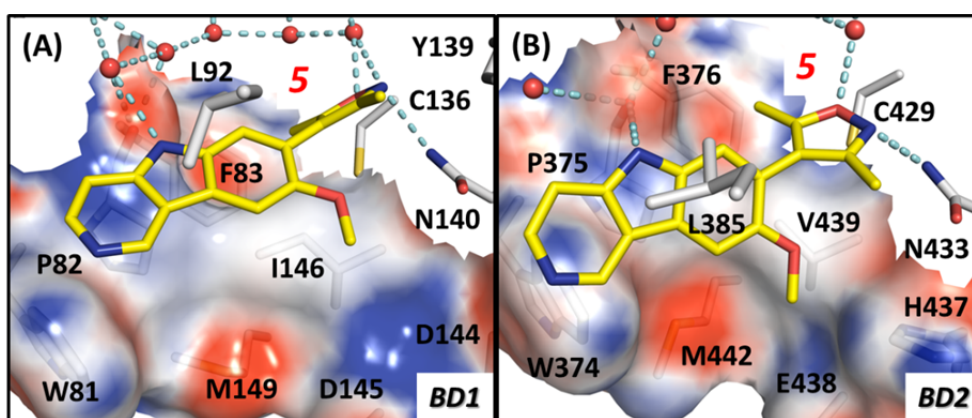


Figure 22 Modeled structures of compound **5** (yellow stick) bound to (A) BRD4 BD1 and (B) BRD4 BD2. Compound **5** is shown in stick with carbon atoms colored in yellow, oxygen atoms in red and nitrogen atoms in blue. Electrostatic potential is mapped to the surface of BRD4 BD1 and BD2 proteins where blue, red, grey correspond to positive, negative and neutral charged regions. Water molecules are shown as red spheres and the hydrogen bonds are denoted by cyan dash lines.

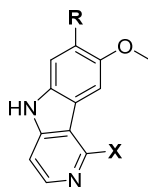
3.3 Structure activity relationship studies of the new class of BET bromodomain inhibitors.

We next performed SAR studies based upon compounds **5** and **6** with the goal of further improving the binding affinities to the BET proteins.

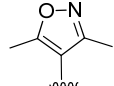
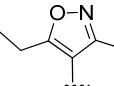
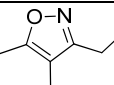
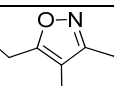
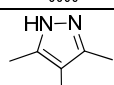
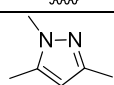
3.3.1 SAR of “head” groups

Replacing R group with other isoxazoles or pyrazoles gave compounds **7-11** (**Table 7**). Enlarging substituents on 3- and 5-positions of isoxazole by adding one carbon atom on either or both sides yielded **7-9**. Compound **7** binds to BRD4 at 1243 nM to BD1 and 478 nM to BD2, about 3-4 fold weaker than **6**. Shifting the ethyl group to the other side further reduced binding affinity of **6** by 10-fold (**8**, K_i =2814 nM to BRD4 BD1, 2182 nM to BRD4 BD2). Employing a 3,5-diethylisoxazole moiety as the R group gave **9**, which binds to BD1 and BD2 at 4842 nM and 1948 nM respectively, even weaker than **8** at BD1. Introducing 3,5-dimethyl-1*H*-pyrazole (**10**) as the head group almost completely eliminated its binding to BRD4 BD1. Replacement of dimethylisoxazole with 1,3,5-trimethyl-1*H*-pyrazole resulted in **11**, which is 4-6 fold weaker than **6**. Hence, 3,5-dimethyloxazole is the best among the head groups explored.

Table 7 SAR of new BET inhibitors with modification “head” groups.



ID	R	X	BRD4 BD1		BRD4 BD2	
			IC ₅₀ (nM)	K _i (nM)	IC ₅₀ (nM)	K _i (nM)
4	-	-	31.7±7.7	9.0±2.9	226±44	74.8±8.6
5		H	4592±72	1644±71	2691±460	824±25

6		Cl	862 ± 100	305 ± 26	579 ± 71	194 ± 24
7		Cl	3868 ± 1972	1243 ± 549	1817 ± 136	478 ± 69
8		Cl	9443 ± 3797	2814 ± 782	13826 ± 3706	2182 ± 132
9		Cl	14022 ± 781	4842 ± 29	6175 ± 549	1948 ± 175
10		Cl	>10000	> 10000	73970 ± 7844	8322 ± 1272
11		Cl	4874 ± 320	1726 ± 17	2580 ± 80	867 ± 107

3.3.2 SAR of five-membered aromatic system as “tail” groups.

Modeling of the “tail” group suggested that replacement of the Cl atom in compound **6** with a 3,5-dimethylisoxazole group yielded **12**, which can occupy the WPF shelf and may enhance the binding affinity. Indeed, compound **12** binds to BRD4 BD1 and BD2 proteins with K_i values of 47.8 nM and 70.1 nM respectively, and is thus 3-times more potent than compound **6**.

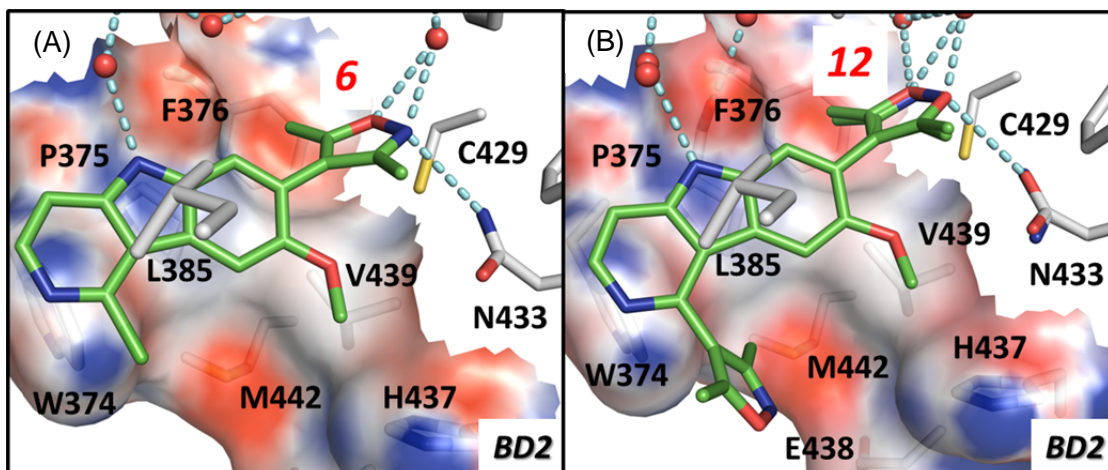


Figure 23 Co-crystal structures of (A) **6** and (B) **12** with BRD4 BD2. Compounds are shown in stick with carbon atoms colored in green, oxygen atoms in red and nitrogen atoms in blue. Electrostatic potential is mapped to the surface of BRD4 BD1 and BD2 proteins where blue, red, grey correspond to positive, negative and neutral charged regions. Water molecules are shown as red spheres and the hydrogen bonds are denoted by cyan dash lines.

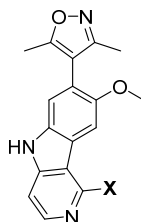
To confirm our predicted binding mode for **12** and facilitate further optimization, we determined a co-crystal structure of **6** and **12** complexed with the BRD4 BD2 protein at 1.33 Å resolution (**Figure 23**). The co-crystal structure for **12** shows that it indeed interacts nicely with the three key regions in BRD4 protein observed in the co-crystal structure of **4** complexed with BRD4 BD1.

The crystal structure also suggests that the WPF shelf can accommodate groups larger than 3,5-dimethylisoxazole. Since 1*H*-pyrazoles have more structural diversity than isoxazoles, we performed additional modifications at this site using 1*H*-pyrazole ring systems (**Table 8**).

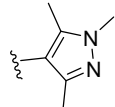
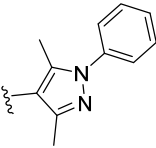
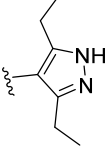
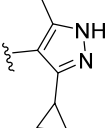
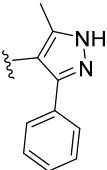
Replacement of the 3,5-dimethylisoxazole group in **12** with a 1*H*-pyrazole group or 3,5-dimethyl-1*H*-pyrazole resulted in compounds **13** and **14**, which have K_i values of 98.8 nM and 247 nM to BRD4 BD1, 2-5 times less potent than **12**. Adding methyl or

phenyl substitutions to the NH group of 3,5-dimethyl-1*H*-pyrazole group in **14** gave **15** and **16**, which bind to BRD4 BD1 with comparable affinities (116 nM and 103 nM), suggesting that this position might be solvent-exposed. Replacement of both of the methyl groups on the “tail” of **14** with ethyl groups resulted in compound **17**, which has a K_i value of 44.1 nM to BRD4 BD1, 6-times more potent than **14**. Changing the “tail” to a 3-cyclopropyl-5-methyl-1*H*-pyrazole group led to compound **18** (RX-37), which has a K_i value of 24.7 nM to BRD4 BD1 and is 10-times more potent than **14** and 2-times more potent than **12**. Replacement of the “tail” group in **14** with a 3-phenyl-5-methyl-1*H*-pyrazole group yielded compound **19**, which binds to BD1 with a similar affinity but is 3-times less potent in BD2 than compound **18**.

Table 8 SAR of new BET inhibitors with modification “tail” groups.



ID	X	BRD4 BD1		BRD4 BD2	
		IC ₅₀ (nM)	K _i (nM)	IC ₅₀ (nM)	K _i (nM)
4	-	31.7±7.7	9.0±2.9	226±44	74.8±8.6
12		134±7	47.8±1.0	221±38	70.1±2.0
13		276±44	98.8±11.6	324±8	100±16
14		702±53	247±29	658±67	201±5

15		327±11	116±5	481±86	134±42
16		301±37	103±3	316±24	98.1±6.1
17		131±11	44.1±6.4	61.9±13.9	16.1±2.8
18		75.5±6.2	24.7±1.0	36.5±8.9	12.2±1.6
19		80.6±1	26.9±1.0	129±45	38.0±2.2

The high-resolution co-crystal structure of **18** complexed with BRD4 BD2 provides a structural basis for its high affinity binding to BDR4 BD2. As shown in **Figure 24A**, **18** binds to BRD4 BD2 in a fashion similar to what was observed for **6** and **12**. The 3,5-dimethylisoxazole sits comfortably in the K-Ac binding pocket; its oxygen atom forms a hydrogen bond with the side chain amide of Asn433, its nitrogen atom is involved in a water-mediated H bond network in which Tyr390, Pro375 as well as the indole amine of γ -carboline are linked *via* six conserved water molecules¹³⁹ (**Figure 24B**). The WPF shelf has hydrophobic interactions with the pyridyl of γ -carboline and the cyclopropyl of the “tail”. The NH group of 1*H*-pyrazole is solvent exposed, which is consistent with the binding data for compounds **15** and **16** (**Table 8**)

(B)

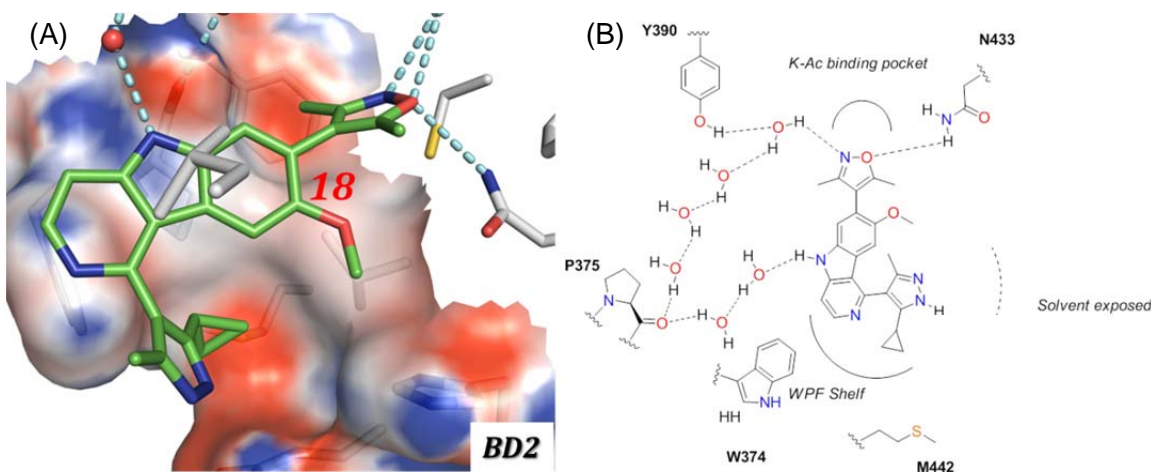


Figure 24 Co-crystal structure and schematic representation of **18** interactions. (A) 3D co-crystal structure of compound **18** and BRD4 BD2. **18** is shown in stick form with carbon atoms colored in green, oxygen atoms in red and nitrogen atoms in blue. Electrostatic potential is mapped to the surface of BRD4 BD2 where blue, red, grey correspond to positive, negative and neutral charged regions. Water molecules are shown as red spheres and the hydrogen bonds are denoted by cyan dash lines. (B) Schematic representation of **18** (RX-37) interactions in K-Ac recognition pocket.

3.4 Selectivity of new BRD4 inhibitors in biochemical and cellular assays

3.4.1 Selectivity among BET family bromodomains

We selected the three most potent inhibitors **17-19** and tested their binding affinities to other bromodomains in the BET family, with compounds **1-4** as references. The results are summarized in **Table 9**, which shows that compounds **17**, **18** and **19** have low nanomolar affinities to both the BD1 and BD2 domains in BRD2 and BRD3 proteins. Compound **18** is the most potent inhibitor with K_i values of 11.1 nM and 11.7 nM to BRD2 BD1 and BD2 domains, and 7.3 nM and 3.2 nM to BRD3 BD1 and BD2 domains, respectively.

Table 9 Binding affinities of new BET inhibitors among BET family members.

ID	K_i (nM)					
	BRD2		BRD3		BRD4	
	BD1	BD2	BD1	BD2	BD1	BD2
1	13.2±4.5	12.5±2.7	6.6±1.2	8.9±1.6	7.6±0.4	10.7±1.1
2	16.6±1.0	5.4±0.2	10.7±1.0	4.0±0.6	10.9±0.6	6.0±0.3
3	56.8±10.0	49.2±6.5	53.9±6.0	30.3±4.5	38.8±5.0	32.3±3.8
4	9.0±4.3	49.6±10.8	7.2±3.0	22.3±3.5	9.0±2.9	74.8±8.6
17	21.0±3.3	15.4±3.2	12.9±2.9	4.2±0.4	44.1±6.4	16.1±2.8
18	11.1±1.0	11.7±3.0	7.3±0.1	3.2±0.5	24.7±1.0	12.2±1.6
19	12.2±1.7	22.2±2.8	10.4±1.0	9.4±1.0	26.9±1.0	38.0±2.2

3.4.2 Selectivity among bromodomains from other families

To test the selectivity of **18** to bromodomains from the BET family, we applied Bio-Layer Interferometry, a label-free technology for assessment of interactions between biomolecules. The binding affinities of **18** to BRD2-4 BD1 and BD2 domains and 9 representative bromodomain-containing proteins from 7 other subfamilies were evaluated. Compounds **1**, **3** and **4** were included as controls.

Table 10 Binding affinities of selected BET inhibitors to other family bromodomains measured by Bio-Layer Interferometry.

Protein	aK_d (nM)			
	1	3	4	18
BRD2(BD1)	14.7±1.9	159±11	54.8±7.8	48.1±4.0
BRD2(BD2)	6.2±1.8	45.4±1.0	70.3±7.3	29.6±6.9

BRD3 (BD1)	13.6±1.0	60.7±10.3	29.8±7.3	17.7±3.6
BRD3 (BD2)	11.7±1.5	40.7±8.5	40.5±7.2	16.3±4.1
BRD4 (BD1)	12.8±2.9	99.4±5.8	52.8±9.2	47.0±14.8
BRD4 (BD2)	6.7±0.7	47.6±2.7	215±29	44.6±22.1
CREBBP		> 10000	3084	670
ATAD2A		> 10000	> 10000	> 10000
ATAD2B				> 10000
TRIM24				~ 10000
BAZ2B				> 10000
MLL1				9500
TAF1B2				> 10000
BRG1				> 10000
PB1BR5				> 10000

^aK_d values were calculated using global fitting.

Compound **18** has K_d values of 16.3-48.1 nM for BET family proteins, which are largely consistent with the binding data obtained from the FP-based, competitive binding assays (**Table 10**). Among the 9 non-BET bromodomain proteins evaluated, compound **18** displays a moderate affinity to CREBBP protein (K_d = 670 nM) but has very low affinities (K_d values ≥ 10,000 nM) for all 8 other bromodomain proteins. These data show that **18** is a potent BET bromodomain inhibitor with selectivity over other bromodomain proteins.

3.5 RX-series BET bromodomain inhibitors selectively induce cell-cycle arrest and apoptosis in leukemia cell-lines.

Previous studies have shown that potent and specific BET inhibitors such as **1**, **3** and **4** potently inhibit cell growth in human acute leukemia cell lines containing the MLL1 chromosomal rearrangement, such as MV4;11 and MOLM-13 cell lines¹¹⁵. Also, BET inhibitors demonstrate selectivity over human acute leukemia cell lines harboring different gene rearrangements such as the K562, which harbors the BCR-ABL fusion protein¹¹¹. We tested three of the most potent BET inhibitors (**17-19**) for their cellular activity and specificity among MV4;11, MOLM-13 and K562 cell lines.

The resulting data (**Table 11**) demonstrated that compounds **17-19** potently inhibit cell growth in the MV4;11 and MOLM-13 cell lines. For example, **18** has IC₅₀ of 20 nM and 66 nM in inhibition of cell growth in MV4;11 and MOLM-13 cell lines, respectively, and is therefore as potent as **1** (JQ-1) but 4-8 times more potent than **3** and **4**. Compounds **17-19** have IC₅₀ values of >2,000 nM in inhibition of cell growth in the K562 cell line harboring BCR-ABL fusion protein, thus displaying excellent cellular specificity.

Table 11 Cell growth inhibitory activity of new BET inhibitors in acute leukemia cell lines^a.

ID\IC ₅₀ (nM)	MV4; 11	MOLM-13	K562
1	24±19	56±24	>2000
3	93±45	241±58	>2000
4	162±112	228±52	>2000
17	23±10	78±12	>2000
18	20±9	66±14	>2000
19	34±15	144±31	>2000

^aCompounds were were co-incubated with cells for 4 days before analysis.

Previous studies have shown that the cytotoxicity of BET inhibitors involves the downregulation of oncogene *c-MYC* and anti-apoptotic *BCL2* in acute leukemia cell lines harboring *MLL1* gene rearrangements¹³⁰. We investigated the mechanism of action for compounds **17** and **18** by western blot analysis in MV4;11 acute leukemia cell lines harboring the MLL1-AF4 fusion gene. As shown in **Figure 25**, compounds **17** and **18** down-regulate the protein levels of *c-Myc* and Bcl-xL in a dose-dependent manner, and both are more efficient than **3** (I-BET-762) and **4** (I-BET-151). Compounds **17** and **18** effectively and dose-dependently induced the cleavage of PARP, a biochemical marker of apoptosis.

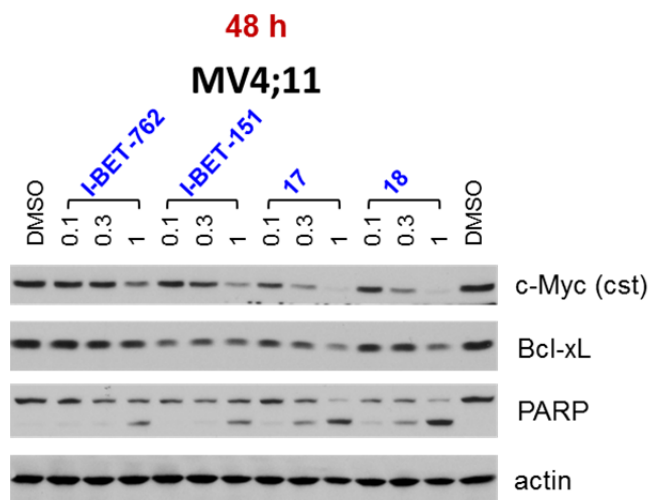


Figure 25 New BET bromodomain inhibitors down-regulate target oncoprotein expression and induce apoptosis in MV4-11 cells.

To further test the ability of compounds **17** and **18** to induce apoptosis in other leukemia cells harboring MLL gene rearrangements, we performed Annexin-V/propidium iodide double staining by flow cytometry in the MOLM-13 cell line

containing the MLL-AF9 fusion. As shown in **Figure 26**, compounds **17** and **18** induced robust apoptosis at concentrations as low as 0.3 μM and were ~ 3 -times more potent than **3** (I-BET-762).

Hence, compounds **17** and **18** effectively down regulate c-Myc as well as anti-apoptotic Bcl-xL, concomitant with apoptosis induction in leukemia cell lines containing MLL fusions. The potency of compounds **17** and **18** is several times greater than that of **3** (I-BET-762), a BET inhibitor in clinical development.

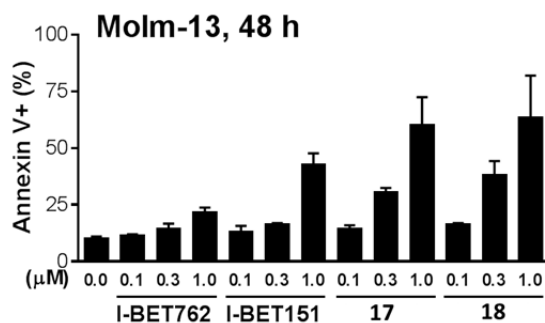


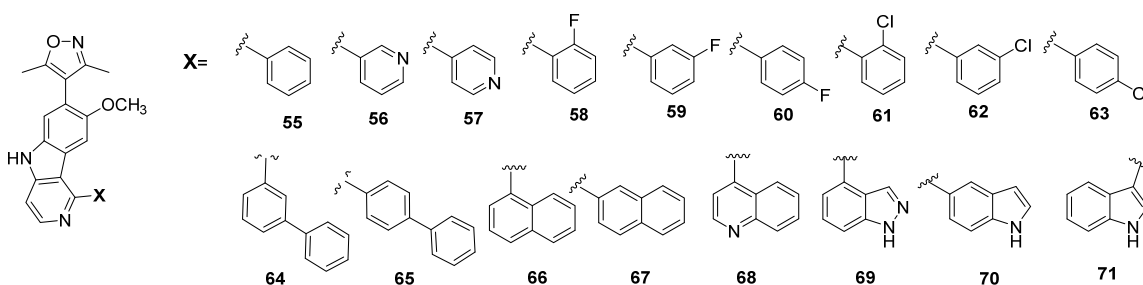
Figure 26 New BET bromodomain inhibitors induce apoptosis in Molm-13 cells.

3.6 SAR of mono- or bicyclic aromatics as “tail” group

Besides the *1H*-pyrazole systems, we also tested other aromatic mono- or bicyclic structures to identify a possible “tail”. Monocyclic groups such as phenyl, pyridyl, fluoro- or chloro- substituted phenyl display binding affinities to BRD4 BD2 of about 100-400 nM, more than 100-fold weaker than **18**. Bicyclic systems gave significant variations in binding affinities when attached at different carbon atoms. For example, angular biphenyl

substituted **64** has a binding affinity to BRD4 BD2 at 354 nM, 7-fold more potent than the linear **65**. Fused ring systems such as naphthyl, quinolinyl, indolyl or indazolyl group in a favored orientation bind even tighter than biphenyl. Compounds **66**, **68** and **71** have K_i values of 31.6 nM, <20 nM and 16.4 nM respectively, which are in a comparable range with the most potent 1*H*-pyrazole analogs (**17**, **18** and **19**).

Table 12 Structure and binding affinities of compounds with mono- and bi-cyclic aromatic “tails”.



ID	BRD4 BD2		ID	BRD4 BD2	
	IC ₅₀ (nM)	K _i (nM)		IC ₅₀ (nM)	K _i (nM)
18	36.5±8.9	12.2±1.6	63	2164±606	418±29
55	514	83.4	64	1011	354
56	873	232	65	10268	2528
57	499±86	98±43	66	283±178	31.6±15.0
58	577	135	67	1077±110	305±20
59	821	223	68	36.3±3.2	< 20
60	1318	404	69	314±34	40.8±5.7
61	928	213	70	490	95.2
62	1087	250	71	197±99	16.4

3.7 Pharmacokinetic and antitumor efficacy studies

Further modification at the “tail” position of the BET inhibitors discussed above gave RX-201 ($K_i=1.4$ nM to BRD4 BD1, $IC_{50}= 26$ nM in MDA-MB-436, structure not shown), which shows good oral PK profile and high plasma and tumor exposure in mice (**Table 13** and **Figure 27**), suggesting this molecule should be orally bioavailable. In efficacy studies using the MD-MBA-436 xenograft, RX-201 shows superior antitumor activity compared with **1** (JQ1) and the clinical compound **2** (OTX015) (**Figure 28**).

Table 13 RX-201 concentrations in mouse plasma and tumor.

25mg/kg(PO)	RX-201 concentration in mouse plasma (ng/mL)				RX-201 concentration in mouse tumor (ng/g)					
	Animal Number				Mouse 1		Mouse 2			
Time points (h)	1	2	Mean	SD	R	L	R	L	Mean	SD
1	4210	10700	7455	4589	4675	4960	2310	3155	3982	1258
3	<1	7680	7680	-	<1	<1	<1	<1	1	-
6	12700	3380	8040	6590	2830	2730	2170	2560	2577	291
24	<1	1.35	1.35	-	167	126	215	170	169	36
48	<1	<1	1	-	99	85	55.5	57	80	21

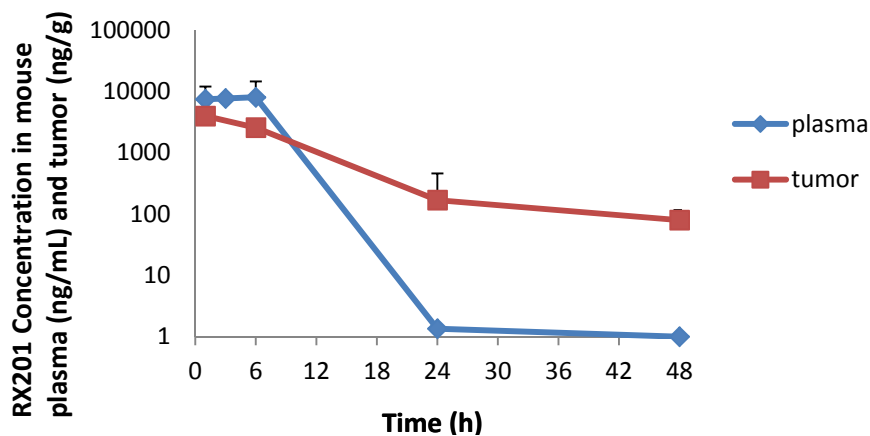


Figure 27 RX-201 concentrations in mice plasma and tumor.

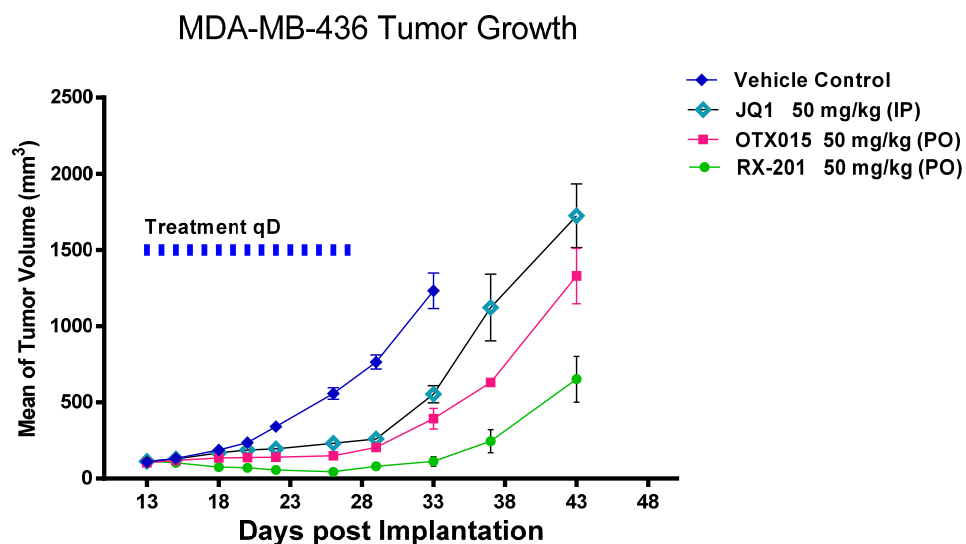
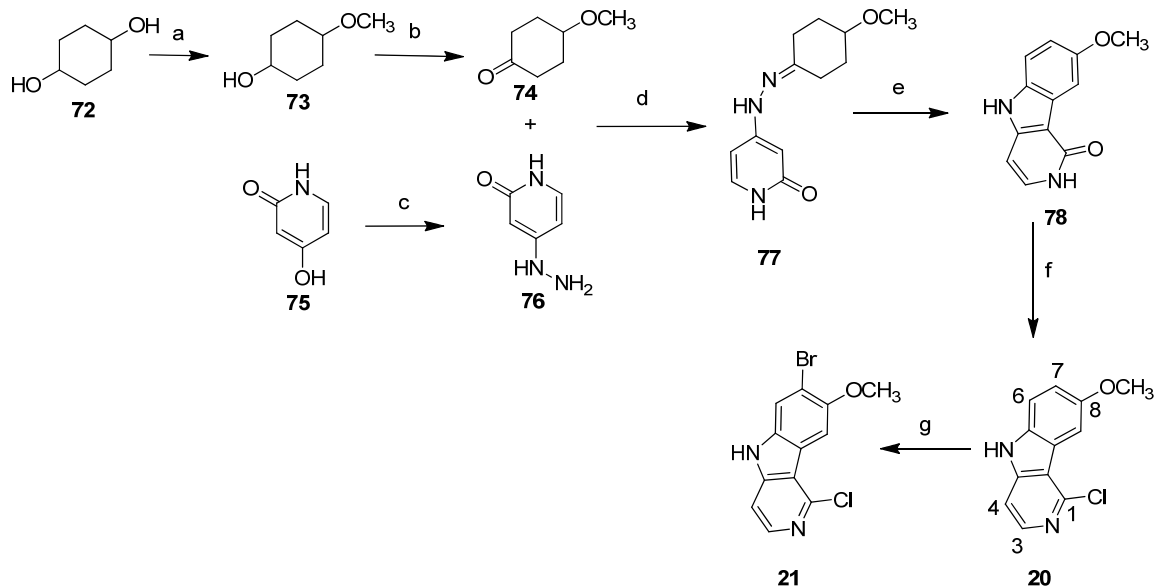


Figure 28 Antitumor activity of RX-201 in a mouse xenograft model.

3.8 Synthesis of γ -carboline-containing compounds as BET bromodomain inhibitors.

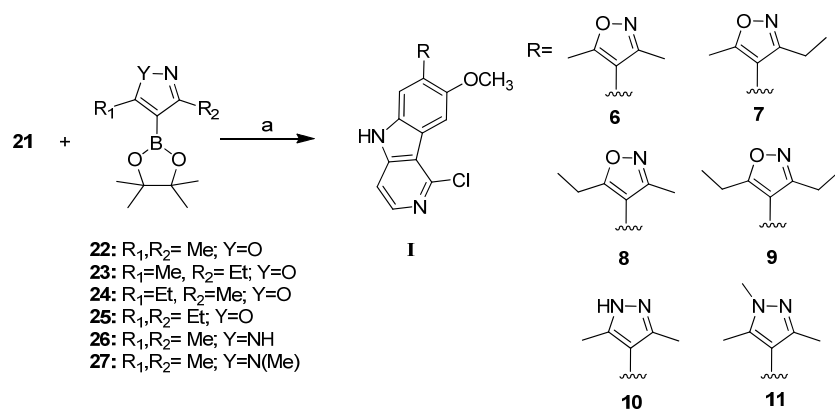
The general synthetic strategy for synthesis of γ -carboline-containing BET bromodomain inhibitors can be generally summarized as γ -carboline core synthesis followed by “head” and “tail” attachment.

The γ -carboline core was synthesized using a reported method¹⁴⁶, in which Fischer indole synthesis was applied to furnish the tricyclic system **78** from its precursor **77**, which was prepared in four steps from the commercially available materials **72** and **75**. Chlorination of **78** gave **20** which was converted to **21** by selective bromination at its 7 position (**Scheme 1**).



Reaction condition: (a) CH_3I , KOH , H_2O , rt, overnight. (b) PCC , DCM , rt, 4h. (c) $\text{H}_2\text{N-NH}_2$, 2-methoxyethanol, reflux, 24h. (d) EtOH , reflux 4h. (e) PhOPh , reflux 0.5 h, then 10% Pd-C reflux, 1.25 h. (f) POCl_3 , reflux 24 h, then 3N HCl 1 hour, neutralized by ammonia. (g) Br_2 , NaOAc , AcOH , overnight;

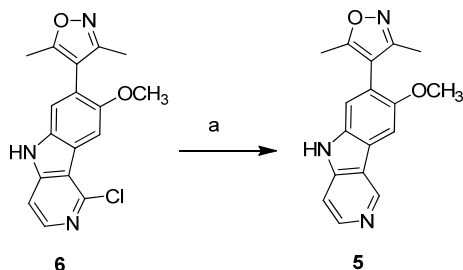
Scheme 1 Synthetic route to γ -carboline core structure.



Reaction conditions: (a) $\text{Pd}(\text{PPh}_3)_4$, K_2CO_3 , Dimethoxyethane, H_2O , reflux.

Scheme 2 General synthetic method for **6-11**.

The core structure **21** was coupled selectively to different boronates (**22-27**) at the “head” position under Suzuki conditions to give compounds **6-11** (**Scheme 2**). **5** was prepared from **6** by stirring under H₂ for 12 hours (**Scheme 3**).

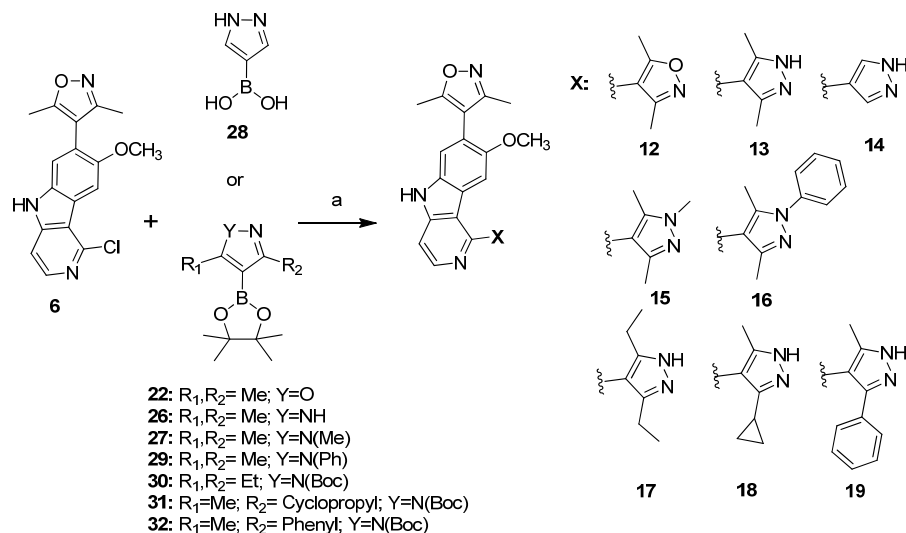


Reaction condition: (a) H₂, Pd/C in MeOH for 12 hours.

Scheme 3 Synthetic method for **5**.

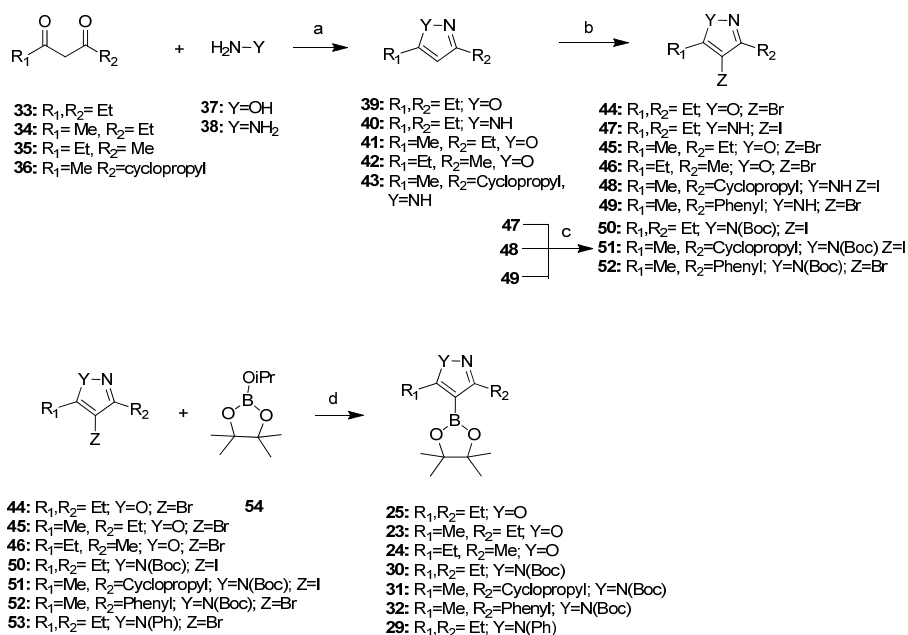
A second Suzuki coupling reaction between **6** and the isoxazole or 1*H*-pyrazole analogs (**22**, **26-32**) led to **12-19** as the final compounds for BET inhibition (**Scheme 4**). Boronates of isoxazole or 1*H*-pyrazole analogs **23-25**, **29-32** were prepared in 3-4 steps from various diketones (**33-36**, **Scheme 5**). Refluxing the diketones with **37** or **38** furnished the five-membered heterocyclics (**39-43**) which were halogenated with *N*-bromosuccinimide (NBS) or *N*-iodosuccinimide (NIS) and consequently converted to the correspondent boronic acid pinacol ester with (**30-32**) or without (**23-25**, **29**) an intermediate Boc protecting step (**Scheme 5**).

The “tail” attachments for **55-71** were made under the same condition used for **12-19**. All the “tail” moieties were purchased in their boronic acid form from commercial sources.



Reaction conditions: (a) Pd(PPh₃)₄, K₂CO₃, Dimethoxyethane, H₂O, reflux.

Scheme 4 General synthetic route for 12-19.



Reaction conditions: (a) EtOH or MeOH/H₂O, reflux; (b) NBS or NIS, DMF, overnight; THF (c) (Boc)₂O, DMAP, 0 °C to rt; (d) BuLi, THF, -78 °C.

Scheme 5 General synthetic route for five-membered heterocyclic boronates.

3.9 Future Directions

Extensive SAR studies of this class of compounds have been performed with the goal of obtaining potent and orally bioavailable BET inhibitors. To date, a number of useful BET inhibitors, including RX-201, have been obtained in our laboratory. Extensive *in vitro* and *in vivo* evaluations to determine their mechanism of action and therapeutic potential as a new class of anticancer drugs are ongoing.

More selective inhibitors of BET family proteins¹⁴⁷ which can discriminate BD1 from BD2 should be able to avoid side-effects stemming from the inhibition of regular biological function by each bromodomain subtype.

In addition to targeting BET family proteins at their bromodomains, other critical PPIs including CTD domains of BRD4 to each subunits of TEFb, mediator binding motif of BRD4⁴⁵, ET domains to Jmjd6 arginine demethylase and Nsd3^{148, 149}, lysine methyltransferase, and nucleosome remodeling related SWI/SNF and CHD4¹⁴⁹ are potential opportunities for therapeutic intervention.

Key safety issues regarding use of epigenetic modifiers as drugs are the long-term effects of a drug on stem cells, germ cells and transgenerational effects which should be monitored closely as clinical trials proceed⁴⁵.

Critical PPIs, downstream target genes, and genomic binding sites relevant to BRD4 dependent disease processes should be further studied in the clinic for an understanding of resistant mechanisms.

3.10 Experiments

3.10.1 Synthetic methods and characterizations of BET bromodomain inhibitors

General Methods

Proton nuclear magnetic resonance (^1H NMR) spectroscopy and carbon nuclear magnetic resonance (^{13}C NMR) spectroscopy were performed in Bruker Advance 300 NMR spectrometers. ^1H chemical shifts are reported with CHD_2OD (3.31 ppm) or HDO (4.70 ppm) as internal standards. The final products were purified by C18 reverse phase semi-preparative HPLC column with solvent A (0.1% TFA in H_2O) and solvent B (0.1% TFA in CH_3CN) as eluents. The final compounds were isolated in their TFA salt form, and the purities, in all cases, were confirmed by analytical HPLC to be >95%.

Synthesis of compound 5

4-(8-Methoxy-5H-pyrido[4,3-b]indol-7-yl)-3,5-dimethylisoxazole (5). 10% Pd-C (5 mg) was suspended in a solution in MeOH of **6** (15 mg, 0.046 mmol). The reaction was stirred for 26 hours under H_2 at room temperature. The Pd-C was removed by filtration and the filtrate was purified by semi-preparative HPLC to give 4 mg (30%) of **5** as a colorless powder after being lyophilized for 24 h. ^1H NMR (300 MHz, MeOD-d_4) δ 9.61 (s, 1H), 8.54 (d, 1H, $J=6.9$ Hz), 8.11 (s, 1H), 7.97 (s, 1H), 7.61 (s, 1H), 4.00 (s, 3H), 2.36 (s, 3H), 2.19 (s, 3H). ESIMS m/z $[\text{M}+\text{H}]^+$ calcd. = 294.33; found = 294.75.

Synthesis of compounds 6-19

4-(1-Chloro-8-methoxy-5H-pyrido[4,3-b]indol-7-yl)-3,5-dimethylisoxazole (**6**).

Compounds **21** (157 mg, 0.5 mmol) and **22** (655 mg, 2.0 mmol), and K₂CO₃ (345 mg, 2.5 mmol) were dissolved in a dimethoxyethane/H₂O (2:1) mixture (75 mL). The reaction system was vacuumed, followed by addition of tetrakis (triphenylphosphine) palladium (0), the system was vacuumed again then filled with N₂. After heating at reflux overnight, the mixture was extracted with EtOAc, and the organic fraction was concentrated before purification by preparative HPLC. 57 mg (35%) of compound **6** was obtained as pale yellow powder after being lyophilized for 24 h. ¹H NMR (300 MHz, MeOD-d₄) δ 8.26 (d, 1H, *J*= 6.0 Hz), 8.09 (s, 1H), 7.60 (d, 1H, *J*= 6.3 Hz), 7.49 (s, 1H), 3.98 (s, 3H), 2.63 (s, 3H), 2.20 (s, 3H). ¹³C NMR (75 MHz, MeOD-d₄) δ 168.07, 161.30, 155.05, 148.78, 143.09, 141.11, 136.57, 122.59, 122.28, 118.84, 116.16, 115.01, 108.08, 105.09, 56.69, 11.69, 10.84. ESIMS *m/z* [M+H]⁺ calcd. = 328.77; found = 328.83.

4-(1-Chloro-8-methoxy-5H-pyrido[4,3-b]indol-7-yl)-3-ethyl-5-methylisoxazole (**7**). This compound was prepared by coupling **21** and **23** under conditions similar to those used for the preparation of **6**. ¹H NMR (300 MHz, MeOD-d₄) δ 8.27 (d, 1H, *J*= 6.3 Hz), 8.02 (s, 1H), 7.64 (d, 1H, *J*= 6.3 Hz), 7.48 (s, 1H), 3.93 (s, 3H), 2.70 (q, 2H, *J*= 7.5 Hz), 2.13 (s, 3H), 1.20 (t, 3H, *J*= 7.5 Hz). ESIMS *m/z* [M+H]⁺ calcd. = 342.80; found = 342.42.

4-(1-Chloro-8-methoxy-5H-pyrido[4,3-b]indol-7-yl)-5-ethyl-3-methylisoxazole (**8**). This compound was prepared by coupling **21** and **24** under conditions similar to those used for the preparation of **6**. ¹H NMR (300 MHz, MeOD-d₄) δ 8.19 (d, 1H, *J*= 5.7 Hz), 8.08 (s,

1H), 7.49 (d, 1H, $J= 5.7$ Hz), 7.43 (s, 1H), 3.96(s, 3H), 2.64 (q, 2H, $J= 7.5$ Hz), 2.34 (s, 3H), 1.12 (t, 3H, $J= 7.5$ Hz). ESIMS m/z $[M+H]^+$ calcd. = 342.80; found = 342.67.

4-(1-Chloro-8-methoxy-5H-pyrido[4,3-b]indol-7-yl)-3,5-diethylisoxazole (**9**). This compound was prepared by coupling **21** and **25** under conditions similar to those used for the preparation of **6**. ^1H NMR (300 MHz, DMSO- d_6) δ 12.06 (s, 1H), 8.22 (d, 1H, $J= 5.7$ Hz), 7.96 (s, 1H), 7.52 (d, 1H, $J= 5.7$ Hz), 7.49 (s, 1H), 3.89 (s, 3H), 2.65 (q, 2H, $J= 7.5$ Hz), 2.53 (q, 2H, $J= 7.5$ Hz), 1.15 (t, 3H, $J= 7.5$ Hz), 1.04 (t, 3H, $J= 7.5$ Hz). ^{13}C NMR (75 MHz, DMSO- d_6), δ 169.85, 163.67, 152.08, 145.84, 143.62, 143.55, 133.92, 119.93, 119.20, 116.06, 114.30, 111.86, 106.71, 103.19, 55.71, 18.94, 18.49, 11.81. ESIMS m/z $[M+H]^+$ calcd. = 356.67; found = 356.83.

1-Chloro-7-(3,5-dimethyl-1H-pyrazol-4-yl)-8-methoxy-5H-pyrido[4,3-b]indole (**10**). This molecule was prepared by coupling **21** and **26** under conditions similar to those used for the preparation of **6**. ^1H NMR (300 MHz, MeOD- d_4) δ 8.24 (d, 1H, $J= 6.0$ Hz), 8.10 (s, 1H), 7.56 (d, 1H, $J= 6.0$ Hz), 7.49 (s, 1H), 3.97 (s, 3H), 2.31 (s, 6H). ^{13}C NMR (75 MHz, MeOD- d_4), δ 154.63, 148.56, 145.51, 142.58, 136.32, 122.52, 121.86, 118.63, 118.34, 116.15, 107.94, 105.19, 101.44, 56.69, 10.75. ESIMS m/z $[M+H]^+$ calcd. = 327.79; found = 327.92.

1-Chloro-8-methoxy-7-(1,3,5-trimethyl-1H-pyrazol-4-yl)-5H-pyrido[4,3-b]indole (**11**). This molecule was prepared by coupling **21** and **27** under conditions similar to those used

for the preparation of **6**. ^1H NMR (300 MHz, MeOD- d_4) δ 8.26 (d, 1H, J = 6.0 Hz), 8.07 (s, 1H), 7.61 (d, 1H, J = 6.3 Hz), 7.45 (s, 1H), 3.95 (s, 3H), 3.88 (s, 3H), 2.24 (s, 3H), 2.20 (s, 3H). ESIMS m/z $[\text{M}+\text{H}]^+$ calcd. = 341.81; found = 342.33.

*4,4'-(8-Methoxy-5H-pyrido[4,3-*b*]indole-1,7-diyl)bis(3,5-dimethylisoxazole)* (**12**). This compound was prepared by coupling **6** and **22** under conditions similar to those used for the preparation of **6**. ^1H NMR (300 MHz, MeOD- d_4) δ 8.63 (d, 1H, J =6.6 Hz), 8.04 (d, 1H, J =6.6 Hz), 7.67 (s, 1H), 7.02 (s, 1H), 3.78 (s, 3H), 2.52 (s, 3H), 2.34 (s, 3H), 2.28 (s, 3H), 2.17 (s, 3H). ^{13}C NMR (75 MHz, MeOD- d_4) δ 172.28, 168.28, 161.12, 160.42, 155.77, 149.23, 138.54, 137.66, 136.81, 124.16, 122.24, 121.46, 117.29, 114.52, 109.87, 109.42, 103.77, 56.42, 12.05, 11.68, 10.79, 10.60. ESIMS m/z $[\text{M}+\text{H}]^+$ calcd. = 389.43; found = 389.50.

*4-(1-(3,5-Dimethyl-1H-pyrazol-4-yl)-8-methoxy-5H-pyrido[4,3-*b*]indol-7-yl)-3,5-dimethylis-oxazole* (**13**). This molecule was prepared in 75% yield by coupling **6** and **26** under conditions similar to those used for the preparation of **6**. ^1H NMR (300 MHz, MeOD- d_4) δ 8.54 (d, 1H, J = 6.9 Hz), 7.95 (d, 1H, J = 6.9 Hz), 7.63 (s, 1H), 7.02 (s, 1H), 3.74 (s, 3H), 2.34 (s, 3H), 2.29 (s, 6H), 2.16 (s, 3H). ^{13}C NMR (75 MHz, MeOD- d_4) δ 168.23, 161.18, 155.58, 148.99, 146.03, 143.05, 137.39, 136.23, 123.63, 122.87, 121.08, 116.98, 114.63, 108.64, 103.98, 56.29, 11.68, 11.41, 10.79. ESIMS m/z $[\text{M}+\text{H}]^+$ calcd. = 388.44; found = 388.42.

4-(8-Methoxy-1-(1H-pyrazol-4-yl)-5H-pyrido[4,3-b]indol-7-yl)-3,5-dimethylisoxazole

(14). This molecule was prepared by coupling **6** and **28** under conditions similar to those used for the preparation of **6**. ¹H NMR (300 MHz, MeOD-d₄) δ 8.48 (s, 2H), 8.45 (d, 1H, *J*=6.9 Hz), 7.89 (d, 1H, *J*=6.9 Hz), 7.63 (s, 1H), 7.61 (s, 1H), 3.82 (s, 3H), 2.35 (s, 3H), 2.17 (s, 3H). ¹³C NMR (75 MHz, MeOD-d₄) δ 168.18, 161.18, 155.28, 149.11, 143.30, 137.25, 135.69, 123.48, 123.01, 119.19, 116.80, 114.66, 113.69, 108.22, 104.50, 56.37, 11.67, 10.80. ESIMS *m/z* [M+H]⁺ calcd. = 360.39; found = 361.17.

4-(8-Methoxy-1-(1,3,5-trimethyl-1H-pyrazol-4-yl)-5H-pyrido[4,3-b]indol-7-yl)-3,5-

dimethylisoxazole (15). This molecule was prepared by coupling **6** and **27** under conditions similar to those used for the preparation of **6**. ¹H NMR (300 MHz, MeOD-d₄) δ 8.54 (d, 1H, *J*= 6.9 Hz), 7.95 (d, 1H, *J*= 6.9 Hz), 7.63 (s, 1H), 7.04 (s, 1H), 3.97 (s, 3H), 3.75 (s, 3H), 2.34 (s, 3H), 2.32 (s, 3H), 2.21 (s, 3H), 2.16 (s, 3H). ESIMS *m/z* [M+H]⁺ calcd. = 402.47; found = 402.75.

4-(1-(3,5-Dimethyl-1-phenyl-1H-pyrazol-4-yl)-8-methoxy-5H-pyrido[4,3-b]indol-7-yl)-

3,5-dimethylisoxazole (16). This molecule was prepared by coupling **6** and **29** under conditions similar to those used for the preparation of **6**. ¹H NMR (300 MHz, MeOD-d₄) δ 8.60 (d, 1H, *J*= 6.6 Hz), 8.00 (d, 1H, *J*= 6.9 Hz), 7.64-7.66 (m, 6H), 7.11 (s, 1H), 3.78 (s, 3H), 2.35 (s, 3H), 2.33 (s, 3H), 2.31 (s, 3H), 2.17 (s, 3H). ¹³C NMR (75 MHz, MeOD-d₄) δ 168.26, 161.16, 155.67, 149.62, 149.10, 142.49, 142.22, 140.20, 137.48, 136.42,

131.02, 130.49, 126.75, 123.83, 122.75, 121.30, 117.06, 114.60, 112.68, 108.87, 103.95, 56.38, 12.56, 11.74, 11.69, 10.81. ESIMS m/z $[M+H]^+$ calcd. = 464.54; found = 464.42.

4-(1-(3,5-Diethyl-1H-pyrazol-4-yl)-8-methoxy-5H-pyrido[4,3-b]indol-7-yl)-3,5-dimethylisoxazole (17). This molecule was prepared in 35% yield by coupling **6** and **30** under conditions similar to those used for the preparation of **6**. ^1H NMR (300 MHz, MeOD- d_4) δ 8.55 (d, 1H, $J= 6.9$ Hz), 7.97 (d, 1H, $J= 6.9$ Hz), 7.64 (s, 1H), 6.92 (s, 1H), 3.70 (s, 3H), 2.65 (m, 4H). 2.34 (s, 3H), 2.16 (s, 3H), 1.10 (t, 6H, $J= 7.5$ Hz). ^{13}C NMR (75 MHz, MeOD- d_4), δ 168.25, 155.57, 148.83, 143.32, 137.42, 136.27, 123.78, 122.91, 121.45, 117.08, 114.59, 108.86, 103.85, 56.30, 30.88, 24.41, 20.51, 13.97, 11.69, 10.81. ESIMS m/z $[M+H]^+$ calcd. = 416.50; found = 416.42.

4-(1-(3-Cyclopropyl-5-methyl-1H-pyrazol-4-yl)-8-methoxy-5H-pyrido[4,3-b]indol-7-yl)-3,5-dimethylisoxazole (18). This molecule was prepared in 19% yield by coupling **6** and **31** under conditions similar to those used for the preparation of **6**. ^1H NMR (300 MHz, MeOD- d_4) δ 8.55 (d, 1H, $J= 6.9$ Hz), 7.96 (d, 1H, $J= 6.6$ Hz), 7.63 (s, 1H), 7.12 (s, 1H), 3.76 (s, 3H), 2.35 (s, 3H), 2.28 (s, 3H), 2.17 (s, 3H), 1.73 (m, 1H), 0.87 (m, 4H). ^{13}C NMR (75 MHz, MeOD- d_4), δ 168.18, 161.15, 155.46, 152.39, 148.94, 145.13, 143.14, 137.35, 136.19, 123.61, 122.93, 121.20, 116.85, 114.63, 110.46, 108.60, 104.41, 56.32, 11.66, 11.01, 10.77, 9.22, 8.45, 8.25. ESIMS m/z $[M+H]^+$ calcd. = 414.48; found = 414.50.

4-(8-Methoxy-1-(5-methyl-3-phenyl-1H-pyrazol-4-yl)-5H-pyrido[4,3-b]indol-7-yl)-3,5-dimethyl-isoxazole (19). This molecule was prepared by coupling **6** and **32** under conditions similar to those used for the preparation of **6**. ¹H NMR (300 MHz, MeOD-d₄) δ 8.54 (d, 1H, *J*= 6.9 Hz), 7.98 (d, 1H, *J*= 6.9 Hz), 7.57 (s, 1H), 7.34 (m, 2H), 7.25 (m, 3H), 6.98 (s, 1H), 3.70 (s, 3H), 2.33 (s, 3H), 2.30 (s, 3H), 2.12 (s, 3H). ¹³C NMR (75 MHz, MeOD-d₄) δ 168.18, 161.13, 155.42, 148.93, 143.24, 137.32, 136.38, 130.28, 128.12, 123.68, 122.65, 121.39, 116.84, 114.58, 108.90, 104.08, 56.33, 11.65, 10.88, 10.76. ESIMS *m/z* [M+H]⁺ calcd. = 450.51; found = 450.75.

1-chloro-8-methoxy-5H-pyrido[4,3-b]indole (20). POCl₃ (20 mL) and **78** were refluxed for 24 h followed by removal of POCl₃ under reduced pressure. The residue was refluxed with HCl for additional 2 h. After cooling, the mixture was neutralized with ammonium hydroxide, and extracted with DCM. Combined organic layer was dried and purified with flash column chromatography (EtOAc: hexane = 1:1 as eluent) to give 0.44 g (64.5%) titled compound as a colorless powder. ¹H NMR (300 MHz, MeOD-d₄) δ 8.26 (d, 1H, *J*=6.3 Hz), 7.94 (d, 1H, *J*=2.1 Hz), 7.61 (m, 2H), 7.31 (dd, 1H, *J*₁= 2.1 Hz, *J*₂= 8.7 Hz), 3.96 (s, 3H).

7-Bromo-1-chloro-8-methoxy-5H-pyrido[4,3-b]indole (21). Compound **20** (377 mg, 1.6 mmol) and NaOAc (197 mg, 2.4 mmol) were dissolved in AcOH (40 mL). Bromine (389 mg, 2.4 mmol) was added dropwise to the reaction system. After stirring at room

temperature overnight, the reaction was quenched with Na₂SO₃ solution. The AcOH was then removed under reduced pressure and H₂O was added followed by extraction with EtOAc. The combined organic fractions were concentrated and purified with preparative HPLC to give 157 mg (31%) of **21** as a colorless powder. ¹H NMR (300 MHz, MeOD-d₄) δ 8.21 (d, 1H, *J*= 5.7 Hz), 8.00 (s, 1H), 7.84 (s, 1H), 7.50 (d, *J*=6.0 Hz), 4.03 (s, 3H).

Synthesis of intermediates **23-25** and **29-32**.

t-Butyl 3-cyclopropyl-5-methyl-4-(4,4,5,5-tetramethyl-1,3,2-dioxaborolan-2-yl)-1H-pyrazole-1-carboxylate (**31**). Compound **51** (1.312 g, 3.77 mmol) was dissolved in THF (30 mL) and cooled to -78 °C under N₂. *n*-Butyl lithium (0.362 g, 5.65 mmol) was added slowly into the solution which was then stirred for 30 min at -78 °C. **54** (0.77 g, 4.14 mmol) was added to the reaction system, and the mixture was stirred at -78 °C for additional 2 h. Upon completion, the reaction was quenched by adding NH₄Cl saturated solution. The mixture was then extracted with EtOAc and dried over anhydrous Na₂SO₄. Purification by flash column chromatography (EtOAc: hexane = 1: 10) gave **31** as a colorless oil (0.459 mg, 35% yield). ¹H NMR (300 MHz, CDCl₃), δ 2.65 (s, 3H), 2.28 (m, 1H), 1.62 (s, 9H), 1.33 (s, 12H), 0.99 (m, 2H), 0.88 (m, 2H).

3-Ethyl-5-methyl-4-(4,4,5,5-tetramethyl-1,3,2-dioxaborolan-2-yl)isoxazole (**23**). This molecule was prepared by treatment of **45** and **54** under conditions similar to those used for the preparation of **31**. Compound **23** was prepared in a mixture with **24**. ¹H NMR (300 MHz, CDCl₃), δ 2.93 (q, *J*=7.5 Hz, 2H), 2.35 (s, 3H), 1.31 (s, 12H), 1.26 (m, 3H).

5-Ethyl-3-methyl-4-(4,4,5,5-tetramethyl-1,3,2-dioxaborolan-2-yl)isoxazole (**24**). This molecule was prepared by treatment of **46** and **54** under conditions similar to those used for the preparation of **31**. **24** was prepared in a mixture with **23**. ¹H NMR (300 MHz, CDCl₃), δ 2.77 (q, *J*=7.5 Hz, 2H), 2.53 (s, 3H), 1.31(s, 12H), 1.26(m, 3H).

t-Butyl-5-cyclopropyl-3-methyl-4-(4,4,5,5-tetramethyl-1,3,2-dioxaborolan-2-yl)-1H-pyrazole-1-carboxylate (**25**). This molecule was prepared by treatment of **44** and **54** under conditions similar to those used for the preparation of **31**. ¹H NMR (300 MHz, CDCl₃), δ 2.93 (q, *J*=7.5 Hz, 2H), 2.77 (q, *J*=7.5 Hz, 2H), 1.31 (s, 12H), 1.26 (m, 6H).

3,5-Dimethyl-1-phenyl-4-(4,4,5,5-tetramethyl-1,3,2-dioxaborolan-2-yl)-1H-pyrazole (**29**). This molecule was prepared by treatment of **53** and **54** under conditions similar to those used for the preparation of **31**. ¹H NMR (300 MHz, CDCl₃), δ 7.35-7.50 (m, 5H), 2.45 (s, 3H), 2.44 (s, 3H), 1.34 (s, 12H).

t-Butyl 3,5-diethyl-4-(4,4,5,5-tetramethyl-1,3,2-dioxaborolan-2-yl)-1H-pyrazole-1-carboxylate (**30**). This molecule was prepared by treatment of **50** and **54** under conditions similar to those used for the preparation of **31**. ¹H NMR (300 MHz, CDCl₃), δ 3.15 (q, *J*=7.5 Hz, 2H), 2.74 (q, *J*=7.5 Hz, 2H), 1.61 (s, 9H), 1.27 (s, 12H), 1.17 (m, 6H).

t-Butyl 5-methyl-3-phenyl-4-(4,4,5,5-tetramethyl-1,3,2-dioxaborolan-2-yl)-1H-pyrazole-1-carboxylate (**32**). This molecule was prepared in 39% yield by reaction of **52** and **54** under conditions similar to those used for the preparation of **31**. ¹H NMR (300 MHz, CDCl₃), δ 7.81 (m, 2H), 7.37 (m, 3H), 2.76 (s, 3H), 1.67 (s, 9H), 1.32 (s, 12H).

Synthesis of compounds **39**, **41** and **42**.

3,5-Diethylisoxazole (**39**). NH₂OH·HCl (**37**, 0.542 g, 7.8 mmol) was neutralized with Na₂CO₃ (0.413 g, 3.9 mmol) in MeOH/H₂O (1:2, 30 mL) solution. **33** (1.0 g, 7.8 mmol) was added into the mixture and heated at reflux overnight. After being cooled to room temperature, the mixture was extracted with Et₂O (40 mL × 2) and the organic layer was dried over anhydrous Na₂SO₄. Removal of solvents gave **39** as a light yellow liquid (0.559 g, 57%). ¹H NMR (300 MHz, CDCl₃), δ 5.85 (s, 1H), 2.63-2.78 (m, 4H), 1.24-1.31 (m, 6H).

3-Ethyl-5-methylisoxazole (**41**). This molecule was prepared by condensation of **34** and **37** under a similar conditions for the preparation of **39**. **41** was made as a mixture with **42** and used in the next step without purification. ¹H NMR (300 MHz, CDCl₃), δ 5.82 (s, 1H), 2.74 (q, *J*=7.5 Hz, 2H), 2.28 (s, 3H), 1.28 (q, *J*=7.5 Hz, 3H).

5-Ethyl-3-methylisoxazole (**42**). This molecule was prepared by treatment of **35** and **37** under conditions similar to those used for the preparation of **39**. **42** was prepared as a

mixture with **41** and used in the next step without purification. ^1H NMR (300 MHz, CDCl_3), δ 5.85 (s, 1H), 2.66 (q, $J=7.5$ Hz, 2H), 2.40 (s, 3H), 1.28 (q, $J=7.5$ Hz, 3H).

Synthesis of **40** and **43**.

3,5-Diethyl-1H-pyrazole (40). **33** (1.128 g, 8.8 mmol) and hydrazine monohydrate **38** (0.44 g, 8.9 mmol) were suspended in H_2O (5 mL). One drop of AcOH was added and the reaction mixture was heated at reflux for 1 h. After cooling to room temperature, the mixture was extracted with EtOAc and dried over anhydrous Na_2SO_4 . Removal of EtOAc gave **40** as a light yellow liquid, (0.96 g, 88%) which was used in the next step without further purification. ^1H NMR (300 MHz, CDCl_3), δ 5.89 (s, 1H), 2.67 (q, $J=7.5$ Hz, 4H), 1.27 (t, $J=7.5$ Hz, 6H).

3-Cyclopropyl-5-methyl-1H-pyrazole (43). This molecule was prepared in 95% yield by reaction of **36** and **38** under conditions similar to those used for the preparation of **40**. ^1H NMR (300 MHz, CDCl_3) δ 9.01 (br, 1H), 5.72 (s, 1H), 2.27 (s, 3H), 1.90 (m, 1H), 0.92 (m, 2H), 0.70 (m, 2H).

Synthesis of **44-48**.

3,5-Diethyl-4-iodo-1H-pyrazole (47). **40** (0.96 g, 7.7 mmol) and N-iodosuccinimide (1.73 g, 7.73 mmol) were dissolved in DMF (8 mL) and stirred at room temperature overnight. Then the reaction mixture was poured into H_2O (80 mL) and the aqueous layer was extracted with EtOAc (50 mL \times 3). The combined organic phases were washed with H_2O

(30 mL × 6) and dried over anhydrous Na₂SO₄. The product was purified using silica gel chromatography and obtained as yellow crystals (1.74 g, 90%). ¹H NMR (300 MHz, CDCl₃), δ 2.65(q, *J*=7.5 Hz, 4H), 1.27 (t, *J*=7.5 Hz, 6H).

4-Bromo-3,5-diethyl-isoxazole (44). This molecule was prepared by treatment of **39** with N-bromosuccinimide (NBS) under conditions similar to those used for the preparation of **47**. ¹H NMR (300 MHz, CDCl₃), δ 2.78 (q, *J*=7.5 Hz, 2H), 2.67 (q, *J*=7.5 Hz, 2H), 1.28-1.34 (m, 6H).

4-Bromo-3-ethyl-5-methylisoxazole (45). This molecule was prepared by treatment of **41** with NBS under conditions similar to those used for the preparation of **47**. **45** was obtained in 71% yield in a mixture with **46**. ¹H NMR (300 MHz, CDCl₃), δ 2.77 (q, *J*=7.5 Hz, 2H), 2.28 (s, 3H), 1.30 (t, *J*=7.5 Hz, 3H).

4-Bromo-5-ethyl-3-methyl-isoxazole (46). This molecule was prepared in 71% yield by treatment of **42** with NBS under conditions similar to those used for the preparation of **47**. **46** was obtained as a mixture with **45**. ¹H NMR (300 MHz, CDCl₃), δ 2.67 (q, *J*=7.5 Hz, 2H), 2.41 (s, 3H), 1.30 (t, *J*=7.5 Hz, 3H).

3-Cyclopropyl-4-iodo-5-methyl-1H-pyrazole (48). This molecule was prepared in 95% yield by treatment of **43** with NIS under conditions similar to those used for the

preparation of **47**. ^1H NMR (300 MHz, CDCl_3) δ 2.23 (s, 3H), 1.83 (m, 1H), 0.95 (m, 2H), 0.80 (m, 2H).

Synthesis of **50-52**.

t-Butyl-3-cyclopropyl-4-iodo-5-methyl-1H-pyrazole-1-carboxylate (**51**). Compound **48** (2.67 g, 10.8 mmol) was dissolved in THF and cooled to 0 $^\circ\text{C}$. $(\text{Boc})_2\text{O}$ (4.7 g, 21.5 mmol) and DMAP (1.32 g, 10.8 mmol) were added successively. After stirring at room temperature for 1 h, the solvent was removed and the crude product was purified by silica gel flash column chromatography (3.41 g, 91% yield). ^1H NMR (300 MHz, CDCl_3), δ 2.52 (s, 3H), 1.82 (m, 1H), 1.61 (s, 9H), 0.98 (m, 2H), 0.90 (m, 2H).

t-Butyl 3,5-diethyl-4-iodo-1H-pyrazole-1-carboxylate (**50**). This molecule was prepared by treatment of **47** with $(\text{Boc})_2\text{O}$ under conditions similar to those used for the preparation of **51**. ^1H NMR (300 MHz, CDCl_3), δ 3.01 (q, $J=7.5$ Hz, 2H), 2.65 (q, $J=7.5$ Hz, 2H), 1.66 (s, 9H), 1.28 (t, $J=7.5$ Hz, 3H), 1.18 (t, $J=7.5$ Hz, 3H).

t-Butyl 4-bromo-5-methyl-3-phenyl-1H-pyrazole-1-carboxylate (**52**). This molecule was prepared by treatment of **49** with $(\text{Boc})_2\text{O}$ under conditions similar to those used for the preparation of **51**. ^1H NMR (300 MHz, CDCl_3), δ 7.94 (m, 2H), 7.45 (m, 3H), 2.62 (s, 3H), 1.69 (s, 9H).

4-(8-methoxy-1-phenyl-5H-pyrido[4,3-b]indol-7-yl)-3,5-dimethylisoxazole (**55**). This molecule was prepared by coupling **6** and phenylboronic acid under conditions similar to those used for the preparation of **6**. ¹HNMR (300 MHz, MeOD-d₄) δ 8.53 (d, 1H, J=6.9 Hz), 7.98 (m, 3H), 7.86 (m, 3H), 7.61 (s, 1H), 7.17 (s, 1H), 3.63 (s, 3H), 2.33 (s, 3H), 2.15 (s, 3H). ESIMS m/z [M+H]⁺ calcd. = 370.42; found = 370.42.

4-(8-methoxy-1-(pyridin-3-yl)-5H-pyrido[4,3-b]indol-7-yl)-3,5-dimethylisoxazole (**56**). This molecule was prepared by coupling **6** and pyridin-3-ylboronic acid under conditions similar to those used for the preparation of **6**. ¹HNMR (300 MHz, MeOD-d₄) δ 9.21 (br, 1H), 9.06 (br, 1H), 8.61 (d, 1H, J=6.9 Hz), 8.49 (d, 1H, J=7.8 Hz), 8.03 (d, 1H, J=6.6 Hz), 7.93 (br, 1H), 7.65 (s, 1H), 7.07 (s, 1H), 3.67 (s, 3H), 2.33 (s, 3H), 2.15 (s, 3H). ESIMS m/z [M+H]⁺ calcd. = 371.41; found = 371.75.

4-(8-methoxy-1-(pyridin-4-yl)-5H-pyrido[4,3-b]indol-7-yl)-3,5-dimethylisoxazole (**57**). This molecule was prepared by coupling **6** and pyridin-4-ylboronic acid under conditions similar to those used for the preparation of **6**. ¹HNMR (300 MHz, MeOD-d₄) δ 9.07 (d, 2H, J= 5.7 Hz), 8.62 (d, 1H, J= 6.9 Hz), 8.06 (m, 3H), 7.65 (s, 1H), 7.12 (s, 1H), 3.67 (s, 3H), 2.33 (s, 3H), 2.15 (s, 3H). ESIMS m/z [M+H]⁺ calcd. = 371.41; found = 372.25.

4-(1-(2-fluorophenyl)-8-methoxy-5H-pyrido[4,3-b]indol-7-yl)-3,5-dimethylisoxazole (**58**). This molecule was prepared by coupling **6** and (2-fluorophenyl)boronic acid under conditions similar to those used for the preparation of **6**. ¹HNMR (300 MHz, MeOD-d₄) δ

8.61 (d, 1H, $J=6.6$ Hz), 8.03 (d, 1H, $J=6.9$ Hz), 7.94 (m, 2H), 7.66 (m, 3H), 6.96 (s, 1H), 3.62 (s, 3H), 2.33 (s, 3H), 2.15 (s, 3H). ESIMS m/z $[M+H]^+$ calcd. = 388.41; found = 388.75 .

4-(1-(3-fluorophenyl)-8-methoxy-5H-pyrido[4,3-b]indol-7-yl)-3,5-dimethylisoxazole (59).

This molecule was prepared by coupling **6** and (3-fluorophenyl)boronic acid under conditions similar to those used for the preparation of **6**. ^1H NMR (300 MHz, MeOD- d_4) δ 8.55 (d, 1H, $J=6.9$ Hz), 8.00 (d, 1H, $J=6.9$ Hz), 7.85 (m, 3H), 7.67 (m, 1H), 7.63 (s, 1H), 7.18 (s, 1H), 3.67 (s, 3H), 2.34 (s, 3H), 2.16 (s, 3H). ESIMS m/z $[M+H]^+$ calcd. = 388.41; found = 388.50 .

4-(1-(4-fluorophenyl)-8-methoxy-5H-pyrido[4,3-b]indol-7-yl)-3,5-dimethylisoxazole (60).

This molecule was prepared by coupling **6** and (4-fluorophenyl)boronic acid under conditions similar to those used for the preparation of **6**. ^1H NMR (300 MHz, MeOD- d_4) δ 8.53 (d, 1H, $J=6.9$ Hz), 8.05 (m, 2H), 7.98 (d, 1H, $J=6.6$ Hz), 7.61 (m, 2H), 7.62 (s, 1H), 7.18 (s, 1H), 3.68 (s, 3H), 2.33 (s, 3H), 2.16 (s, 3H). ESIMS m/z $[M+H]^+$ calcd. = 388.41; found = 389.08.

4-(1-(2-chlorophenyl)-8-methoxy-5H-pyrido[4,3-b]indol-7-yl)-3,5-dimethylisoxazole (61).

This molecule was prepared by coupling **6** and (2-chlorophenyl)boronic acid under conditions similar to those used for the preparation of **6**. ^1H NMR (300 MHz, MeOD- d_4) δ 8.62 (d, 1H, $J=6.9$ Hz), 8.04 (d, 1H, $J=6.6$ Hz), 7.89 (m, 3H), 7.80 (m, 1H), 7.63 (s, 1H),

6.64 (s, 1H), 3.56 (s, 3H), 2.32 (s, 3H), 2.14 (s, 3H). ESIMS m/z $[M+H]^+$ calcd. = 404.87; found = 404.92.

4-(1-(3-chlorophenyl)-8-methoxy-5H-pyrido[4,3-b]indol-7-yl)-3,5-dimethylisoxazole (62).

This molecule was prepared by coupling **6** and (3-chlorophenyl)boronic acid under conditions similar to those used for the preparation of **6**. ^1H NMR (300 MHz, MeOD- d_4) δ 8.56 (d, 1H, $J=6.9$ Hz), 8.09 (d, 1H, $J=1.2$ Hz), 8.02 (d, 1H, $J=6.9$ Hz), 7.85-7.93 (m, 3H), 7.65 (s, 1H), 7.20 (s, 1H), 3.69 (s, 3H), 2.34 (s, 3H), 2.16 (s, 3H). ESIMS m/z $[M+H]^+$ calcd. = 404.87; found = 405.00 .

4-(1-(4-chlorophenyl)-8-methoxy-5H-pyrido[4,3-b]indol-7-yl)-3,5-dimethylisoxazole (63).

This molecule was prepared by coupling **6** and (4-chlorophenyl)boronic acid under conditions similar to those used for the preparation of **6**. ^1H NMR (300 MHz, MeOD- d_4) δ 8.54(d, 1H, $J=6.9$ Hz), 8.00 (d, 2H, $J=8.7$ Hz), 7.98 (d, 1H, $J=6.6$ Hz), 7.88 (d, 2H, $J=8.7$ Hz), 7.62 (s, 1H), 7.19 (s, 1H), 3.69 (s, 3H), 2.33 (s, 3H), 2.16 (s, 3H). ESIMS m/z $[M+H]^+$ calcd. = 404.87; found =405.33 .

4-(1-([1,1'-biphenyl]-3-yl)-8-methoxy-5H-pyrido[4,3-b]indol-7-yl)-3,5-dimethylisoxazole

(64). This molecule was prepared by coupling **6** and [1,1'-biphenyl]-3-ylboronic acid under conditions similar to those used for the preparation of **6**. ^1H NMR (300 MHz, MeOD- d_4) δ 8.56 (d, 1H, $J= 6.9$ Hz), 8.29 (s, 1H), 8.15 (m, 1H), 7.98 (m, 3H), 7.81 (d,

2H, $J=7.2$ Hz), 7.62 (s, 1H), 7.50 (m, 3H), 7.26 (s, 1H), 3.50 (s, 3H), 2.32 (s, 3H), 2.14 (s, 3H). ESIMS m/z $[M+H]^+$ calcd. =446.52; found = 446.75 .

4-(1-([1,1'-biphenyl]-4-yl)-8-methoxy-5H-pyrido[4,3-b]indol-7-yl)-3,5-dimethylisoxazole (**65**). This molecule was prepared by coupling **6** and [1,1'-biphenyl]-4-ylboronic acid under conditions similar to those used for the preparation of **6**. ^1H NMR (300 MHz, MeOD- d_4) δ 8.55 (d, 1H, $J= 6.9$ Hz), 8.13 (d, 2H, $J= 8.7$ Hz), 8.08 (d, 2H, $J= 8.4$ Hz), 7.99 (d, 1H, $J= 6.6$ Hz), 7.83 (dd, 2H, $J_1= 7.8$ Hz, $J_2= 1.2$ Hz), 7.63 (s, 1H), 7.48-7.59 (m, 3H), 7.31 (s, 1H), 3.66 (s, 3H), 2.34 (s, 3H), 2.16 (s, 3H). ESIMS m/z $[M+H]^+$ calcd. = 446.52 ; found = 446.92.

4-(8-methoxy-1-(naphthalen-1-yl)-5H-pyrido[4,3-b]indol-7-yl)-3,5-dimethylisoxazole (**66**). This molecule was prepared by coupling **6** and naphthalen-1-ylboronic acid under conditions similar to those used for the preparation of **6**. ^1H NMR (300 MHz, MeOD- d_4) δ 8.65 (d, 1H, $J= 6.9$ Hz), 8.40 (d, 1H, $J= 8.1$ Hz), 8.22 (d, 1H, $J= 8.4$ Hz), 8.09 (d, 1H, $J= 6.9$ Hz), 7.93 (m, 2H), 7.70 (m, 1H), 7.59 (s, 1H), 7.54 (m, 1H), 6.10 (s, 1H), 3.11 (s, 3H), 2.27 (s, 1H), 2.07 (s, 1H). ^{13}C NMR (300 MHz, MeOD- d_4) δ 166.5, 159.5, 153.4, 147.3, 146.6, 135.8, 134.5, 133.7, 131.9, 130.3, 128.8, 128.4, 128.3, 128.1, 127.1, 125.4, 124.0, 121.8, 120.9, 119.5, 115.1, 112.9, 107.6, 103.1, 54.0, 10.0, 9.1. ESIMS m/z $[M+H]^+$ calcd. = 420.48 ; found = 420.75.

4-(8-methoxy-1-(naphthalen-2-yl)-5H-pyrido[4,3-b]indol-7-yl)-3,5-dimethylisoxazole

(67). This molecule was prepared by coupling **6** and naphthalen-2-ylboronic acid under conditions similar to those used for the preparation of **6**. ¹HNMR (300 MHz, MeOD-d₄) δ 8.57 (d, 1H, *J* = 6.9 Hz), 8.36 (d, 1H, *J* = 8.4 Hz), 8.17 (dd, 2H, *J*₁ = 6.9 Hz, *J*₂ = 1.5 Hz), 8.04 (dd, 1H, *J*₁ = 8.4 Hz, *J*₂ = 1.8 Hz), 8.00 (d, 1H, *J* = 6.6 Hz), 7.75 (m, 2H), 7.63 (s, 1H), 7.26 (s, 1H), 3.48 (s, 3H), 2.32 (s, 3H), 2.14 (s, 3H). ESIMS *m/z* [M+H]⁺ calcd. = 420.48; found = 420.92 .

4-(8-methoxy-1-(quinolin-4-yl)-5H-pyrido[4,3-b]indol-7-yl)-3,5-dimethylisoxazole **(68)**.

This molecule was prepared by coupling **6** and quinolin-4-ylboronic acid under conditions similar to those used for the preparation of **6**. ¹HNMR (300 MHz, MeOD-d₄) δ 9.31 (d, 1H), 8.74 (d, *J* = 6.9 Hz, 1H), 8.40 (d, *J* = 8.4 Hz, 1H), 8.16 (d, *J* = 6.9 Hz, 1H), 7.99-8.05 (m, 2H), 7.63-7.69 (m, 3H), 6.11 (s, 1H), 3.15 (s, 3H), 2.28 (s, 3H), 2.08 (s, 3H). ¹³CNMR (300 MHz, MeOD-d₄) δ 168.23, 161.02, 155.27, 150.52, 149.25, 146.69, 143.59, 137.82, 136.76, 134.28, 131.54, 129.05, 128.72, 126.99, 126.70, 124.51, 124.23, 121.71, 120.87, 117.11, 114.39, 110.03, 104.57, 55.90, 11.65, 10.74. ESIMS *m/z* [M+H]⁺ calcd. = 421.47; found = 421.58.

4-(1-(1H-indol-5-yl)-8-methoxy-5H-pyrido[4,3-b]indol-7-yl)-3,5-dimethylisoxazole **(70)**.

This molecule was prepared by coupling **6** and (1H-indol-5-yl)boronic acid under conditions similar to those used for the preparation of **6**. ¹HNMR (300 MHz, MeOD-d₄) δ 8.47 (d, 1H, *J* = 6.6 Hz), 8.25 (d, 1H, *J* = 1.5 Hz), 7.91 (d, 1H, *J* = 6.6 Hz), 7.84 (d, 1H, *J* =

8.4 Hz), 7.70 (dd, 1H, $J_1 = 8.4$ Hz, $J_2 = 1.8$ Hz), 7.60 (s, 1H), 7.53 (d, 1H, $J = 3.0$ Hz), 7.42 (s, 1H), 6.76 (d, 1H, $J = 3.3$ Hz), 3.56 (s, 3H), 2.33 (s, 3H), 2.15 (s, 3H). ^{13}C NMR (300 MHz, MeOD- d_4), δ 166.52, 159.57, 153.41, 150.70, 147.47, 138.01, 135.66, 133.92, 128.47, 127.17, 121.82, 121.66, 121.59, 121.44, 121.32, 117.44, 115.02, 113.09, 112.09, 106.44, 103.31, 102.08, 54.53, 10.05, 9.18. ESIMS m/z $[\text{M}+\text{H}]^+$ calcd. = 409.46; found = 409.67.

4-(1-(1H-indol-3-yl)-8-methoxy-5H-pyrido[4,3-b]indol-7-yl)-3,5-dimethylisoxazole (71).

This molecule was prepared by coupling **6** and (1H-indol-3-yl)boronic acid under conditions similar to those used for the preparation of **6**. ^1H NMR (300 MHz, MeOD- d_4) δ 8.46 (d, 1H, $J = 6.9$ Hz), 8.13 (s, 1H), 7.89 (d, 1H, $J = 6.6$ Hz), 7.72 (d, 1H, $J = 8.7$ Hz), 7.59 (s, 1H), 7.40 (m, 2H), 7.25 (m, 1H), 7.01 (s, 1H), 3.30 (s, 3H), 2.33 (s, 3H), 2.14 (s, 3H). ESIMS m/z $[\text{M}+\text{H}]^+$ calcd. = 409.46; found = 409.67.

4-methoxycyclohexanol (73). An aqueous solution (20 mL) of 1,4-cyclohexanediol (17.5 g, 150 mmol) and KOH (9.3 g, 170 mmol) was heated to reflux for one h. After cooling to room temperature, water was removed under reduced pressure, and then CH_3I (32.0 g, 230 mmol) was added. After 24 h stirring at room temperature, the reaction mixture was quenched with 100 mL water and extracted with CHCl_3 (100 mL \times 3). The combined organic fraction was dried and then purified in flash column chromatography (eluted with EtOAc:hexane = 1:1) to give 7.14 g (36%) pale yellow liquid as the title compound.

4-methoxycyclohexanone (74). **73** (7.14 g, 54.8 mmol) was dissolved in DCM (60 mL), and added slowly into a pyridinium chlorochromate (23.65 g, 109.7 mmol) DCM solution (120 mL). The resulting mixture was stirred for 4 h under a N₂ atmosphere. Pyridinium chlorochromate was filtered with H type silica gel, and the filtrate was concentrated to give 2.47 g (35%) titled compound as a pale yellow oil. ¹HNMR (300 MHz, CDCl₃) δ 3.61 (t, 1H, *J*=2.4 Hz), 3.40 (s, 3H), 2.56 (m, 2H), 2.26 (m, 2H), 2.10 (m, 2H), 1.96 (m, 2H).

4-hydrazinylpyridin-2(1H)-one (76). **75** (4.97 g, 44.7 mmol) was slowly added to a solution in 2-methoxyethanol (100 mL) of H₂N-NH₂ (9.19 g, 290 mmol). The mixture was heated to reflux for 24 h, after which the solvent was removed and 4.57 g (81.6%) title compound was obtained by recrystallization from EtOH. ¹HNMR (300 MHz, D₂O) δ 7.67 (s, 1H), 7.24 (d, 2H, *J*=7.2 Hz), 6.30 (s, 1H), 6.04 (d, 2H, *J*=7.2 Hz), 5.73 (s, 1H), 3.62 (s, 2H).

4-(2-(4-methoxycyclohexylidene)hydrazinyl)pyridin-2(1H)-one (77). **76** (2.07 g, 16.5 mmol) was suspended in **74** (2.33 g, 18.2 mmol) solution in absolute EtOH (100 mL). After being heated to reflux for 2 h, the reaction mixture was concentrated to half of its original volume. The resulting precipitates were filtered and dried to give 3.02 g (77.0%) colorless solid. ¹HNMR (300 MHz, DMSO-d₆) δ 10.50 (s, 1H), 9.28 (s, 1H), 7.07 (d, 1H,

$J=7.2$ Hz), 6.01 (d, 1H, $J=5.7$ Hz), 5.67 (d, 1H, $J=2.1$ Hz), 3.45 (m, 1H), 3.28 (s, 3H), 2.35 (m, 2H), 2.20 (m, 2H), 1.86 (m, 2H), 1.62 (m, 2H).

*8-methoxy-5H-pyrido[4,3-*b*]indol-1-ol* (**78**). **77** (1 g, 4.27 mmol) was dissolved in diphenyl ether (20 mL). The solution was heated to reflux under N₂ protection for 30 min. After cooling to room temperature, 10% Pd-C (0.3 g) was added to the mixture which was heated to reflux again for 75 min. Then hexane (40 mL) was added into the cooled mixture. The resulting precipitates were filtered and taken up into boiling AcOH (55 mL), then filtered again to get rid of Pd-C. The filtrate was concentrated to give yellow solid which is boiled in 8 mL EtOH and filtered to give 0.63 g (63.1%) of a pale yellow solid as the title compound. ¹HNMR (300 MHz, DMSO-*d*₆) δ 11.54 (s, 1H), 11.03 (s, 1H), 7.60 (d, 1H, $J=2.1$ Hz), 7.37 (d, 1H, $J=8.7$ Hz), 7.25 (m, 1H), 6.90 (dd, 1H, $J_1=2.7$ Hz, $J_2=8.7$ Hz), 6.46 (d, 1H, $J=7.2$ Hz), 3.81 (s, 3H).

3.10.2 Biochemical assays

3.10.2.1 Fluorescence polarization assay

Competitive fluorescence polarization (FP) binding assays were performed to quantitate the binding affinities of designed compounds to the BRD2-BRD4 BD1 and BD2 domains. For the development of competitive FP binding assays, we designed and synthesized a FAM labeled fluorescent probe based upon ZBA248, a potent BET inhibitor we have developed whose chemical structure is provided in the our patent¹⁵⁰. Equilibrium dissociation constants (K_d) values of ZBA248 to these six proteins were

determined from protein saturation experiments by monitoring the total fluorescence polarization of mixtures composed with the fluorescent probe at a fixed concentration and proteins with increasing concentrations up to full saturation. Serial dilutions of each tested protein were mixed with ZBA248 to a final volume of 200 μ l in the assay buffer (100 mM phosphate buffer, pH = 6.5, with 0.01% Triton X-100). The final probe concentration for all assays was 1.5 nM. Plates were incubated at room temperature for 30 min with gentle shaking to ensure equilibrium. FP values in millipolarization units (mP) were measured using the Infinite M-1000 plate reader (Tecan U.S., Research Triangle Park, NC) in Microfluor 1 96-well, black, round-bottom plates (Thermo Scientific, Waltham, MA) at an excitation wavelength of 485 nm and an emission wavelength of 530 nm. The K_d values for the interaction with ZBA248, calculated by fitting the sigmoidal dose-dependent FP, increases as a function of protein concentrations and analyzed with Graphpad Prism 6.0 software (Graphpad Software, San Diego, CA), are 2.0, 2.2, 6.5, 0.6, 5.5, and 3.0 nM to BRD2 BD1 and 2, BRD3 BD1 and 2, and BRD4 BD1 and 2, respectively.

The IC_{50} values of compounds were determined in competitive binding experiments. Mixtures of 10 μ l of the compound in an assay buffer with 40% ethylene glycol and 190 μ l of preincubated protein/probe complex solution in the assay buffer were added into assay plates which were incubated at room temperature for 30 min with gentle shaking. Final concentrations of proteins were 3, 6, 15, 2, 10, and 6 nM in assays for BD1 and BD2 of BRD2, BRD3, and BRD4 BD2, respectively. The final probe concentration in all competitive experiments was 1.5 nM. Negative controls containing

protein/probe complex only (equivalent to 0% inhibition), and positive controls containing only free probes (equivalent to 100% inhibition), were included on each assay plate. FP values were measured as described above. IC₅₀ values were determined by nonlinear regression fitting of the competition curves. K_i values of competitive inhibitors were obtained directly by nonlinear regression fitting, based upon the K_d values of the probe to different proteins, and the concentrations of the proteins and probes in the competitive assays^{151, 152}.

3.10.2.2 Bio-layer Interferometry (BLI)

BLI experiments were performed using an OctetRED96 instrument from PALL/ForteBio. All experiments were performed at 25 °C using PBS (pH 7.4) as the assay buffer, to which 0.1% BSA and 0.01% Tween-20 were added to reduce nonspecific interactions. 0.5% DMSO was also introduced to increase compound solubility. Assays were conducted in Greiner 96 well black flat-bottom microplates containing the protein solutions, pure assay buffer for dissociation, and serial dilutions of the compounds being tested. During the experiment, sample plates were continuously shaken at 1000 RPM to eliminate a mass transport effect.

Biotinylated proteins prepared using the Thermo EZ-Link long-chain biotinylation reagent were immobilized on Super Streptavidin (SSA) biosensors by dipping sensors into plate wells containing protein solutions whose concentrations were pre-determined from control experiments to achieve the best signal to noise ratio. Sensor saturation was typically achieved in 10-15 min. Biotinylated blocked Streptavidin (SAV-

B4) sensors were prepared as the inactive reference controls following the protocol provided by the manufacturer. Sensors loaded with proteins were moved and dipped into wells with pure assay buffer then washed in the buffer for 10 min to eliminate loose nonspecific bound protein and establish a stable base line. Assessment was conducted of association-dissociation cycles of compounds started by moving and dipping sensors into the solutions of the compounds and pure buffer wells alternately starting from the lowest concentration of compound. Association and dissociation times were carefully determined to ensure full association and dissociation.

Buffer-only reference was included in all assays. Raw kinetic data collected were processed with the Data Analysis software provided by the manufacturer using double reference subtraction in which both buffer-only reference and inactive protein reference were subtracted. The resulting data were analyzed based on a 1:1 binding model from which k_{on} and k_{off} values were obtained and then K_d values were calculated.

3.10.3 Cellular assays

Cell lines obtained from the American Type Culture Collection (ATCC) were used within three months of thawing fresh vials. Cells were maintained in the recommended culture medium with 10% FBS at 37 °C and an atmosphere of 5% CO₂. The effect of BET inhibitors on cell viability was determined in a 4-day proliferation assay as described previously¹⁵³. Cells were seeded in 96-well white opaque cell culture plates at a density of 3,000-10,000 cells/well in 75 µL of culture medium. Each compound tested was serially diluted in the appropriate medium, and 75 µL of a diluted

solution containing the compound was added to the appropriate wells of the plate. After the addition of the tested compound, the cells were incubated at 37 °C in an atmosphere of 5% CO₂ for 4 days. Cell viability was determined using the CellTiter-Glo® Luminescent Cell Viability Assay Kit (Promega, Madison, WI) according to the manufacturer's instructions. The luminescent signal was measured using a Tecan Infinite M1000 multimode microplate reader (Tecan, Morrisville, NC). The readings were normalized to the DMSO-treated cells and the IC₅₀ values were calculated by nonlinear regression analysis using the GraphPad Prism 5 software.

3.10.4 Molecular modeling

The co-crystal structures of BRD4 BD1 in a complex with compound **3** (PDB entry: 3ZYU), BRD4 BD2 in a complex with GW841819X (PDB entry: 2YEM) and BRD4 BD2 in a complex with compound **6** were used to model the binding poses of designed compounds with BRD4 BD1 and BRD4 BD2. Chain A of the BRD4 BD1 crystal structure was first extracted and protons were added using the “protonate 3D” module in MOE¹⁵⁴ where protonation states of His residues at pH 7.0 were determined by considering neighboring residues in the structure. All water molecules from the crystal structure were saved. The same procedures were used for BRD4 BD2 protein. The designed compound structures were drawn and optimized using the MOE program. All the binding poses of designed compounds with BRD4 BD1 were modeled using the GOLD program (version 4.0.1)^{155, 156}. The center of the binding site for BRD4 BD1 was set at C136 and that for BRD4 BD2 at C429. The radius of the binding site in both cases was defined as 11 Å, large enough to cover the entire binding pocket. At the binding site,

water molecules A2129, A2137 and A2178 of BRD4 BD1 (PDB entry: 3ZYU) were included during the docking simulations where flags of on, toggle, toggle were set individually and allowed to spin for optimal hydrogen bond interaction. In each genetic algorithm (GA) run, a maximum number of 200,000 operations were performed on a population of 5 islands each of 100 individuals. Operator weights for crossover, mutation and migration were set to 95, 95 and 10 respectively. The docking simulations were terminated after 20 runs for each ligand. ChemScore implemented in Gold 4.0.1 was used as the fitness function to evaluate the docked poses. The 20 conformations ranked highest by each fitness function were saved for analysis of the predicted docking modes.

3.10.5 Crystallization and structure determination

BRD4 BD2 (residues 333-460) was concentrated to ~8 mg/mL and incubated with a 2-fold excess of the inhibitor prior to crystallization setup. Crystals were grown in 50% polyethylene glycol 600, 0.1 M Tris pH 8.0, and 0.01 to 0.10 M ATP. Data were collected at the Advance Photon Source at Argonne National Lab on the LS-CAT beamlines 21-ID-F. The complex was crystallized in space group P21212 and contained 1 molecule per asymmetric unit. Data were processed with HKL2000¹⁵⁷ and the structure was solved by molecular replacement with Phaser¹⁵⁸ using PDB code 2OUO as a model. The structure was refined with Buster¹⁵⁹ and electron density maps fit with COOT¹⁶⁰. Coordinates and restraints for the compound were developed using Grade with the mogul+qm option¹⁵⁹. The co-crystal structures were validated using Molprobability¹⁶¹, Parvati¹⁶², and Whatcheck¹⁶³. Ligand statistics were obtained from the Uppsala Electron-Density Server¹⁶⁴.

3.10.6 Pharmacokinetic analysis

Quantitative analysis of drug concentration in mouse plasma and tumor tissue was completed using the previously reported method¹⁶⁵.

3.10.7 *In vivo* antitumor efficacy

The antitumor activity of RX-201 in MDA-MB-436 xenograft model was tested using the previously reported method¹⁶⁶.

CHAPTER 4

Perspective of targeting protein-protein interactions using peptide or non-peptide small-molecules for cancer targeted therapy

In the previous two chapters, the application of either stapled peptides or non-peptidic small-molecules to block PPIs with oncogenic significance is described. These two projects have different backgrounds such as the level of biological understanding, shape of PPI interfaces and availability of known ligands. These features allow design of two types of molecules serving either as a pharmacological tool to validate the target or as a clinical candidate with improved drug-like properties.

The RAP1 project starts with limited biological information and no reported ligand and design of a tool molecule to study biological consequences is a priority for the project. Due to its large and hydrophobic features at the RAP1/TRF2 interface, a peptide, a fragment of the protein, was the initial direct chemical entity. In contrast, BET bromodomains have already been validated as targets with four clinical drugs developed by different institutions (Clinicaltrials.gov). Therefore, the aim of this project is to develop a new scaffold that has superior anticancer activity than other clinical compounds. I would like to discuss some of my experience and understanding gained over five years regarding application of these two types of molecules in the area of inhibition of oncogenic PPIs.

As mentioned earlier, a peptide represents a straightforward ligand design strategy for PPI targets. Oncogenic PPIs are largely unexplored and employment of natural or

structurally modified peptides will accelerate ligand discovery and target validation. Peptide-based molecules can be applied as biochemical tools for small-molecule screening⁸⁶, they can penetrate cell membranes to bind to intracellular targets enabling a study of the biology of the system³⁸, or they can be converted to a “drug-like” peptide mimetic that may benefit patients clinically¹⁶⁷. Although a peptide would appear to have applications as broad as those of small molecules, the length, charge and conformation of the specific peptide sequence will largely determine its fate.

As discussed in Chapter 1, the peptide ligand of XIAP: Smac, is a four-amino acid sequence, AVPI, with all hydrophobic side chains. Such a simple and charge free nature facilitated conversion of the tetrapeptide into clinical compounds. Clinical molecules (**Figure 1**), still retain a largely peptide scaffold and carry a net positive charge that was thought to be favorable for membrane penetration and water solubility¹⁶⁸.

For more complex peptides, the task is more difficult. For example, α -helices containing PPI interfaces such as MDM2/p53, RAP1/TRF2 and Bcl-2 family members have all been probed by stapled peptides^{38, 169}. These molecules were used to establish biochemical assays, or as tool molecules to study biology in cells. However, none of the stapled peptides or even peptides with secondary structure entered clinical trials targeting intracellular oncogenic targets. In fact not every stapled peptide even works well in cells¹⁷⁰. As discussed in both Walensky's¹⁷¹ and our studies, stapling alone does not guarantee high helical propensity, target protein binding affinity or potent cellular activity. And fine-tuning of the sequence is necessary to obtain potent and cell-permeable stapled

peptides. As shown in **Figure 29**, charge difference at the terminal residues of one stapled peptide can lead to diverse cellular performance¹⁷¹. This notwithstanding, it is still unclear whether or not a stapled α -helix can be used as drug. Efforts to put stapled peptides into human studies are continually being made; an example is ATSP-7041¹⁶⁹, a first-in-class p53 re-activator under development by Aileron and Roche and currently in preclinical trials. However, no structured peptide has been reported to have clinical value in oncogenic PPI inhibition, suggesting the difficulty and limitation of peptides in this field.

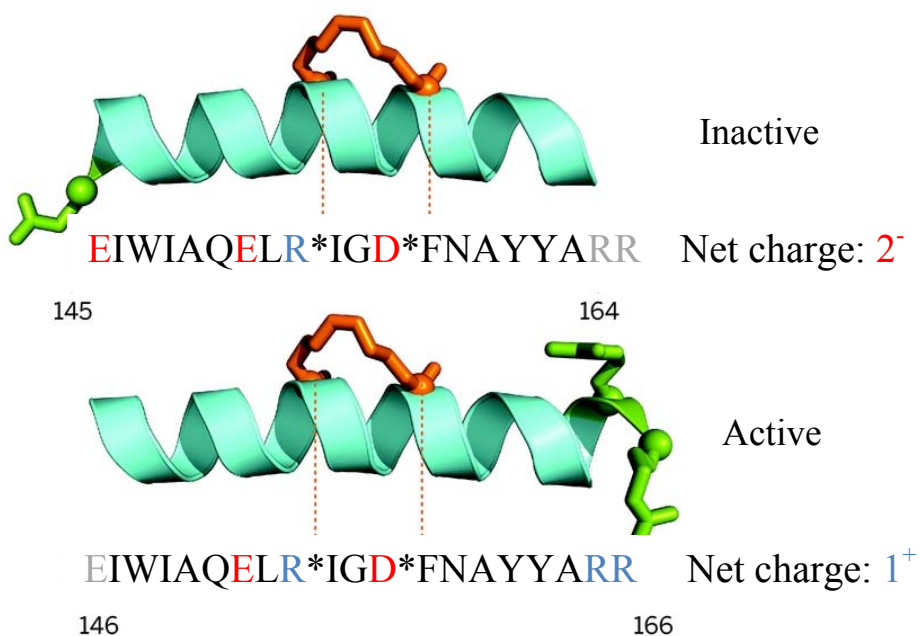


Figure 29 Charge difference is important in cellular activity of stapled peptides.

Non-peptide small-molecule probes on the other hand can easily be converted to “drug-like” molecules that function *in vivo*, but one of the difficulties regarding design of

small-molecular PPI inhibitors is the larger surface area compared with traditional targets like enzymes or receptors. This normally results in inhibitor molecules with larger structural complexity and diversity, and requires more efforts in lead discovery and optimization. The discovery of clinical compounds ABT-263, MI-77301 and I-BET762 employs various screening techniques such as fragment-based screening, virtual screening, and phenotypic and chemoproteomic screening^{48, 139, 172}. Compared to peptides which are normally a fragment of one PPI member, screening of initial leads and subsequent optimization are costly in terms of resources and risks. Unlike peptides, small-molecules are not endogenous ligands for PPIs, so the specificity of the molecule should be carefully examined at the outset. As PPI interfaces are mostly hydrophobic, exclusion of false-positive results and careful interpretation of SAR are primary concerns. Finally, preparation of small-molecules involves multi-step syntheses which are clearly more complicated than (largely automated) peptide synthesis.

To summarize my understanding with peptide and small-molecular PPI inhibitors, in view of the advantages of peptides in early stage studies, they can be used to probe unexplored PPI interfaces. This effort could provide new biological discoveries and preliminary SAR that will guide the discovery of small molecules, therefore pushing the project further into deeper biological and even human studies which may finally benefit patients in the clinic.

REFERENCES

1. <http://www.cancerresearchuk.org/>. Worldwide cancer mortality statistics.
2. Dobbstein, M.; Moll, U. Targeting tumour-supportive cellular machineries in anticancer drug development. *Nature reviews. Drug discovery* **2014**, *13*, 179-96.
3. Goodman, L. S.; Wintrobe, M. M.; et al. Nitrogen mustard therapy; use of methyl-bis (beta-chloroethyl) amine hydrochloride and tris (beta-chloroethyl) amine hydrochloride for Hodgkin's disease, lymphosarcoma, leukemia and certain allied and miscellaneous disorders. *Journal of the American Medical Association* **1946**, *132*, 126-32.
4. Hertz, R.; Li, M. C.; Spencer, D. B. Effect of methotrexate therapy upon choriocarcinoma and chorioadenoma. *Proceedings of the Society for Experimental Biology and Medicine. Society for Experimental Biology and Medicine* **1956**, *93*, 361-6.
5. Johnson, I. S.; Armstrong, J. G.; Gorman, M.; Burnett, J. P., Jr. The Vinca Alkaloids: A New Class of Oncolytic Agents. *Cancer research* **1963**, *23*, 1390-427.
6. Gordon, M.; Hollander, S. Review of platinum anticancer compounds. *Journal of medicine* **1993**, *24*, 209-65.
7. Jordheim, L. P.; Durantel, D.; Zoulim, F.; Dumontet, C. Advances in the development of nucleoside and nucleotide analogues for cancer and viral diseases. *Nature reviews. Drug discovery* **2013**, *12*, 447-64.
8. Schiff, P. B.; Horwitz, S. B. Taxol stabilizes microtubules in mouse fibroblast cells. *Proceedings of the National Academy of Sciences of the United States of America* **1980**, *77*, 1561-5.
9. Muggia, F.; Kudlowitz, D. Novel taxanes. *Anti-cancer drugs* **2014**, *25*, 593-8.
10. Buchdunger, E.; Zimmermann, J.; Mett, H.; Meyer, T.; Muller, M.; Druker, B. J.; Lydon, N. B. Inhibition of the Abl protein-tyrosine kinase in vitro and in vivo by a 2-phenylaminopyrimidine derivative. *Cancer research* **1996**, *56*, 100-4.
11. van Oosterom, A. T.; Judson, I.; Verweij, J.; Stroobants, S.; Donato di Paola, E.; Dimitrijevic, S.; Martens, M.; Webb, A.; Scot, R.; Van Glabbeke, M.; Silberman, S.; Nielsen, O. S. Safety and efficacy of imatinib (STI571) in metastatic gastrointestinal stromal tumours: a phase I study. *Lancet* **2001**, *358*, 1421-3.
12. Dagher, R.; Cohen, M.; Williams, G.; Rothmann, M.; Gobburu, J.; Robbie, G.; Rahman, A.; Chen, G.; Staten, A.; Griebel, D.; Pazdur, R. Approval summary: imatinib mesylate in the treatment of metastatic and/or unresectable malignant gastrointestinal stromal tumors. *Clinical cancer research : an official journal of the American Association for Cancer Research* **2002**, *8*, 3034-8.
13. Baselga, J.; Averbuch, S. D. ZD1839 ('Iressa') as an anticancer agent. *Drugs* **2000**, *60* Suppl 1, 33-40; discussion 41-2.
14. Cohen, M. H.; Williams, G. A.; Sridhara, R.; Chen, G.; Pazdur, R. FDA drug approval summary: gefitinib (ZD1839) (Iressa) tablets. *The oncologist* **2003**, *8*, 303-6.
15. Baselga, J.; Tripathy, D.; Mendelsohn, J.; Baughman, S.; Benz, C. C.; Dantis, L.; Sklarin, N. T.; Seidman, A. D.; Hudis, C. A.; Moore, J.; Rosen, P. P.; Twaddell, T.; Henderson, I. C.; Norton, L. Phase II study of weekly intravenous trastuzumab (Herceptin) in patients with HER2/neu-overexpressing metastatic breast cancer. *Seminars in oncology* **1999**, *26*, 78-83.
16. Ryan, Q.; Ibrahim, A.; Cohen, M. H.; Johnson, J.; Ko, C. W.; Sridhara, R.; Justice, R.; Pazdur, R. FDA drug approval summary: lapatinib in combination with capecitabine for

- previously treated metastatic breast cancer that overexpresses HER-2. *The oncologist* **2008**, 13, 1114-9.
17. Groenendijk, F. H.; Bernardis, R. Drug resistance to targeted therapies: deja vu all over again. *Molecular oncology* **2014**, 8, 1067-83.
 18. Weisberg, E.; Griffin, J. D. Mechanisms of resistance imatinib (STI571) in preclinical models and in leukemia patients. *Drug resistance updates : reviews and commentaries in antimicrobial and anticancer chemotherapy* **2001**, 4, 22-8.
 19. Krystal, G. W. Mechanisms of resistance to imatinib (STI571) and prospects for combination with conventional chemotherapeutic agents. *Drug resistance updates : reviews and commentaries in antimicrobial and anticancer chemotherapy* **2001**, 4, 16-21.
 20. Flaherty, K. T.; Infante, J. R.; Daud, A.; Gonzalez, R.; Kefford, R. F.; Sosman, J.; Hamid, O.; Schuchter, L.; Cebon, J.; Ibrahim, N.; Kudchadkar, R.; Burris, H. A., 3rd; Falchook, G.; Algazi, A.; Lewis, K.; Long, G. V.; Puzanov, I.; Lebowitz, P.; Singh, A.; Little, S.; Sun, P.; Allred, A.; Ouellet, D.; Kim, K. B.; Patel, K.; Weber, J. Combined BRAF and MEK inhibition in melanoma with BRAF V600 mutations. *The New England journal of medicine* **2012**, 367, 1694-703.
 21. Spigel, D. R.; Burris, H. A., 3rd; Greco, F. A.; Shipley, D. L.; Friedman, E. K.; Waterhouse, D. M.; Whorf, R. C.; Mitchell, R. B.; Daniel, D. B.; Zangmeister, J.; Bass, J. D.; Hainsworth, J. D. Randomized, double-blind, placebo-controlled, phase II trial of sorafenib and erlotinib or erlotinib alone in previously treated advanced non-small-cell lung cancer. *Journal of clinical oncology : official journal of the American Society of Clinical Oncology* **2011**, 29, 2582-9.
 22. Teicher, B. A.; Ara, G.; Herbst, R.; Palombella, V. J.; Adams, J. The proteasome inhibitor PS-341 in cancer therapy. *Clinical cancer research : an official journal of the American Association for Cancer Research* **1999**, 5, 2638-45.
 23. Kane, R. C.; Bross, P. F.; Farrell, A. T.; Pazdur, R. Velcade: U.S. FDA approval for the treatment of multiple myeloma progressing on prior therapy. *The oncologist* **2003**, 8, 508-13.
 24. Richon, V. M.; Emiliani, S.; Verdin, E.; Webb, Y.; Breslow, R.; Rifkind, R. A.; Marks, P. A. A class of hybrid polar inducers of transformed cell differentiation inhibits histone deacetylases. *Proceedings of the National Academy of Sciences of the United States of America* **1998**, 95, 3003-7.
 25. Mann, B. S.; Johnson, J. R.; Cohen, M. H.; Justice, R.; Pazdur, R. FDA approval summary: vorinostat for treatment of advanced primary cutaneous T-cell lymphoma. *The oncologist* **2007**, 12, 1247-52.
 26. Arrowsmith, C. H.; Bountra, C.; Fish, P. V.; Lee, K.; Schapira, M. Epigenetic protein families: a new frontier for drug discovery. *Nature reviews. Drug discovery* **2012**, 11, 384-400.
 27. Trepel, J.; Mollapour, M.; Giaccone, G.; Neckers, L. Targeting the dynamic HSP90 complex in cancer. *Nature reviews. Cancer* **2010**, 10, 537-49.
 28. Whitesell, L.; Lindquist, S. L. HSP90 and the chaperoning of cancer. *Nature reviews. Cancer* **2005**, 5, 761-72.
 29. Nero, T. L.; Morton, C. J.; Holien, J. K.; Wielens, J.; Parker, M. W. Oncogenic protein interfaces: small molecules, big challenges. *Nature reviews. Cancer* **2014**, 14, 248-62.
 30. Azzarito, V.; Long, K.; Murphy, N. S.; Wilson, A. J. Inhibition of alpha-helix-mediated protein-protein interactions using designed molecules. *Nature Chemistry* **2013**, 5, 161-173.
 31. Higuero, A. P.; Jubb, H.; Blundell, T. L. Protein-protein interactions as druggable targets: recent technological advances. *Current opinion in pharmacology* **2013**, 13, 791-6.
 32. Arkin, M. R.; Tang, Y.; Wells, J. A. Small-molecule inhibitors of protein-protein interactions: progressing toward the reality. *Chemistry & biology* **2014**, 21, 1102-14.

33. Pollak, M. N. Insulin-like growth factors and neoplasia. *Novartis Foundation symposium* **2004**, 262, 84-98; discussion 98-107, 265-8.
34. Hartman, G. D.; Egbertson, M. S.; Halczenko, W.; Laswell, W. L.; Duggan, M. E.; Smith, R. L.; Naylor, A. M.; Manno, P. D.; Lynch, R. J.; Zhang, G.; et al. Non-peptide fibrinogen receptor antagonists. 1. Discovery and design of exosite inhibitors. *Journal of Medicinal Chemistry* **1992**, 35, 4640-2.
35. Two i.v. antiplatelet agents marketed for coronary disease. *American journal of health-system pharmacy : AJHP : official journal of the American Society of Health-System Pharmacists* **1998**, 55, 1440, 1443.
36. Bogan, A. A.; Thorn, K. S. Anatomy of hot spots in protein interfaces. *Journal of molecular biology* **1998**, 280, 1-9.
37. Cukuroglu, E.; Engin, H. B.; Gursoy, A.; Keskin, O. Hot spots in protein-protein interfaces: Towards drug discovery. *Progress in biophysics and molecular biology* **2014**.
38. Walensky, L. D.; Kung, A. L.; Escher, I.; Malia, T. J.; Barbuto, S.; Wright, R. D.; Wagner, G.; Verdine, G. L.; Korsmeyer, S. J. Activation of apoptosis in vivo by a hydrocarbon-stapled BH3 helix. *Science* **2004**, 305, 1466-1470.
39. Lipinski, C. A. Lead- and drug-like compounds: the rule-of-five revolution. *Drug discovery today. Technologies* **2004**, 1, 337-41.
40. Lipinski, C. A.; Lombardo, F.; Dominy, B. W.; Feeney, P. J. Experimental and computational approaches to estimate solubility and permeability in drug discovery and development settings. *Advanced drug delivery reviews* **2001**, 46, 3-26.
41. Holcik, M.; Korneluk, R. G. Functional characterization of the X-linked inhibitor of apoptosis (XIAP) internal ribosome entry site element: role of La autoantigen in XIAP translation. *Molecular and cellular biology* **2000**, 20, 4648-57.
42. Wilkinson, J. C.; Cepero, E.; Boise, L. H.; Duckett, C. S. Upstream regulatory role for XIAP in receptor-mediated apoptosis. *Molecular and cellular biology* **2004**, 24, 7003-14.
43. Huang, Y.; Park, Y. C.; Rich, R. L.; Segal, D.; Myszka, D. G.; Wu, H. Structural basis of caspase inhibition by XIAP: differential roles of the linker versus the BIR domain. *Cell* **2001**, 104, 781-90.
44. Dhalluin, C.; Carlson, J. E.; Zeng, L.; He, C.; Aggarwal, A. K.; Zhou, M. M. Structure and ligand of a histone acetyltransferase bromodomain. *Nature* **1999**, 399, 491-6.
45. Shi, J.; Vakoc, C. R. The mechanisms behind the therapeutic activity of BET bromodomain inhibition. *Molecular Cell* **2014**, 54, 728-36.
46. Sattler, M.; Liang, H.; Nettlesheim, D.; Meadows, R. P.; Harlan, J. E.; Eberstadt, M.; Yoon, H. S.; Shuker, S. B.; Chang, B. S.; Minn, A. J.; Thompson, C. B.; Fesik, S. W. Structure of Bcl-xL-Bak peptide complex: recognition between regulators of apoptosis. *Science* **1997**, 275, 983-6.
47. Kussie, P. H.; Gorina, S.; Marechal, V.; Elenbaas, B.; Moreau, J.; Levine, A. J.; Pavletich, N. P. Structure of the MDM2 oncoprotein bound to the p53 tumor suppressor transactivation domain. *Science* **1996**, 274, 948-53.
48. Oltersdorf, T.; Elmore, S. W.; Shoemaker, A. R.; Armstrong, R. C.; Augeri, D. J.; Belli, B. A.; Bruncko, M.; Deckwerth, T. L.; Dinges, J.; Hajduk, P. J.; Joseph, M. K.; Kitada, S.; Korsmeyer, S. J.; Kunzer, A. R.; Letai, A.; Li, C.; Mitten, M. J.; Nettlesheim, D. G.; Ng, S.; Nimmer, P. M.; O'Connor, J. M.; Oleksijew, A.; Petros, A. M.; Reed, J. C.; Shen, W.; Tahir, S. K.; Thompson, C. B.; Tomaselli, K. J.; Wang, B.; Wendt, M. D.; Zhang, H.; Fesik, S. W.; Rosenberg, S. H. An inhibitor of Bcl-2 family proteins induces regression of solid tumours. *Nature* **2005**, 435, 677-81.

49. Tse, C.; Shoemaker, A. R.; Adickes, J.; Anderson, M. G.; Chen, J.; Jin, S.; Johnson, E. F.; Marsh, K. C.; Mitten, M. J.; Nimmer, P.; Roberts, L.; Tahir, S. K.; Xiao, Y.; Yang, X.; Zhang, H.; Fesik, S.; Rosenberg, S. H.; Elmore, S. W. ABT-263: a potent and orally bioavailable Bcl-2 family inhibitor. *Cancer research* **2008**, *68*, 3421-8.
50. Vassilev, L. T.; Vu, B. T.; Graves, B.; Carvajal, D.; Podlaski, F.; Filipovic, Z.; Kong, N.; Kammlott, U.; Lukacs, C.; Klein, C.; Fotouhi, N.; Liu, E. A. In vivo activation of the p53 pathway by small-molecule antagonists of MDM2. *Science* **2004**, *303*, 844-8.
51. Zhao, Y.; Yu, S.; Sun, W.; Liu, L.; Lu, J.; McEachern, D.; Shargary, S.; Bernard, D.; Li, X.; Zhao, T.; Zou, P.; Sun, D.; Wang, S. A potent small-molecule inhibitor of the MDM2-p53 interaction (MI-888) achieved complete and durable tumor regression in mice. *Journal of Medicinal Chemistry* **2013**, *56*, 5553-61.
52. Wang, S.; Sun, W.; Zhao, Y.; McEachern, D.; Meaux, I.; Barriere, C.; Stuckey, J. A.; Meagher, J. L.; Bai, L.; Liu, L.; Hoffman-Luca, C. G.; Lu, J.; Shangary, S.; Yu, S.; Bernard, D.; Aguilar, A.; Dos-Santos, O.; Besret, L.; Guerif, S.; Pannier, P.; Gorge-Bernat, D.; Debussche, L. SAR405838: an optimized inhibitor of MDM2-p53 interaction that induces complete and durable tumor regression. *Cancer research* **2014**, *74*, 5855-65.
53. Livingston, D.; Alexander, S.; Bond, J.; Briggs, T.; Fraley, A.; Hale, S.; Landsman, T.; Martinelli, R.; Shortsleeves, K.; Terrett, N.; Walsh, N. Identification and Characterization of Synthetic Small Molecule Macrocyclic Antagonists of Human IL17A. *Arthritis and Rheumatism* **2012**, *64*, S770-S770.
54. Wang, Y.; Coulombe, R.; Cameron, D. R.; Thauvette, L.; Massariol, M. J.; Amon, L. M.; Fink, D.; Titolo, S.; Welchner, E.; Yoakim, C.; Archambault, J.; White, P. W. Crystal structure of the E2 transactivation domain of human papillomavirus type 11 bound to a protein interaction inhibitor. *Journal of Biological Chemistry* **2004**, *279*, 6976-6985.
55. Shore, D. RAP1: a protean regulator in yeast. *Trends in genetics : TIG* **1994**, *10*, 408-12.
56. de Lange, T. Shelterin: the protein complex that shapes and safeguards human telomeres. *Genes Dev* **2005**, *19*, 2100-10.
57. Sfeir, A.; Kabir, S.; van Overbeek, M.; Celli, G. B.; de Lange, T. Loss of Rap1 Induces Telomere Recombination in the Absence of NHEJ or a DNA Damage Signal. *Science* **2010**, *327*, 1657-1661.
58. Greenwood, J.; Cooper, J. P. Trapping Rap1 at the telomere to prevent chromosome end fusions. *Embo Journal* **2009**, *28*, 3277-3278.
59. Xin, H. W.; Liu, D.; Zhou, S. Y. The telosome/shelterin complex and its functions. *Genome Biology* **2008**, *9*, 232.1-232.7.
60. Kanoh, J.; Ishikawa, F. Composition and conservation of the telomeric complex. *Cellular and molecular life sciences : CMLS* **2003**, *60*, 2295-302.
61. Blasco, M. A. Telomeres and human disease: ageing, cancer and beyond. *Nature reviews. Genetics* **2005**, *6*, 611-22.
62. Kovalchuk, O.; Hendricks, C. A.; Cassie, S.; Engelward, A. J.; Engelward, B. P. In vivo recombination after chronic damage exposure falls to below spontaneous levels in "recombomice". *Molecular cancer research : MCR* **2004**, *2*, 567-73.
63. Martinez, P.; Thanasoula, M.; Carlos, A. R.; Gomez-Lopez, G.; Tejera, A. M.; Schoeftner, S.; Dominguez, O.; Pisano, D. G.; Tarsounas, M.; Blasco, M. A. Mammalian Rap1 controls telomere function and gene expression through binding to telomeric and extratelomeric sites. *Nature Cell Biology* **2010**, *12*, 768-80.
64. Papai, G.; Tripathi, M. K.; Ruhlmann, C.; Layer, J. H.; Weil, P. A.; Schultz, P. TFIIA and the transactivator Rap1 cooperate to commit TFIID for transcription initiation. *Nature* **2010**, *465*, 956-60.

65. Yeung, F.; Ramirez, C. M.; Mateos-Gomez, P. A.; Pinzaru, A.; Ceccarini, G.; Kabir, S.; Fernandez-Hernando, C.; Sfeir, A. Nontelomeric role for Rap1 in regulating metabolism and protecting against obesity. *Cell reports* **2013**, *3*, 1847-56.
66. Martinez, P.; Gomez-Lopez, G.; Garcia, F.; Mercken, E.; Mitchell, S.; Flores, J. M.; de Cabo, R.; Blasco, M. A. RAP1 protects from obesity through its extratelomeric role regulating gene expression. *Cell reports* **2013**, *3*, 2059-74.
67. Teo, H. L.; Ghosh, S.; Luesch, H.; Ghosh, A.; Wong, E. T.; Malik, N.; Orth, A.; de Jesus, P.; Perry, A. S.; Oliver, J. D.; Tran, N. L.; Speiser, L. J.; Wong, M.; Saez, E.; Schultz, P.; Chanda, S. K.; Verma, I. M.; Tergaonkar, V. Telomere-independent Rap1 is an IKK adaptor and regulates NF-kappa B-dependent gene expression. *Nature Cell Biology* **2010**, *12*, 758-U26.
68. Chen, Y.; Rai, R.; Zhou, Z. R.; Kanoh, J.; Ribeyre, C.; Yang, Y.; Zheng, H.; Damay, P.; Wang, F.; Tsujii, H.; Hiraoka, Y.; Shore, D.; Hu, H. Y.; Chang, S.; Lei, M. A conserved motif within RAP1 has diversified roles in telomere protection and regulation in different organisms. *Nature structural & molecular biology* **2011**, *18*, 213-21.
69. Verdine, G. Drugging "Undruggable" Targets Using Stapled Peptides. *Biopolymers* **2009**, *92*, 296-296.
70. Duong, M. T.; Sahin, E. RAP1: protector of telomeres, defender against obesity. *Cell reports* **2013**, *3*, 1757-8.
71. Chapman, R. N.; Dimartino, G.; Arora, P. S. A highly stable short alpha-helix constrained by a main-chain hydrogen-bond surrogate. *Journal of the American Chemical Society* **2004**, *126*, 12252-12253.
72. Wang, D. Y.; Liao, W.; Arora, P. S. Binding properties of artificial a helices derived from a hydrogen-bond surrogate: Application to Bcl-xL. *Angewandte Chemie-International Edition* **2005**, *44*, 6525-6529.
73. Henchey, L. K.; Porter, J. R.; Ghosh, I.; Arora, P. S. High Specificity in Protein Recognition by Hydrogen-Bond-Surrogate alpha-Helices: Selective Inhibition of the p53/MDM2 Complex. *Chembiochem* **2010**, *11*, 2104-2107.
74. Henchey, L. K.; Kushal, S.; Dubey, R.; Chapman, R. N.; Olenyuk, B. Z.; Arora, P. S. Inhibition of Hypoxia Inducible Factor 1-Transcription Coactivator Interaction by a Hydrogen Bond Surrogate alpha-Helix. *Journal of the American Chemical Society* **2010**, *132*, 941+.
75. Kneissl, S.; Loveridge, E. J.; Williams, C.; Crump, M. P.; Allemann, R. K. Photocontrollable Peptide-Based Switches Target the Anti-Apoptotic Protein Bcl-X-L. *Chembiochem* **2008**, *9*, 3046-3054.
76. Andrews, M. J. I.; Tabor, A. B. Forming stable helical peptides using natural and artificial amino acids. *Tetrahedron* **1999**, *55*, 11711-11743.
77. Garner, J.; Harding, M. M. Design and synthesis of alpha-helical peptides and mimetics. *Organic & Biomolecular Chemistry* **2007**, *5*, 3577-3585.
78. Galande, A. K.; Bramlett, K. S.; Trent, J. O.; Burris, T. P.; Wittliff, J. L.; Spatola, A. F. Potent inhibitors of LXXLL-based protein-protein interactions. *Chembiochem* **2005**, *6*, 1991-1998.
79. Judice, J. K.; Tom, J. Y.; Huang, W.; Wrin, T.; Vennari, J.; Petropoulos, C. J.; McDowell, R. S. Inhibition of HIV type 1 infectivity by constrained alpha-helical peptides: implications for the viral fusion mechanism. *Proceedings of the National Academy of Sciences of the United States of America* **1997**, *94*, 13426-30.
80. Harrison, R. S.; Shepherd, N. E.; Hoang, H. N.; Ruiz-Gomez, G.; Hill, T. A.; Driver, R. W.; Desai, V. S.; Young, P. R.; Abbenante, G.; Fairlie, D. P. Downsizing human, bacterial, and viral proteins to short water-stable alpha helices that maintain biological potency. *Proceedings of the National Academy of Sciences of the United States of America* **2010**, *107*, 11686-91.

81. Blackwell, H. E.; Grubbs, R. H. Highly efficient synthesis of covalently cross-linked peptide helices by ring-closing metathesis. *Angewandte Chemie-International Edition* **1998**, *37*, 3281-3284.
82. Schafmeister, C. E.; Po, J.; Verdine, G. L. An all-hydrocarbon cross-linking system for enhancing the helicity and metabolic stability of peptides. *Journal of the American Chemical Society* **2000**, *122*, 5891-5892.
83. Walensky, L. D.; Pitter, K.; Morash, J.; Oh, K. J.; Barbuto, S.; Fisher, J.; Smith, E.; Verdine, G. L.; Korsmeyer, S. J. A stapled BID BH3 helix directly binds and activates BAX. *Molecular Cell* **2006**, *24*, 199-210.
84. Kim, Y. W.; Kutchukian, P. S.; Verdine, G. L. Introduction of All-Hydrocarbon $i,i+3$ Staples into alpha-Helices via Ring-Closing Olefin Metathesis. *Organic Letters* **2010**, *12*, 3046-3049.
85. Hilinski, G. J.; Kim, Y. W.; Hong, J.; Kutchukian, P. S.; Crenshaw, C. M.; Berkovitch, S. S.; Chang, A.; Ham, S.; Verdine, G. L. Stitched alpha-helical peptides via bis ring-closing metathesis. *Journal of the American Chemical Society* **2014**, *136*, 12314-22.
86. Kawamoto, S. A.; Coleska, A.; Ran, X.; Yi, H.; Yang, C. Y.; Wang, S. Design of Triazole-Stapled BCL9 alpha-Helical Peptides to Target the beta-Catenin/B-Cell CLL/lymphoma 9 (BCL9) Protein-Protein Interaction. *Journal of Medicinal Chemistry* **2012**, *55*, 1137-46.
87. Grigoryev, Y. Stapled peptide to enter human testing, but affinity questions remain. *Nature medicine* **2013**, *19*, 120.
88. Park, S. H.; Raines, R. T. Fluorescence polarization assay to quantify protein-protein interactions. *Methods in molecular biology* **2004**, *261*, 161-6.
89. Lakowicz, J. R. *Principles of fluorescence spectroscopy*. 3rd ed. ed.; Springer: New York, 2006.
90. Katayama, H.; Hojo, H.; Ohira, T.; Nakahara, Y. An efficient peptide ligation using azido-protected peptides via the thioester method. *Tetrahedron Letters* **2008**, *49*, 5492-5494.
91. Cheng, R. P.; Gellman, S. H.; DeGrado, W. F. beta-Peptides: from structure to function. *Chemical reviews* **2001**, *101*, 3219-32.
92. Bernal, F.; Tyler, A. F.; Korsmeyer, S. J.; Walensky, L. D.; Verdine, G. L. Reactivation of the p53 tumor suppressor pathway by a stapled p53 peptide. *Journal of the American Chemical Society* **2007**, *129*, 5298-5298.
93. Werder, M.; Hauser, H.; Abele, S.; Seebach, D. beta-peptides as inhibitors of small-intestinal cholesterol and fat absorption. *Helvetica Chimica Acta* **1999**, *82*, 1774-1783.
94. Boersma, M. D.; Haase, H. S.; Peterson-Kaufman, K. J.; Lee, E. F.; Clarke, O. B.; Colman, P. M.; Smith, B. J.; Horne, W. S.; Fairlie, W. D.; Gellman, S. H. Evaluation of diverse alpha/beta-backbone patterns for functional alpha-helix mimicry: analogues of the Bim BH3 domain. *Journal of the American Chemical Society* **2012**, *134*, 315-23.
95. Lau, Y. H.; de Andrade, P.; Skold, N.; McKenzie, G. J.; Venkitaraman, A. R.; Verma, C.; Lane, D. P.; Spring, D. R. Investigating peptide sequence variations for 'double-click' stapled p53 peptides. *Organic & Biomolecular Chemistry* **2014**, *12*, 4074-7.
96. Yap, J. L.; Cao, X.; Vanommeslaeghe, K.; Jung, K. Y.; Peddaboina, C.; Wilder, P. T.; Nan, A.; MacKerell, A. D., Jr.; Smythe, W. R.; Fletcher, S. Relaxation of the rigid backbone of an oligoamide-foldamer-based alpha-helix mimetic: identification of potent Bcl-xL inhibitors. *Organic & Biomolecular Chemistry* **2012**, *10*, 2928-33.
97. Rodriguez, J. M.; Nevola, L.; Ross, N. T.; Lee, G. I.; Hamilton, A. D. Synthetic inhibitors of extended helix-protein interactions based on a biphenyl 4,4'-dicarboxamide scaffold. *Chembiochem : a European journal of chemical biology* **2009**, *10*, 829-33.

98. Lee, J. H.; Zhang, Q.; Jo, S.; Chai, S. C.; Oh, M.; Im, W.; Lu, H.; Lim, H. S. Novel pyrrolopyrimidine-based alpha-helix mimetics: cell-permeable inhibitors of protein-protein interactions. *Journal of the American Chemical Society* **2011**, 133, 676-9.
99. Huang, X. Y. Fluorescence polarization competition assay: The range of resolvable inhibitor potency is limited by the affinity of the fluorescent ligand. *Journal of biomolecular screening* **2003**, 8, 34-38.
100. Nikolovska-Coleska, Z.; Wang, R. X.; Fang, X. L.; Pan, H. G.; Tomita, Y.; Li, P.; Roller, P. P.; Krajewski, K.; Saito, N. G.; Stuckey, J. A.; Wang, S. M. Development and optimization of a binding assay for the XIAP BIR3 domain using fluorescence polarization. *Analytical biochemistry* **2004**, 332, 261-273.
101. Luo, P. Z.; Baldwin, R. L. Mechanism of helix induction by trifluoroethanol: A framework for extrapolating the helix-forming properties of peptides from trifluoroethanol/water mixtures back to water. *Biochemistry* **1997**, 36, 8413-8421.
102. MOE. Montreal, Q., Canada: Chemical Computing Group. .
103. Lu, J.; Bai, L.; Sun, H.; Nikolovska-Coleska, Z.; McEachern, D.; Qiu, S.; Miller, R. S.; Yi, H.; Shangary, S.; Sun, Y.; Meagher, J. L.; Stuckey, J. A.; Wang, S. SM-164: a novel, bivalent Smac mimetic that induces apoptosis and tumor regression by concurrent removal of the blockade of cIAP-1/2 and XIAP. *Cancer research* **2008**, 68, 9384-93.
104. Bird, A. Perceptions of epigenetics. *Nature* **2007**, 447, 396-8.
105. Helin, K.; Dhanak, D. Chromatin proteins and modifications as drug targets. *Nature* **2013**, 502, 480-8.
106. Haynes, S. R.; Dollard, C.; Winston, F.; Beck, S.; Trowsdale, J.; Dawid, I. B. The bromodomain: a conserved sequence found in human, Drosophila and yeast proteins. *Nucleic acids research* **1992**, 20, 2603.
107. Tamkun, J. W.; Deuring, R.; Scott, M. P.; Kissinger, M.; Pattatucci, A. M.; Kaufman, T. C.; Kennison, J. A. brahma: a regulator of Drosophila homeotic genes structurally related to the yeast transcriptional activator SNF2/SWI2. *Cell* **1992**, 68, 561-72.
108. Zeng, L.; Zhou, M. M. Bromodomain: an acetyl-lysine binding domain. *FEBS letters* **2002**, 513, 124-8.
109. Denis, G. V. Bromodomain coactivators in cancer, obesity, type 2 diabetes, and inflammation. *Discovery medicine* **2010**, 10, 489-99.
110. Filippakopoulos, P.; Qi, J.; Picaud, S.; Shen, Y.; Smith, W. B.; Fedorov, O.; Morse, E. M.; Keates, T.; Hickman, T. T.; Felletar, I.; Philpott, M.; Munro, S.; McKeown, M. R.; Wang, Y.; Christie, A. L.; West, N.; Cameron, M. J.; Schwartz, B.; Heightman, T. D.; La Thangue, N.; French, C. A.; Wiest, O.; Kung, A. L.; Knapp, S.; Bradner, J. E. Selective inhibition of BET bromodomains. *Nature* **2010**, 468, 1067-73.
111. Zuber, J.; Shi, J.; Wang, E.; Rappaport, A. R.; Herrmann, H.; Sison, E. A.; Magoon, D.; Qi, J.; Blatt, K.; Wunderlich, M.; Taylor, M. J.; Johns, C.; Chicas, A.; Mulloy, J. C.; Kogan, S. C.; Brown, P.; Valent, P.; Bradner, J. E.; Lowe, S. W.; Vakoc, C. R. RNAi screen identifies Brd4 as a therapeutic target in acute myeloid leukaemia. *Nature* **2011**, 478, 524-8.
112. Lockwood, W. W.; Zejnullahu, K.; Bradner, J. E.; Varmus, H. Sensitivity of human lung adenocarcinoma cell lines to targeted inhibition of BET epigenetic signaling proteins. *Proceedings of the National Academy of Sciences of the United States of America* **2012**, 109, 19408-13.
113. Feng, Q.; Zhang, Z.; Shea, M. J.; Creighton, C. J.; Coarfa, C.; Hilsenbeck, S. G.; Lanz, R.; He, B.; Wang, L.; Fu, X.; Nardone, A.; Song, Y.; Bradner, J.; Mitsiades, N.; Mitsiades, C. S.; Osborne, C. K.; Schiff, R.; O'Malley, B. W. An epigenomic approach to therapy for tamoxifen-resistant breast cancer. *Cell research* **2014**.

114. Asangani, I. A.; Dommeti, V. L.; Wang, X.; Malik, R.; Cieslik, M.; Yang, R.; Escara-Wilke, J.; Wilder-Romans, K.; Dhanireddy, S.; Engelke, C.; Iyer, M. K.; Jing, X.; Wu, Y. M.; Cao, X.; Qin, Z. S.; Wang, S.; Feng, F. Y.; Chinnaiyan, A. M. Therapeutic targeting of BET bromodomain proteins in castration-resistant prostate cancer. *Nature* **2014**.
115. Dawson, M. A.; Prinjha, R. K.; Dittmann, A.; Giotopoulos, G.; Bantscheff, M.; Chan, W. I.; Robson, S. C.; Chung, C. W.; Hopf, C.; Savitski, M. M.; Huthmacher, C.; Gudgin, E.; Lugo, D.; Beinke, S.; Chapman, T. D.; Roberts, E. J.; Soden, P. E.; Auger, K. R.; Mirguet, O.; Doehner, K.; Delwel, R.; Burnett, A. K.; Jeffrey, P.; Drewes, G.; Lee, K.; Huntly, B. J.; Kouzarides, T. Inhibition of BET recruitment to chromatin as an effective treatment for MLL-fusion leukaemia. *Nature* **2011**, 478, 529-33.
116. Pastori, C.; Daniel, M.; Penas, C.; Volmar, C. H.; Johnstone, A. L.; Brothers, S. P.; Graham, R. M.; Allen, B.; Sarkaria, J. N.; Komotar, R. J.; Wahlestedt, C.; Ayad, N. G. BET bromodomain proteins are required for glioblastoma cell proliferation. *Epigenetics : official journal of the DNA Methylation Society* **2014**, 9, 611-20.
117. Nicodeme, E.; Jeffrey, K. L.; Schaefer, U.; Beinke, S.; Dewell, S.; Chung, C. W.; Chandwani, R.; Marazzi, I.; Wilson, P.; Coste, H.; White, J.; Kirilovsky, J.; Rice, C. M.; Lora, J. M.; Prinjha, R. K.; Lee, K.; Tarakhovskiy, A. Suppression of inflammation by a synthetic histone mimic. *Nature* **2010**, 468, 1119-23.
118. Zhu, J.; Gaiha, G. D.; John, S. P.; Pertel, T.; Chin, C. R.; Gao, G.; Qu, H.; Walker, B. D.; Elledge, S. J.; Brass, A. L. Reactivation of latent HIV-1 by inhibition of BRD4. *Cell reports* **2012**, 2, 807-16.
119. Banerjee, C.; Archin, N.; Michaels, D.; Belkina, A. C.; Denis, G. V.; Bradner, J.; Sebastiani, P.; Margolis, D. M.; Montano, M. BET bromodomain inhibition as a novel strategy for reactivation of HIV-1. *Journal of leukocyte biology* **2012**, 92, 1147-54.
120. Puissant, A.; Frumm, S. M.; Alexe, G.; Bassil, C. F.; Qi, J.; Chanthery, Y. H.; Nekritz, E. A.; Zeid, R.; Gustafson, W. C.; Greninger, P.; Garnett, M. J.; McDermott, U.; Benes, C. H.; Kung, A. L.; Weiss, W. A.; Bradner, J. E.; Stegmaier, K. Targeting MYCN in neuroblastoma by BET bromodomain inhibition. *Cancer discovery* **2013**, 3, 308-23.
121. Anand, P.; Brown, J. D.; Lin, C. Y.; Qi, J.; Zhang, R.; Artero, P. C.; Alaiti, M. A.; Bullard, J.; Alazem, K.; Margulies, K. B.; Cappola, T. P.; Lemieux, M.; Plutzky, J.; Bradner, J. E.; Haldar, S. M. BET bromodomains mediate transcriptional pause release in heart failure. *Cell* **2013**, 154, 569-82.
122. Borah, J. C.; Mujtaba, S.; Karakikes, I.; Zeng, L.; Muller, M.; Patel, J.; Moshkina, N.; Morohashi, K.; Zhang, W.; Gerona-Navarro, G.; Hajjar, R. J.; Zhou, M. M. A small molecule binding to the coactivator CREB-binding protein blocks apoptosis in cardiomyocytes. *Chemistry & biology* **2011**, 18, 531-41.
123. Jang, M. K.; Mochizuki, K.; Zhou, M.; Jeong, H. S.; Brady, J. N.; Ozato, K. The bromodomain protein Brd4 is a positive regulatory component of P-TEFb and stimulates RNA polymerase II-dependent transcription. *Molecular Cell* **2005**, 19, 523-34.
124. Boehm, D.; Calvanese, V.; Dar, R. D.; Xing, S.; Schroeder, S.; Martins, L.; Aull, K.; Li, P. C.; Planelles, V.; Bradner, J. E.; Zhou, M. M.; Siliciano, R. F.; Weinberger, L.; Verdin, E.; Ott, M. BET bromodomain-targeting compounds reactivate HIV from latency via a Tat-independent mechanism. *Cell Cycle* **2013**, 12, 452-62.
125. Wang, F.; Liu, H.; Blanton, W. P.; Belkina, A.; Lebrasseur, N. K.; Denis, G. V. Brd2 disruption in mice causes severe obesity without Type 2 diabetes. *The Biochemical journal* **2010**, 425, 71-83.

126. Lenburg, M. E.; Sinha, A.; Faller, D. V.; Denis, G. V. Tumor-specific and proliferation-specific gene expression typifies murine transgenic B cell lymphomagenesis. *The Journal of biological chemistry* **2007**, *282*, 4803-11.
127. Matzuk, M. M.; McKeown, M. R.; Filippakopoulos, P.; Li, Q.; Ma, L.; Agno, J. E.; Lemieux, M. E.; Picaud, S.; Yu, R. N.; Qi, J.; Knapp, S.; Bradner, J. E. Small-molecule inhibition of BRDT for male contraception. *Cell* **2012**, *150*, 673-84.
128. Adachi, K. *e. a.* Thienotriazolodiazepine compound and a medicinal use thereof. *International Patent No. PCT/JP2006/310709 (WO/2006/129623)* **2006**.
129. Miyoshi, S., Ooike, S., Iwata, K., Hikawa, H., Sugaraha, K. . Antitumor agent. *International Patent No. PCT/JP2008/073864 (WO/2009/084693)* **2009**.
130. Delmore, J. E.; Issa, G. C.; Lemieux, M. E.; Rahl, P. B.; Shi, J.; Jacobs, H. M.; Kastritis, E.; Gilpatrick, T.; Paranal, R. M.; Qi, J.; Chesi, M.; Schinzel, A. C.; McKeown, M. R.; Heffernan, T. P.; Vakoc, C. R.; Bergsagel, P. L.; Ghobrial, I. M.; Richardson, P. G.; Young, R. A.; Hahn, W. C.; Anderson, K. C.; Kung, A. L.; Bradner, J. E.; Mitsiades, C. S. BET bromodomain inhibition as a therapeutic strategy to target c-Myc. *Cell* **2011**, *146*, 904-17.
131. Zhang, W.; Prakash, C.; Sum, C.; Gong, Y.; Li, Y.; Kwok, J. J.; Thiessen, N.; Pettersson, S.; Jones, S. J.; Knapp, S.; Yang, H.; Chin, K. C. Bromodomain-containing protein 4 (BRD4) regulates RNA polymerase II serine 2 phosphorylation in human CD4+ T cells. *The Journal of biological chemistry* **2012**, *287*, 43137-55.
132. Bartholomeeusen, K.; Xiang, Y.; Fujinaga, K.; Peterlin, B. M. Bromodomain and extra-terminal (BET) bromodomain inhibition activate transcription via transient release of positive transcription elongation factor b (P-TEFb) from 7SK small nuclear ribonucleoprotein. *The Journal of biological chemistry* **2012**, *287*, 36609-16.
133. Spiltoir, J. I.; Stratton, M. S.; Cavaasin, M. A.; Demos-Davies, K.; Reid, B. G.; Qi, J.; Bradner, J. E.; McKinsey, T. A. BET acetyl-lysine binding proteins control pathological cardiac hypertrophy. *Journal of molecular and cellular cardiology* **2013**, *63*, 175-9.
134. Zou, Z.; Huang, B.; Wu, X.; Zhang, H.; Qi, J.; Bradner, J.; Nair, S.; Chen, L. F. Brd4 maintains constitutively active NF-kappaB in cancer cells by binding to acetylated RelA. *Oncogene* **2013**.
135. Li, Z.; Guo, J.; Wu, Y.; Zhou, Q. The BET bromodomain inhibitor JQ1 activates HIV latency through antagonizing Brd4 inhibition of Tat-transactivation. *Nucleic acids research* **2013**, *41*, 277-87.
136. <http://www.endeavourvision.com/news-n155-c70-OncoEthix+In-Licenses+OTX015>, a. a. h. OncoEthix In-Licenses OTX015, an anticancer Bromodomain inhibitor from Mitsubishi Tanabe Pharma Corporation. **June 15, 2012**.
137. Clinicaltrials.gov. NCT02259114.
138. Braun, T.; Coude, M. M.; Berrou, J.; Bertrand, S.; Riveiro, E.; Herait, P.; Baruchel, A.; Dombret, H.; Gardin, C. Preclinical Study Of The Bromodomain Inhibitor OTX015 In Acute Myeloid (AML) and Lymphoid (ALL) Leukemias. *Blood* **2013**, *122*.
139. Hewings, D. S.; Rooney, T. P.; Jennings, L. E.; Hay, D. A.; Schofield, C. J.; Brennan, P. E.; Knapp, S.; Conway, S. J. Progress in the development and application of small molecule inhibitors of bromodomain-acetyl-lysine interactions. *Journal of Medicinal Chemistry* **2012**, *55*, 9393-413.
140. Clinicaltrials.gov. NCT01587703.
141. Clinicaltrials.gov. NCT01987362.
142. Clinicaltrials.gov. NCT01949883.
143. Clinicaltrials.gov. NCT02157636.
144. clinicaltrials.gov. NCT02158858.

145. Chung, C. W.; Coste, H.; White, J. H.; Mirguet, O.; Wilde, J.; Gosmini, R. L.; Delves, C.; Magny, S. M.; Woodward, R.; Hughes, S. A.; Boursier, E. V.; Flynn, H.; Bouillot, A. M.; Bamborough, P.; Brusq, J. M.; Gellibert, F. J.; Jones, E. J.; Riou, A. M.; Homes, P.; Martin, S. L.; Uings, I. J.; Toum, J.; Clement, C. A.; Boullay, A. B.; Grimley, R. L.; Blandel, F. M.; Prinjha, R. K.; Lee, K.; Kirilovsky, J.; Nicodeme, E. Discovery and characterization of small molecule inhibitors of the BET family bromodomains. *Journal of Medicinal Chemistry* **2011**, *54*, 3827-38.
146. Bisagni, E.; Nguyen, C. H.; Pierre, A.; Pepin, O.; Decointet, P.; Gros, P. 1-Amino-Substituted 4-Methyl-5h-Pyrido[4,3-B]Indoles (Gamma-Carbolines) as Tricyclic Analogs of Ellipticines - a New Class of Antineoplastic Agents. *Journal of Medicinal Chemistry* **1988**, *31*, 398-405.
147. Picaud, S.; Da Costa, D.; Thanasopoulou, A.; Filippakopoulos, P.; Fish, P. V.; Philpott, M.; Fedorov, O.; Brennan, P.; Bunnage, M. E.; Owen, D. R.; Bradner, J. E.; Taniere, P.; O'Sullivan, B.; Muller, S.; Schwaller, J.; Stankovic, T.; Knapp, S. PFI-1, a highly selective protein interaction inhibitor, targeting BET Bromodomains. *Cancer research* **2013**, *73*, 3336-46.
148. Liu, W.; Ma, Q.; Wong, K.; Li, W.; Ohgi, K.; Zhang, J.; Aggarwal, A. K.; Rosenfeld, M. G. Brd4 and JMJD6-associated anti-pause enhancers in regulation of transcriptional pause release. *Cell* **2013**, *155*, 1581-95.
149. Rahman, S.; Sowa, M. E.; Ottinger, M.; Smith, J. A.; Shi, Y.; Harper, J. W.; Howley, P. M. The Brd4 extraterminal domain confers transcription activation independent of pTEFb by recruiting multiple proteins, including NSD3. *Molecular and cellular biology* **2011**, *31*, 2641-52.
150. BET bromodomain inhibitors and therapeutic method using the same. *PCT/US2014/022953*.
151. Wang, Z. X. An exact mathematical expression for describing competitive binding of two different ligands to a protein molecule. *FEBS Lett* **1995**, *360*, 111-4.
152. Zhang, R. M.; Mayhood, T.; Lipari, P.; Wang, Y. L.; Durkin, J.; Syto, R.; Gesell, J.; McNemar, C.; Windsor, W. Fluorescence polarization assay and inhibitor design for MDM2/p53 interaction. *Analytical Biochemistry* **2004**, *331*, 138-146.
153. Bai, L.; Chen, J.; McEachern, D.; Liu, L.; Zhou, H.; Aguilar, A.; Wang, S. BM-1197: A Novel and Specific Bcl-2/Bcl-xL Inhibitor Inducing Complete and Long-Lasting Tumor Regression In Vivo. *PLoS one* **2014**, *9*, e99404.
154. MOE, Chemical Computing Group: Montreal, Quebec, Canada.
155. Jones, G.; Willett, P.; Glen, R. C.; Leach, A. R.; Taylor, R. Development and validation of a genetic algorithm for flexible docking. *Journal of molecular biology* **1997**, *267*, 727-48.
156. Verdonk, M. L.; Cole, J. C.; Hartshorn, M. J.; Murray, C. W.; Taylor, R. D. Improved protein-ligand docking using GOLD. *Proteins* **2003**, *52*, 609-23.
157. Otwinowski, Z.; Minor, W. Processing of X-ray diffraction data collected in oscillation mode. *Macromolecular Crystallography, Pt A* **1997**, *276*, 307-326.
158. McCoy, A. J.; Grosse-Kunstleve, R. W.; Adams, P. D.; Winn, M. D.; Storoni, L. C.; Read, R. J. Phaser crystallographic software. *Journal of Applied Crystallography* **2007**, *40*, 658-674.
159. Bricogne G., B. E., Brandle M., Flensburg C., Keller P., Paciorek W., Roversi P., Sharff A., Smart O. S., Vornrhein C., Womack T. O. *W.T.O. Buster version 2.10.0* **2011**.
160. Emsley, P.; Lohkamp, B.; Scott, W. G.; Cowtan, K. Features and development of Coot. *Acta crystallographica. Section D, Biological crystallography* **2010**, *66*, 486-501.
161. Chen, V. B.; Arendall, W. B., 3rd; Headd, J. J.; Keedy, D. A.; Immormino, R. M.; Kapral, G. J.; Murray, L. W.; Richardson, J. S.; Richardson, D. C. MolProbity: all-atom structure validation for macromolecular crystallography. *Acta crystallographica. Section D, Biological crystallography* **2010**, *66*, 12-21.

162. Zucker, F.; Champ, P. C.; Merritt, E. A. Validation of crystallographic models containing TLS or other descriptions of anisotropy. *Acta crystallographica. Section D, Biological crystallography* **2010**, 66, 889-900.
163. Hoofstede, R. W.; Vriend, G.; Sander, C.; Abola, E. E. Errors in protein structures. *Nature* **1996**, 381, 272.
164. Kleywegt, G. J.; Harris, M. R.; Zou, J. Y.; Taylor, T. C.; Wahlby, A.; Jones, T. A. The Uppsala Electron-Density Server. *Acta crystallographica. Section D, Biological crystallography* **2004**, 60, 2240-9.
165. Ramalingam, P.; Ko, Y. T. A validated LC-MS/MS method for quantitative analysis of curcumin in mouse plasma and brain tissue and its application in pharmacokinetic and brain distribution studies. *J Chromatogr B Analyt Technol Biomed Life Sci* **2014**, 969, 101-8.
166. Sheng, R.; Sun, H.; Liu, L.; Lu, J.; McEachern, D.; Wang, G.; Wen, J.; Min, P.; Du, Z.; Lu, H.; Kang, S.; Guo, M.; Yang, D.; Wang, S. A potent bivalent Smac mimetic (SM-1200) achieving rapid, complete, and durable tumor regression in mice. *J Med Chem* **2013**, 56, 3969-79.
167. Cai, Q.; Sun, H.; Peng, Y.; Lu, J.; Nikolovska-Coleska, Z.; McEachern, D.; Liu, L.; Qiu, S.; Yang, C. Y.; Miller, R.; Yi, H.; Zhang, T.; Sun, D.; Kang, S.; Guo, M.; Leopold, L.; Yang, D.; Wang, S. A potent and orally active antagonist (SM-406/AT-406) of multiple inhibitor of apoptosis proteins (IAPs) in clinical development for cancer treatment. *J Med Chem* **2011**, 54, 2714-26.
168. Deshayes, S.; Morris, M. C.; Divita, G.; Heitz, F. Cell-penetrating peptides: tools for intracellular delivery of therapeutics. *Cell Mol Life Sci* **2005**, 62, 1839-49.
169. Chang, Y. S.; Graves, B.; Guerlavais, V.; Tovar, C.; Packman, K.; To, K. H.; Olson, K. A.; Kesavan, K.; Gangurde, P.; Mukherjee, A.; Baker, T.; Darlak, K.; Elkin, C.; Filipovic, Z.; Qureshi, F. Z.; Cai, H.; Berry, P.; Feyfant, E.; Shi, X. E.; Horstick, J.; Annis, D. A.; Manning, A. M.; Fotouhi, N.; Nash, H.; Vassilev, L. T.; Sawyer, T. K. Stapled alpha-helical peptide drug development: a potent dual inhibitor of MDM2 and MDMX for p53-dependent cancer therapy. *Proc Natl Acad Sci U S A* **2013**, 110, E3445-54.
170. Okamoto, T.; Zobel, K.; Fedorova, A.; Quan, C.; Yang, H.; Fairbrother, W. J.; Huang, D. C.; Smith, B. J.; Deshayes, K.; Czabotar, P. E. Stabilizing the pro-apoptotic BimBH3 helix (BimSAHB) does not necessarily enhance affinity or biological activity. *ACS Chem Biol* **2013**, 8, 297-302.
171. Drahl, C. Stapled peptides hit puberty, with attendant drama. *CHEMICAL & ENGINEERING NEWS* **2013**, 91, 26-28.
172. Ding, K.; Lu, Y.; Nikolovska-Coleska, Z.; Qiu, S.; Ding, Y.; Gao, W.; Stuckey, J.; Krajewski, K.; Roller, P. P.; Tomita, Y.; Parrish, D. A.; Deschamps, J. R.; Wang, S. Structure-based design of potent non-peptide MDM2 inhibitors. *J Am Chem Soc* **2005**, 127, 10130-1.